Geochemical study on isotope ratio of dissolved oxygen and argon anomaly in the northwestern Pacific Ocean

（北西太平洋の溶存酸素同位体比およびアルゴン異常の地球化学的研究）

KEEDAKKADAN, Habeeb Rahman

Doctor of Philosophy, Science

Graduate School of Environmental Studies, Nagoya University

2016

Acknowledgment

Over the past three it has taken to complete my Ph. D thesis, many people have helped me along the way, and I am eternally thankful for their assistance. I would like to take this opportunity to thank all the persons who have made it possible for me to commence and complete this enormous task. I would like to acknowledge and commend them for their efforts, cooperation and collaboration that have worked towards the successes of this study.

I am deeply grateful to my Professor Takeshi Nakatsuka and supervising guide Dr. Osamu Abe for patiently taking me through this difficult task of environmental research. I express my deep and sincere gratitude to my guide for conceptualisation and implementation of this research topic, in addition to his peerless guidance and motivation all the way through my doctoral research. He is not only my academic supervisor, but also a real mentor and friend who let me know how to treat life with patience and fair-mindedness across my stay in Japan.

I am deeply grateful to the Japanese Government and Ministry of Education, Culture, Sports, Science, and Technology for the financial support for my study. I thank Dr Prosenjit Ghosh and Professor chandramohanakumar for their recommendation and reference letters for the admission in Nagoya University. I thank interviewing committee for awarding MEXT scholarship.

I am thankful to Dr. MORIMOTO Maki for her valuable suggestions, help and encouragement during the tenure of my work and my smooth stay in japan as an international student. I do not have words to acknowledge her for kind help to do official and unofficial works. I thank her for helping me to understand Japanese papers and documents from the university and other authorities.

I extend my special gratitude towards Dr. chenxi xu for his help as a tutor during my study in Nagoya University. That was made me a smooth and fast setting up of official and daily life in Japan. I thank person who assigned Xu san as my tutor. I extend my special gratitude towards associate professor Christina Lim, international student adviser graduate school of environmental studies, for her orientations and advices helped me for smooth academic and daily life in japan. I also express thanks toward International Residence – Yamate officials and staffs for a very luxurious comfortable stay during first year of my course.

I extend my special gratitude towards Dr. V. V. S. S Sarma, Scientists, National Institute of Oceanography, Goa for collecting water samples during MR 07-01 cruise. I thank Principal Investigators and staff of MR 13-04 and MR 14-02 for a safe and comfortable cruise. I would like to thank Chief Chef and restaurant workers of

staff MR 13-04 and MR 14-02 who prepared special spicy delicious food. I express my sincere thanks to marine workers who analysed hydrographical parameters during both cruises.

I am thankful to Aneesah Nishaat for her help in finding and making contract for a private apartment. I am sincerely thankful to my friend Yuka Mochida (持田侑香) for her help in interacting with Japanese people and translating Japanese documents for last three years.

I acknowledge the help and encouragement rendered by my colleagues, Yasui san, LI Zhen, Dr Naoyuki Kurita and Dr Masaki Sano. I owe my heartfelt thanks to my dear friends Dr. Klm Manoj, Dr Renjith, Dr Gireesh Kumar, Dr Ratheesh Kumar, Dr. Namdev Vatmurge, Dr G Venkata Ramana, Dr. Sathiyanarayanan Murugan, Sreenadh S Pillai and Vinay Elothunkal for their support and encouragement.

I would like to thank my beloved father, mother, wife and sister, for their support, patience, and for their continued inspiration over the years.

Words are insufficient to convey my gratefulness for the prayers and encouragement of my parents and sister during the entire course and this research programme.

Above all, I thank the Almighty God Allah for blessing me with the potential to complete this work successfully.

Keedakkadan Habeeb Rahman

Abstract

Ocean is a fundamental component of climate system, it covers 70 % of earth's surface carrying 97 % of all water on the earth. The ocean water control and distributes solar energy through water circulation all over the world. Ocean plays a major role in the existence of life on the earth by providing vital essentials like food, oxygen, water and minerals through the active geochemical cycles. It acts as a largest storage house for greenhouse gases and minerals. However last few decades natural and anthropogenic processes resulting sea level rise and global warming that altered its natural habitat have seriously affected the world ocean. Observation and simulation based studies have employed to understand the properties of world ocean and its effect in the climate system. In this study, I have used stable isotope ratios of oxygen and noble gas anomalies along with other hydrographical parameters to understand the physical and biological properties of Pacific Ocean.

Isotope ratio of dissolved oxygen has been used to evaluate processes of primary production and oxygen consumption in aquatic ecosystem. After the discovery in 1999 that tropospheric oxygen contains the memory of mass-independent isotope fractionation during stratospheric ozone formation and consumption, dissolved oxygen can be divided into atmospheric and photosynthetic sources using its triple isotopic consumption. More recently, exact determination of primary production become available by the combined analysis with oxygen to argon ratio that could reduce the uncertainty due to temperature variation and bubble mediated gas transfer process between air and water.

Oceanic studies of triple isotopic composition of dissolved oxygen have been conducted in the mixed layer and below to evaluate present ocean primary productivity. On the other hand, behavior of triple isotopic composition of dissolved oxygen in the subsurface ocean below euphotic zone has not been investigated. The subsurface $\Delta^{17}O$, which is defined as a difference from mass dependent raw, was considered as a new tracer to reconstruct past primary productivity.

In this study, (1) development of cryogenic separation of an oxygen-argon mixture in the natural air samples for the determination of isotope and molecular ratios, (2) determination of equilibrium isotope fractionation factor of molecular oxygen between gas and liquid phase, and distribution of triple isotopic composition of dissolved oxygen and argon anomaly along 155 °E transect in the northwestern Pacific Ocean were conducted. Argon anomaly is identical

to saturation degree of argon and can be obtained from measurements of oxygen to argon ratio and dissolved oxygen concentration.

(1) Development of cryogenic separation of an oxygen argon mixture in natural air samples

Gas chromatography based methods haven developed for separation of oxygen or oxygen-argon mixture from natural air samples; however, these chromatographic methods require ultra-high purity helium as a carrier gas and the depletion of helium reservoir is a growing global concern. I developed simpler, higher portability and helium free cryogenic separation methods for the determination of isotope and molecular ratio analysis. Atmospheric or dissolved air samples were trapped into a single 5A molecular sieve column at liquid nitrogen temperature, and then only oxygen-argon mixture would be eluted after increasing column temperature to -92 °C. Repeated measurements of atmospheric air yielded a reproducibility (1 σ) of 0.044 ‰, 15 per meg and 1.9 ‰ for $\delta^{18}O$, $\Delta^{17}O$ and $\delta(O_2/Ar)$ values respectively

(2) Determination of equilibrium isotope fractionation factor of molecular oxygen between gas and liquid phases

Using cryogenic separation method developed, equilibrium isotope fractionation factor of molecular oxygen between gas and liquid phases were determined, the equilibrium isotopic composition of dissolved oxygen with atmosphere is an essential end member for the estimation of gross primary productivity using triple isotope method however, present arguments are the existence of temperature dependency and/or the difference of experimentally obtained results due to the approaches of generating equilibrium water. In this study isotope ratios of equilibrated dissolved oxygen by stirring and bubbling methods were determined with regard to seawater and deionized water. Significant differences were not recognised in $\delta^{18}O$ and $\Delta^{17}O$ values due to equilibrium methods and $\Delta^{17}O$ value was in good agreement with recently reported results. On the other hand, significant difference of $\delta^{18}O$ value were found between seawater and deionized water.

(3) Distribution of triple isotopic composition of dissolved oxygen and argon anomaly along 155 °E transect in the northwestern Pacific Ocean.

To investigate triple isotopic composition of dissolved oxygen and argon anomaly in the surface water, seawater samples were collected at a depth between surface and 1000 m from 8

stations along 155 °E transect (the equator, 5 °N, 10 °N, 10 °N, 15 °N, 20 °N, 24 °N, 30 °N and 36 °N) in the northwestern pacific ocean.

The maximum values of $\Delta^{17}O$ and argon anomaly were found consistently in the thermocline between the equator and 20 °N. The maximum value of $\Delta^{17}O$ was formed by accumulating photosynthetic oxygen in this zone where was shielded from atmosphere. Vertical diapycnal mixing caused the maximum value of argon anomaly. A constant value of 65 ± 19 per meg was found in the north pacific intermediate water (NPIW), which is represented as a potential density of 26.8.

Contents

Chapter 1

Introduction

Chapter 2

Material and method

Chapter 3

Results

Chapter 4

Discussions and Conclusions

Chapter 5

Chapter 1

Introduction

Existence of human being in this planet was being tightly bonded with world ocean processes. Ocean helps the existence of life by providing food, actively involving the geochemical cycling of water (Ramanathan et al. 2001; Wajsowicz and Schopf 2001: Oki and Kanae 2006), gases (Falkowski et al. 1998: Del Giorgio and Duarte 2002) and minerals (Treguer et al. 1995), and also it control the earth's climate drastically through circulation, gas exchange and largest storage greenhouse gases like carbon dioxide. World Ocean receives water, minerals, gases, dissolved substances from land and atmosphere through rain, run off and atmosphere, and eventually a portion of them will be used for the marine life activities and remaining will be stored either in the form of dissolved substances or deposited in the basin as sediments. Ocean has a very active role in the geochemical cycling of elements, minerals, water etc. Hence, understanding of ocean is very important for studying earth system, climate processes, climate change global warming and sea level rise along with atmosphere. In this study I were looking more deeply in to chemical, physical and oceanographic properties of Pacific Ocean, especially for northwestern Pacific Ocean. In order to understand these properties, I have used primarily dissolved oxygen triple isotopes and argon saturation along with hydrographical parameters. Dissolved oxygen isotope ratios in the open ocean are a measure biological activity (photosynthesis and respiration) and gas exchange in the mixed layer and deep water. It always does have a strong inverse relations ship with concentration of dissolved oxygen. The studies on triple oxygen isotope is a relatively new field in isotope geochemistry and it was widely used to study biosphere oxygen production and marine gross oxygen production. The behavior of biologically inactive noble gas concentration in the ocean water was rarely understood and very few applications were discovered. Few decades before the applications of noble gas concentration and its saturation in the oceanic environment was started and now the method has wide applications to determine gas exchange coefficients, bubble mediated seawater super saturation and water mass mixing heating and cooling creates the argon supersaturation or undersaturation in the water. In order to study these processes, it is important to have a simple and accurate method to estimate oxygen isotope and argon concentrations in the dissolved gas samples. Thus I have established a new cryogenic method

to purify oxygen–argon mixture in the natural air samples, it has several advantages over other available methods.

1.1 Oxygen concentration and isotopic compositions

Oxygen constitutes about 47.2 % of earth's crust by mass and second most abundant gas in the atmosphere and third in our galaxy (Wedepohl 1995: Chiappini et al. 2003; Javoy et al. 2010; Lyons et al. 2014). The production of gaseous oxygen was started around 3-3.5 billion years ago and it was well documented along with banded iron formation (Lyons et al. 2014). It was believed that the oxygen was produced from water as a result of photosynthesis by unicellular organisms. In 1773 Carl Wilhelm Scheele discovered this biologically important gas. Our earth's atmosphere constitutes about 21 % molecular oxygen and which recycled through photosynthesis and respiration (Lyons et al. 2014). While talking about oxygen cycle and photosynthesis, the world ocean has an important role. It was believed that about 50-85 % of atmospheric oxygen was produced by marine phytoplankton and was recycled through respiration and gas exchange (Falkowski 1994). Thus it is important to study the production and utilization of oxygen in the world ocean. Such a study can be made possible by measuring dissolved oxygen concentration in the water. In 1888 Winkler proposed a method to determine dissolved oxygen in water samples, later on O_2 sensors were involved in the determination of oceanic O_2 concentration accurately. Surface water contains about 4-6 mL/L of dissolved oxygen.

Isotopes are the same atoms, whose nucleus containing same number of protons and electrons but a different number of electrons. There are different isotopes like stable and radioactive, the stable isotopes have a neutron to proton ratio close to unity or a maximum of 1.5. The difference in chemical and physical properties of these isotopes due to different mass number of an element is known as isotope effect. The abundance of isotopes in the nature varies widely as a function of mass number, lighter isotopes will be more abundant than the heavier ones. Oxygen has three isotopes, ^{16}O, ^{17}O and ^{18}O having a natural abundance of 99.76 %, 0.04 % and 0.2% respectively (Nier 1950). Isotopic Fractionation is a separation process during a phase transition or reactions, during this process lighter isotope will have more preference than heavier one. The main processes cause isotope fractionation are, 1) isotope exchange reactions, 2) kinetic processes.

Pioneer studies of stable isotopes and its fractionation were carried out by (Bigeleisen and Mayer 1947; Urey 1947: Oneil 1986). Isotope exchange reactions are physicochemical

processes in which light or heavy isotopes exchange each other between different phases or between individual molecules. Best example for isotope exchange reaction is the precipitation for calcium carbonate in water, in which ^{18}O and ^{16}O between water and carbonate exchanges

$$H_2{}^{18}O + 1/3CaC^{16}O_3 \leftrightarrow H_2{}^{16}O + 1/3\ CaC^{18}O_3$$

Here the fractionation factor is the ratio of number of any two isotopes in one chemical compound to the corresponding ratio for other chemical compound.

$$\alpha = \frac{R_{reactants}}{R_{products}}$$

$$\alpha = (^{18}O/^{16}O)_{CaCO3} / (^{18}O/^{16}O)_{H2O}$$

In the isotope geochemistry, it very common to express isotopes as ratios of heavy to light isotopes. Differences between two isotopes of one element is very small to measure them individually with enough precision is difficult to impossible for most isotope systems. By comparing a sample ratio to a standard ratio, the difference between these two can be determined much more precisely. Delta δ is the isotope ratio of a particular element relative to standard times 1000.

$$\delta^{18}O = \left(\frac{R_{sample} - R_{standard}}{R_{standard}}\right)$$

Where R is the ratio of heavy/light isotope.

Isotopic compounds can have a significant fractionation during phase transfer processes because of the difference in the vapor pressure of each isotopic compound. Such isotopic fractionation can be treated as an isotopic fractional distillation and is expressed by Rayleigh equation (Rayleigh 1896). During the face transfer, ratio of heavy to light isotope molecule in the two phase changes, this process is temperature dependent, higher temperature lesser will be the difference between isotopic composition of two phases. This fractionation is called isotopic fractionation associated with equilibrium exchange reaction between two phases (α).

$$\alpha_{A\text{-}B} = R_A/R_B$$

Where A and B are the two phases or compounds, R is the ratio of heavy isotope to light isotope of compound A and B. the value of α is usually differ within few percent from

unity, however the observed maximum α value of 4 is associated hydrogen isotope fractionations.

$$\alpha_{A\text{-}B} = (\delta A)/ (\delta B)$$

Fractionation factor usually proportional to the temperature, thus the 1000 ln α is linearly proportional to 1/T, (T = temperature in Kelvin)

Kinetic fractionations are quite different, but similar to the equilibrium fractionation, which are associated with incomplete or unidirectional evaporation, biologically mediated reactions and diffusion. The magnitude kinetic fractionation depends on the reaction pathway, reaction rate and strength of bonds being broken or formed. Kinetic fractionation factors are usually larger than the equilibrium fraction. The bonds between lighter isotopes are easier to break than the bond between heavier isotopes, because of their large vibrational energy than the bonds between heavier isotopes. Hence the light isotopes can react faster and enriched in the products, so reactants will be enriched with heavier isotopes and product will be with lighter isotopes.

Isotopic fractionation is

$$\alpha = R_p/R_s$$

Where R_p and R_s are the ratios of heavy isotope to light isotope in the products and reactants respectively.

Isotope enrichment factor ε is

$$\varepsilon_{p\text{-}s} = (\alpha\text{-}1)$$

The Rayleigh equation for isotopic fractionation

Rayleigh equation originally derived for the fractionation distillation of mixed liquids, this can be approximated for partitioning of stable isotopes between two reservoirs under certain conditions, 1) material is continuously removed for a system containing the molecules of two or more isotopes, 2) removal process described by fractionation factor α, 3) the fractionation factor α does not change during the process. Under these condition the Rayleigh equation can be written for isotopic fraction is

$$(R/R_o) = (X_1/X_{1o})^{(\alpha-1)}$$

Where R is the ratio of isotopes in the reactant, R_o is the initial ratio, X_1 is the concentration of abundant of lighter isotope, X_{1o} is the initial concentration.

Substitute $f = X_1/X_{1o}$,

$$R = R_o f^{(\alpha-1)}$$

And the equation can be approximated for δ, under certain conditions like α is near 1, δ_o values near 0 and less than 10.

$$\delta \approx \delta_o \ f^{(\alpha-1)}$$

1.2 Biological stable isotope fractionation

Biological fractionation is a best example for kinetic isotope reaction, which is a unidirectional consumption/production reactions. Biological organisms preferentially use lighter isotopes than the heavier ones, thus any kind of biological product will highly depleted in terms of isotopes. This significant fractionation during biological activity is mainly because of the energy associated with breaking of molecular bonds. Bonds between lighter isotopes possess higher vibrational energy than the heavier molecules, thus a biological species needs to spend small amount of energy to break/react lighter molecules than the heavier molecules.

Bond dissociation energy is a measure of bond strength between two atoms, ground state vibrational energy of a bond is

$$E = ½\ h\nu$$

Where h is the Plank's constant and ν is the vibrational frequency and that can be expressed in terms of Hooke's law

$$\nu = 1/2\pi\sqrt{k/\mu}$$

Where μ is the reduced mass,

$$\mu = \left(\frac{m1 \times m2}{m1+m2}\right)$$

Thus the strength of a bond is

$$E = \left(\frac{h\sqrt{k}}{4\pi}\right)\sqrt{\frac{1}{\mu}}$$

Thus bond strength is proportional to $\sqrt{\frac{1}{\mu}}$

For the ratio of the bond energies of oxygen isotopic molecules are

$^{16}O^{18}O/^{16}O^{16}O = 0.972$

Thus slower reaction steps show more fractionation than faster steps, because organisms have time to be more selective.

Thus the isotopes fractionate either through equilibrium processes or kinetic or both. In short most of the fractionations are related to the mass of isotopic molecules and also in some cases the temperature. Thus this isotopic fractionation can be broadly classified into two.

1.3 Mass dependent isotope fractionation

In general, isotopic fractionations are mostly mass dependent during any kind of terrestrial processes, because at a thermodynamic equilibrium the isotopic distributions are strictly governed by the mass difference of isotopes of elements. That means, the elements having more than two isotopes the fractionation of one isotope must be relative to the other isotopes. For example, the enrichment of ^{18}O relative to ^{16}O is observed to be approximately twice as large as the enrichment of ^{17}O relative to ^{16}O. Approximately $\delta^{17}O = 0.52\delta^{18}O$. However recently the studies about fractionation of multiple stable isotopes reviled that, there can be slight variation in the fractionation constants (Luz et al. 1999; Miller 2002; Young et al. 2002:Yeung et al. 2012;). This mass dependent fractionation of isotopes can be easily understandable from the slope linear line of three isotopes of oxygen (Matsuhisa et al. 1978).

1.4 Marine Photosynthesis

Photosynthesis is a process of conversion of light energy to chemical energy as carbohydrates by green plants and algae. These processes are begin when light energy absorbed

by proteins that contain green chlorophyll pigments, and the sugars are produced in light reactions that is called Calvin cycle. During photosynthesis carbon dioxide is converter to sugars in a process called carbon fixation, and water molecules break down to form oxygen. A general equation for photosynthesis is

$$n CO_2 + 2n\ H_2O + h\nu\ (\text{light energy}) = (CH_2O)n + n\ O_2 + n\ H_2O$$

This reaction is an endothermic process, to make it feasible the system need to supply light energy.

The oxygen produced during light dependent reaction of photosynthesis is from the water through the photolysis

$$2\ H_2O + 2\ NADP^+ + 3\ ADP + 3\ Pi + \text{light} \rightarrow 2\ NADPH + 2H^+ + 3ATP + O_2$$

The Hill's reaction confirmed the source of oxygen is pyrolysis of water not the oxygen present in the CO_2

Simply Hill's reaction is, when isolated chloroplasts are illuminated in presence of an electron acceptor, the acceptor is reduced and molecular oxygen evolved.

$$2H_2O + 2A + \text{chloroplast} + \text{light} \rightarrow 2\ AH_2 + O_2$$

Where A is an electron acceptor (eg: ferric potassium oxalate ($K_3[Fe(C_2O_4)_3]. 3\ H_2O$))

Therefore the isotopic composition of plant is controlling factor of isotopic ratios of photosynthetically produced oxygen.

In the isotopic geochemistry the importance of the production of oxygen by photosynthesis from water is very important. Early 1950s the researchers were noticed the dissolved oxygen is ocean is enriched in $\delta^{18}O$ by relative to atmospheric oxygen. In the ocean the concentration and isotopic composition of dissolved oxygen was mainly controlled by the gas exchange, respiration and photosynthesis. Gas exchange always brings dissolved oxygen in ocean towards an equilibrium value for both concentration and isotope ratios. The equilibrium value of oxygen isotope ratios $\delta^{18}O$ and $\delta^{17}O$ were around 0.7 and 0.35 respectively (Benson et al. 1979; Keedakkadan and Abe 2015). This equilibrium isotope fractionation was found to be dependent on temperature of equilibrium system (Benson et al. 1979). The production of oxygen in the ocean is by photosynthesis, and the process was believed to be no fractionation during the break down of water molecules. The measured $\delta^{18}O$ of dissolved oxygen for Amazon River basis was between 15-30 ‰ (Quay et al. 1995). The oxygen isotope

ratios of photosynthetically produced oxygen was measured by Craig and found the water isotope ratios have no significant difference from the oxygen isotope ratios (Craig 1957), and which is substantially compared to atmospheric oxygen. The fractionation factor during the formation of oxygen by photosynthesis was calculated as 1.000 ±0.002 (Helman et al. 2005; Quay et al. 1993). Relative to Vienna standard mean ocean water the isotopic composition of photosynthetically produced oxygen is same. There is a small difference of -5 ‰ for $\delta^{17}O$ of marine waters compared to VSMOW but not for $\delta^{18}O$ (Luz and Barkan 2010). Oxygen isotopic composition of WSMOW was measured for $\delta^{17}O$ and $\delta^{18}O$ as -11.9 ‰ and -23.3 relative to atmospheric oxygen respectively (Barkan and Luz 2005; Barkan and Luz 2011; Kaiser and Abe 2012).

1.5 Isotopic fractionation during respiration

Figure 35 shows the mass dependent fractionation of dissolved oxygen by respiration. The isotopic composition of dissolved oxygen and its properties were studied deeply to explain biological activity respiration, circulation. The measurement of tropospheric oxygen isotopic composition $\delta^{18}O$ values are much positive, and the value is around 23.8 ‰, this is known as dole effect and it is because of the oxygen consumption process (Dole 1936). This oxygen consumption process include respiration (Kroopnick and Craig 1976), photorespiration (Guy et al. 1993). Each of these processes has different fractionations, the cytochrome pathway, alternative oxidase pathway, photorespiration, Mehler reaction (Guy et al. 1993; Helman et al. 2005). Cytochrome path way is the mitochondrial respiration, which is associated with an isotopic fractionation of 18 ‰ (Helman et al. 2005). Oxidase reaction is an alternative path way for the production of energy, the cycle is carried out by an enzyme called alternative oxidase under stress conditions, and this process is associated with production of less energy (Mehler 1951). The oxygen isotopic fractionation associated with this process is 28 ‰ (Angert et al. 2003). Under certain conditions like low CO_2, high oxygen or high temperature, the photosynthetic enzyme RuBisCO bind with oxygen to produce plant toxic ammonia along with utilization of one ATP and NADPH. Even though it is an energy losing process, it happens mainly C3 Plants and cause to reduce efficiency of photosynthesis, significantly reducing photosynthetic output by 25 %. This oxygen uptake associated with RuBisCO has an oxygen isotopic fractionation about 21.7 ‰ (Guy et al. 1993). Another process that can fractionate oxygen isotope is Mehler reaction. In plant chloroplast can use oxygen as electron acceptor to

form O_2^-, which is then redly converted to potentially toxic hydrogen peroxide. This Mehler reaction is associated with oxygen isotopic fractionation of 15.3 ‰ (Guy et al. 1993). These all process together causes the Dole effect, and the difference between marine and terrestrial fractionation is small and is about 3-4 ‰ (Luz and Barkan 2011).

The dole effect was measuring since 1936. The standard method to measure the isotope ratios of water is the equilibration reaction with CO_2. Using this method I can precisely measure the $\delta^{18}O$ but not for $\delta^{17}O$, this is because of the masking of much more abundant ^{13}C measured in the same molecular mass 45. Later Brenninkmeijer developed an alternative method to measure $\delta^{17}O$ in CO_2, but the method was suffered large uncertainty (Brenninkmeijer and Rockmann 1998). However more recently Barkan introduced a high accuracy measurement by the fluorination of water molecule. Thus it demands another method to convert water to oxygen. A simple way to breakdown water to oxygen is fluorination using CoF_3 (cobalt fluoride). This was carried out using 10g of CoF_3 in a 25 cm nickel tube at 370 °C, and pass 2 μL water, then collect the produced oxygen using 5A molecular sieve at liquid nitrogen temperature. Using this method the $\delta^{17}O$ and $\delta^{18}O$ of atmospheric oxygen was measured as 12.8 ‰ and 23.88 ‰, for SLAP -29.48 ‰ and -55.11 ‰ respectively. The analytical precision of this method was 0.01 and 0.03 for $\delta^{17}O$ and $\delta^{18}O$ respectively (Barkan and Luz 2005). Another potentially new technique that could be used for the determination of $\delta^{17}O$ and $\delta^{18}O$ of CO_2 is through the isotope exchange between O_2 and CO_2 over hot platinum (Mahata et al. 2013). Using this method I can determine the isotope ratio of water, which was equilibrated with CO_2.

1.6 Isotopic composition of atmospheric oxygen

The production of gaseous oxygen was started around 3-3.5 billion years ago and it was well documented along with banded iron formation. It was believed that the oxygen was produced from water as result of photosynthesis by unicellular organisms. Our earth's atmosphere constitutes about 21 % molecular oxygen and which recycled through photosynthesis and respiration. While talking about oxygen cycle and photosynthesis, the world ocean has an important role. Recent geological time the atmospheric oxygen concentration was remarkably constant. The amount of oxygen present in the atmosphere is $3x10^{19}$ mole, and is large while comparing with oxidized and reducing carbon. The combustion of all reduced carbon would cause a reduction of atmospheric oxygen concentration only by 2-3 % (Broecker 1970). A small variation in the atmospheric oxygen can be expected due to the

seasonal variation in the oxidation reduction processes, and the concentration of atmospheric oxygen increases as result of fossil fuel burning, thus equivalent amount of oxygen concentration reduction can be expected. In the ocean oxygen is simply dissolve which is proportional to the partial pressure of atmospheric oxygen, thus any small change in the atmospheric oxygen concentration will be taken care of dissolved oxygen in the oxygen.

Photosynthetic oxygen and isotopic faction due to different oxygen consumption processes and the oxygen isotope exchange control isotopic composition of atmospheric oxygen during the process of ozone cycle (Luz et al. 1999: Bender 2000). The oxygen isotopic composition was higher than that of average seawater and the value is 23.8 ‰ is called dole effect (Dole 1936). A detail of this was explained in the previous section.

1.7 Mass independent oxygen isotope fractionation

Thiemens & Heidenreich 1983 (Thiemens and Heidenreich 1983) discovered the first chemically produced mass independent isotope fractionation. This discovery initiated a wide application to understand physical chemistry, atmospheric chemistry, paleoclimate, biological oxygen productivity and solar system origin and evolution. It was shown that the production of ozone from molecular oxygen, the product isotope ^{17}O and ^{18}O was equally fractionated rather than terrestrial mass dependent fractionation of 0.5. Mauersberger 1981 (Mauersberger 1981) measured isotopic composition of stratospheric ozone and reported 400 % enrichment in ^{18}O. Later (Mauersberger 1987) measured ^{17}O of stratospheric ozone and confirmed the mass independent fractionation, which was then further confirmed by the ground based FTIR measurement (Schueler et al. 1990). This isotopic signature of ozone was then transferred to other molecules like sulphate, nitrate and carbon dioxide.

The source of mass independent oxygen isotopic fraction in the atmospheric oxygen is the isotope exchange associated with the ozone formation and dissociation in stratosphere. Ozone is an inorganic molecule having tri-atomic oxygen with molecular formula O_3. Its boiling point is -112 °C, ozone is a bend molecule having a bond angle of 116.78° and O-O bond length is 1.272Å, the molecular symmetry C_{2V}. It is allotrope of oxygen having distinctively pungent smell, it is less stable than oxygen. Ozone is formed after the interaction of ultra-violate rays with oxygen. The concentration of ozone in the atmosphere is 10ppb, the 90 % ozone resides in the stratosphere between a depths at 10-17 km above the earth's surface

and extend up to about 50 km. remaining ozone is in the lower region of the atmosphere called troposphere, which is called ozone layer. Ozone in the lower atmosphere is associated with smog and it is produced by pollution. Stratospheric have an important role in the existence of life in the earth, thus it plays a beneficial role in the atmosphere by absorbing ultra-violet radiation. Absorption of UV rays by ozone creates heat, thus creating hot region in the upper atmosphere, which is opposite to the general behavior of atmosphere, which is decrease of temperature by increase in altitude.

The production of ozone in the stratosphere is when ultra-violet radiation reacts oxygen molecule, this process is called chapman cycle, and is produced through the following steps (Chapman 1930; Lammerzahl et al. 2002)

Oxygen molecule pyrolysed by solar energy

$$h\nu + O_2 \rightarrow 2O^{\cdot}$$

This oxygen radicle reacts with another oxygen molecule

$$O^{\cdot} + O_2 \rightarrow O3$$

Ozone can then reacts with another oxygen radicle to produce O_2

$$O_3 + O^{\cdot} \rightarrow 2O_2$$

Ozone can then react with photon to produce O_2

$$O_3 + h\nu \rightarrow O_2 + O^{\cdot}$$

It is very clear that in stratosphere the ozone is getting created and destroyed by ultraviolet radiation. This is a natural process that has been taking place for millions of years. In the atmosphere oxygen is continuously produced by photosynthesis, thus oxygen layer has the capability of regenerating itself.

Ozone in the earth's surface is toxic to human and other living organisms, because ozone is very reactive and it can oxidize the living tissues. Which also have bad effects with crop production, forest growth. The atmospheric ozone depletion was a global concern, which is more severe in Antarctic region. A study conducted during 1980 to 1984 at Antarctica's Halley Bay shows an ozone depletion of about 30% in the Antarctic spring season (Solomon et al. 1986). It was difficult to explain this ozone depletion in the Antarctic area during spring. A unique feature of Antarctic lower stratosphere is high frequency stratospheric cloud,

providing a substrate for the heterogeneous reaction. A heterogeneous reaction between HCl and $ClONO_2$ was explained as possible reason for this observation (Solomon et al. 1986).

The depletion of ozone is associated with chlorofluorocarbons, which is containing chlorine, fluorine and carbon. This compound is extremely stable and thus which can cross troposphere into stratosphere. This long lifetime allows the molecule to interact with high-energy radiation in the upper atmosphere, which leads to breakdown of CFC molecule to produce chlorine. This chlorine acts as a catalyst to destroy so much of oxygen, this chlorine initiate the breakdown of ozone and combine with a free oxygen to produce an oxygen molecule. After each cycle the chlorine gets regenerated and undergo a new cycle, a single chlorine molecule can destroy thousands of ozone molecules (Molina and Rowland 1974; Solomon et al. 1986; Molina and Molina 1987).

$$Cl + O_3 \rightarrow ClO + O_2$$

$$ClO + O. \rightarrow Cl + O_2$$

$$O_3 + O. \rightarrow 2O_2$$

This interaction of oxygen and ozone with ultraviolet radiation is very fast and it produces a mass independent isotopic fractionation. Since the discovery of mass independent oxygen isotopic fraction in the meteorites (Clayton et al. 1973) and laboratory in 1983 (Thiemens and Heidenreich 1983), it has been subjected to numerous studies to explain the phenomenon. Thiemens and Heidenreich ascribed self-shielding as the mechanism responsible for the observed mass independent fractionation in the atmospheric oxygen during the formation of ozone. However this mechanism was useful only to explain laboratory finding according to theoretical consideration (Navon and Wasserburg 1985). The rate isotopic exchange exceeds that of ozone formation and thus original isotopic anomaly is removed by mass dependent isotope exchange before it may be sequestered in a stable molecular product. In 1986 Thiemens and Heidenreich proposed role of molecular symmetry in the formation as a mediating factor in fractionating the isotopes in a mass independent manner. The governing factor was the lifetime of the excited state O_3* molecule, immediately formed during oxygen atom molecule collision is an enhanced asymmetric species with respect to the symmetric one.

This enhanced lifetime arises owing the doubling of the asymmetric states with respect to symmetric state.

Harthorn and Marcus (1999) developed an intra-molecular theory of mass independent isotope fraction in ozone (Hathorn and Marcus 1999; Hathorn and Marcus 2000). This theory explains the trace amount of ^{17}O or ^{18}O an isotope denoted by Q, that can form an asymmetric molecule QOO in addition to symmetric one OQO, whereas ^{16}O with $^{32}O_2$ can only for symmetric a symmetric species OOO. There are several issues to be answered regarding the isotopic fractionation of ozone in the stratosphere like why symmetric isotopomer also enhanced, difference between the isotope enhancement in laboratory experiment and stratosphere and also the influence of ambient pressure.

This mass independent fractionation of oxygen partially transferred to carbon dioxide in the middle atmosphere.

$$O+O_2 + M \rightarrow O_3^* + M$$

$$O_3^* + M \rightarrow O_3 + M^*$$

$$O_3 + h\nu \rightarrow O. + O_2$$

$$O. + CO_2 \rightarrow CO_3^* \rightarrow O. + CO_2$$

$$O. + CO_2 \rightarrow CO_3^* \rightarrow O. + CO_2$$

The observed three isotopes slope of stratospheric CO_2 ranges from 1.2 to 1.7, much higher than for O_3. As a result, oxygen become anomalously depleted and CO_2 will enriched in terms of oxygen isotope ratios. There is no stratospheric loss term for the enrichment in the CO_2, net stratospheric enrichment lost are lost only at the earth's surface by isotope exchange with liquid water in the leaves and in the ocean (Farquhar et al. 1993; Yung et al. 1997). In contrast oxygen does not exchange isotope with water, and depletion disappears only through the consumption of O_2 by respiration and its replacement by photosynthesis. This respiratory and photosynthetic fluxes are small compared with stratospheric fractionation, thus the anomaly in the oxygen isotope accumulates to a measurable level relative to atmospheric oxygen (Luz et al. 1999).

As a result of these cycle the atmospheric oxygen has a signature of mass independent isotopic fraction during the formation of ozone. This phenomenon was then applied for the

determination of global oxygen production (Luz et al. 1999) and then it was revised for the marine oxygen gross production (Luz and Barkan 2000).

1.8 Assessing gross production with the triple oxygen isotope method

Gross/net oxygen production in ocean water was estimating using traditional methods like studying in situ changes of dissolved oxygen (Emerson 1987), in vitro O_2 incubations in light/dark bottles (Robinson et al. 2002), In vitro O_2 incubations with $H_2{}^{18}O$ (Grande et al. 1989), ^{14}C incubation (Steemann Nielsen, 1952; Grande et al. 1989), and chlorophyll measurements, O_2/Ar methods (Craig and Hayward 1987). Another in situ method was derived for the measurement of determination of gross productivity using mass independent fractionation factor in the dissolved oxygen triple isotope ratios (Luz et al. 1999; Luz and Barkan 2000). This method has unique advantages over the traditional methods and also it has disadvantages associated with its mass balance calculations. The method relayed on both dissolved oxygen isotope ratio measurement and the estimation of piston velocity using wind speed. The calculation of piston velocity from wind speed was associated with an error about 30 %. Before explaining the method, I need to discuss the basic principle behind this method.

As explain earlier the oxygen in the atmosphere was depleted ^{17}O while comparing with meteoric water fraction and biologically produced has an excess of ^{17}O while comparing with atmospheric oxygen. This ^{17}O excess was denoted as $\Delta^{17}O$. This phenomenon was then applied for the determination of global oxygen production (Luz et al. 1999) and then it was revised for the marine oxygen gross production (Luz and Barkan 2000). There are several definitions used for the denoting this ^{17}O excess in the atmosphere, which has been compiled by Kaiser according to mathematical importance (Kaiser 2011).

$$\Delta^{17}O = \delta^{17}O - \lambda\delta^{18}O \quad \text{(Thiemens et al. 1995)}$$

$$\Delta^{17}O = 1 + \delta^{17}O - (1 + \delta^{18}O)^{\lambda} \quad \text{(Farquhar et al. 1998)}$$

$$\Delta^{17}O = 1 + \delta^{17}O / (1 + \delta^{18}O)^{\lambda} - 1 \quad \text{(Miller 2002)}$$

$$\Delta^{17}O = \ln(1 + \delta^{17}O) - \lambda(1 + \delta^{18}O) \quad \text{(Angert et al. 2003)}$$

The coefficient λ was chosen by different authors to ensure that $\Delta^{17}O$ has certain desired mathematical proportion. I used the value of λ as 0.518 for the further calculation of $\Delta^{17}O$ in the whole study according to some latest literature. (Luz and Barkan 2009; Stanley et al. 2009).

In order to derive the quantitative estimate of gross oxygen production in the ocean Luz considered oxygen isotope mass balance in the oceanic mixed layer at steady state with respect to oxygen concentration and $\Delta^{17}O$, and vertical and horizontal mixing with deep water was neglected. According to theory, in the absence of biological action $\Delta^{17}O$ of dissolved oxygen will be close to equilibrium value that is it will be approximately equal to $\Delta^{17}O_{equ}$. $\Delta^{17}O$ balance in the mixed layer is given by

$$I\,\Delta^{17}O_{eq} + GP\,\Delta^{17}O_{max} = E\,\Delta^{17}O_{dis} + R\,\Delta^{17}O_{dis}$$

Where I and E are the rate of atmospheric O_2 invasion and evasion, GP is the gross oxygen production and R is total oxygen consumption. A detailed derivation of the equation as follows,

$$\frac{dO_2}{dt} = P + G_{in} - C - G_{gout}$$

$$\frac{d\left[\left(\frac{^{18}O}{^{16}O}\right)_d O_2\right]}{dt} = \left(\frac{^{18}O}{^{16}O}\right)_{max} P + \left(\frac{^{18}O}{^{16}O}\right)_a \propto^{18}_{gin} G_{gin} - \left(\frac{^{18}O}{^{16}O}\right)_d (\propto^{18}_{C} C - \propto^{18}_{gout} G_{gout})$$

$$\frac{d\left[\left(\frac{^{17}O}{^{16}O}\right)_d O_2\right]}{dt} = \left(\frac{^{17}O}{^{16}O}\right)_{max} P + \left(\frac{^{17}O}{^{16}O}\right)_a \propto^{17}_{gin} G_{gin} - \left(\frac{^{17}O}{^{16}O}\right)_d (\propto^{17}_{C} C - \propto^{17}_{gout} G_{gout}$$

As I considered the left hand side of the above equation will be zero

$$\left(\frac{^{18}O}{^{16}O}\right)_d \left(\propto_C^{18} C - \propto_{gout}^{18} G_{gout}\right) = \left(\frac{^{18}O}{^{16}O}\right)_{max} P + \left(\frac{^{18}O}{^{16}O}\right)_a \left(\propto_{gin}^{18} G_{gin}\right) \quad (2)$$

$$\left(\frac{^{17}O}{^{16}O}\right)_d \left(\propto_C^{17} C - \propto_{gout}^{17} G_{gout}\right) = \left(\frac{^{17}O}{^{16}O}\right)_{max} P + \left(\frac{^{17}O}{^{16}O}\right)_a \left(\propto_{gin}^{17} G_{gin}\right) \quad (3)$$

$$P + G_{in} = C + G_{gout} \quad (1)$$

(1)- (2)

$$P - \left(\frac{^{18}O}{^{16}O}\right)_{max} P + G_{in} - \left(\frac{^{18}O}{^{16}O}\right)_d \left(\propto_{gin}^{18} G_{gin}\right)$$

$$= C - \left(\frac{^{18}O}{^{16}O}\right)_d \left(\propto_C^{18} C - \propto_{gout}^{18} G_{gout}\right) + G_{gout}$$

$$P\left(1 - \left(\frac{^{18}O}{^{16}O}\right)_{max}\right) + G_{in}\left(1 - \left(\frac{^{18}O}{^{16}O}\right)_a \propto_{gin}^{18}\right) = C\left(1 - \left(\frac{^{18}O}{^{16}O}\right)_d \propto_C^{18}\right) +$$

$$G_{gout}\left(1 - \left(\frac{^{18}O}{^{16}O}\right)_d\right) \propto_{gout}^{18} \quad (4)$$

Similarly (1)-(3) is

$$P\left(1 - \left(\frac{^{17}O}{^{16}O}\right)_{max}\right) + G_{in}\left(1 - \left(\frac{^{17}O}{^{16}O}\right)_a \propto_{gin}^{17}\right) = C\left(1 - \left(\frac{^{17}O}{^{16}O}\right)_d \propto_C^{17}\right) +$$

$$G_{gout}\left(1 - \left(\frac{^{17}O}{^{16}O}\right)_d\right) \propto_{gout}^{17} \quad (5)$$

$$(1 - AB) \cong (1 - A) + (1 - B)$$

And substitute $(1-\propto) = \varepsilon$

$$P(\delta^{18}O)_{max} + G_{in}(\delta^{18}O)_{in} + G\varepsilon_{gin}^{18} = C(\delta^{18}O)_d + C\varepsilon_c^{18} + G_{out}(\delta^{18}O)_d +$$

$$G_{out}\varepsilon_{gout}^{18} \quad (6)$$

$$P(\delta^{17}O)_{max} + G_{in}(\delta^{17}O)_{in} + G\varepsilon^{17}_{gin} = C(\delta^{17}O)_d + C\varepsilon^{17}_c + G_{out}(\delta^{17}O)_d + G_{out}\varepsilon^{17}_{gout} \quad (7)$$

While representing all the δ values with respect to atmospheric air $(\delta^{18}O)_{in}$ and $(\delta^{17}O)_{in}$ will become zero

(7)-0.521(6)

$$P\left(\delta^{17}O - 0.521\delta^{18}O\right)_{max} + G_{in}\left(\varepsilon^{17}_{gin} - 0.521\varepsilon^{18}_{gin}\right) = C\left(\delta^{17}O - 0.521\delta^{18}O\right)_d + C\left(\varepsilon^{17}_c - 0.521\varepsilon^{18}_c\right) + G_{out}\left(\delta^{17}O - 0.521\delta^{18}O\right)_d + G_{out}\left(\varepsilon^{17}_{gout} - 0.521\varepsilon^{18}_{gout}\right)$$

$$P\Delta_{max} + G_{in}\left(\varepsilon^{17}_{gin} - 0.521\varepsilon^{18}_{gin}\right) = C\Delta_d + G_{out}\Delta_{diss} + C\left(\varepsilon^{17}_c - 0.521\varepsilon^{18}_c\right) + G_{out}\left(\varepsilon^{17}_{gout} - 0.521\varepsilon^{18}_{gout}\right)$$

Since consumption and gas out are mass dependent processes. A small fractionation occurs during invasion, Δ_{eq}

$$\left(\varepsilon^{17}_c - 0.521\varepsilon^{18}_c\right) = 0$$

$$\left(\varepsilon^{17}_{gout} - 0.521\varepsilon^{18}_{gout}\right) = 0$$

$$\left(\varepsilon^{17}_{gin} - 0.521\varepsilon^{18}_{gin}\right) = \Delta_{eq}$$

$$P\Delta_{max} + G_{in}\Delta_{eq} = C\Delta_d + G_{out}\Delta_d \quad (8)$$

$$P\Delta_{max} + G_{in}\Delta_{eq} = (C + G_{out})\Delta_d \quad (9)$$

Substitute

$G_{in} + P = C + G_{out}$ (Mass balance) from equation (1) and $G_{in} = KC_o$

$$G_{in}\left(\Delta_{eq} - \Delta_d\right) + P(\Delta_{max} - \Delta_d) = 0$$

$$P = KC_o\left(\Delta_d - \Delta_{eq}\right)/(\Delta_{max} - \Delta_d)$$

Here P = Gross oxygen production,

K= Piston velocity,

C_0= Equilibrium O_2 concentration.

The ratio of net and gross production also can be calculated using oxygen isotope anomaly (Hendricks et al. 2004), the advantage of this method is that, its calculation excludes gas exchange coefficient. The equation can be derived as

$$h\frac{dC}{dt} = G - R + K(C_0 - C)$$

$$\delta^*_{dis}O = \frac{\left(\frac{G}{kC_0}\right)(\delta^*_w O + 1) + (\delta^*_{sat}O + 1)}{\left(\frac{G}{kC_0}\right) + 1 - \left(\left(\frac{G}{kC_0}\right) + 1 - \left(\frac{C}{C_0}\right)\right)(1 - \alpha^*_R)} - 1$$

$$\delta^*_{dis}O = \frac{\left(\frac{C}{C_0}-1\right)(\delta^*_w O+1)+\left(\frac{N}{G}\right)(\delta^*_0 O+1)}{\left(\frac{C}{C_0}\right)-1+\left(\frac{N}{G}\right)-\left(1-\left(\frac{N}{G}\right)\right)\left(\left(\frac{C}{C_0}\right)-1\right)(1-\alpha^*_R)} - 1 \qquad (10)$$

$$N = kC_0\left(\frac{C}{C_0} - 1\right)$$

$$\frac{G}{kC_{sat}} = \frac{\Delta^{17}O_0 - \Delta^{17}O_{dis}}{\Delta^{17}O_{dis} - \Delta^{17}O_W}$$

$$N/G \approx \left(\frac{C}{C_0} - 1\right)\frac{\Delta^{17}O_{dis} - \Delta^{17}O_W}{\Delta^{17}O_0 - \Delta^{17}O_{dis}}$$

Using above explained mass balance of dissolved oxygen isotope ratios in ocean, it very simple to estimate gross oxygen production in the ocean. Another use of this calculation is to determine α_R for mixed layer, where oxygen production and respiration takes place simultaneously. The equation (10) can be used for the calculation of oxygen isotope

fractionation during the marine respiration for mixed layer by rearranging it for α_R. The estimation of variability of photosynthetic production of oxygen in ocean is important to understand global carbon and oxygen cycles and ultimately carbon fixing and responds to future climate forcing. Initially scientists were using in vitro determination methods like ^{14}C labeled incubation, ^{18}O incubation, dissolved oxygen methods has very large uncertainty. There are many studies compared in vitro and in situ estimates of marine production indicate that marine productivity are underestimated by bottle rate approaches (Karl et al. 2003; Williams et al. 2004: Juranek and Quay 2005).

1.9 Calculation of ^{18}O isotope fractionation during respiration by marine organisms in the mixed layer

Triple oxygen isotope ratio method can be used to determine respiratory oxygen isotope fraction in the mixed layer, where oxygen production and utilization coexists. The equation below can be used for the calculation of α_R using the measured triple oxygen isotope ratios.

$$\delta^*_{\mathrm{dis}}\mathrm{O} = \frac{\left(\frac{\mathrm{C}}{C_0} - 1\right)(\delta^*_{\mathrm{w}}\mathrm{O} + 1) + \left(\frac{\mathrm{N}}{\mathrm{G}}\right)(\delta^*_0\mathrm{O} + 1)}{\left(\frac{\mathrm{C}}{\mathrm{C}_0}\right) - 1 + \left(\frac{\mathrm{N}}{\mathrm{G}}\right) - \left(1 - \left(\frac{\mathrm{N}}{\mathrm{G}}\right)\right)\left(\left(\frac{\mathrm{C}}{\mathrm{C}_0}\right) - 1\right)(1 - \alpha^*_{\mathrm{R}})} - 1$$

Where C_0= Equilibrium O_2 concentration

C= O_2 concentration

$$N/G \approx \left(\frac{\mathrm{C}}{\mathrm{C}_0} - 1\right)\frac{\Delta^{17}\mathrm{O}_{\mathrm{dis}} - \Delta^{17}\mathrm{O}_{\mathrm{W}}}{\Delta^{17}\mathrm{O}_0 - \Delta^{17}\mathrm{O}_{\mathrm{dis}}}$$

$\delta_0{}^*O$ = Equilibrium δ^*O of dissolved oxygen (calculated from temperature)

$\delta_w{}^*O$= isotope ratio of photosynthetic O_2

$\delta_w{}^*O$ = measured isotope ratio of dissolved oxygen

1.10 The dissolved oxygen isotope anomaly at equilibrium with atmosphere ($\Delta^{17}O_{eq}$)

The value of piston velocity can be calculated from the wind speed according to (Wanninkhof 1992). As production over residence time of oxygen in the mixed layer is about

10 to 30 days depending on wind speed, thus we generally use 10 days averaged wind speed for the estimation of gas exchange coefficient. The equilibrium oxygen concentration (C_0) can be calculated from temperature and salinity of seawater. The $\Delta^{17}O_{max}$ is maximum Δ^{17}O due to photosynthesis and $\Delta^{17}O_{eq}$ is the equilibrium isotope effect, caused by small change in the value of λ because of the different oxygen isotope fraction during different processes of respiration as explained later. The value of Δ^{17}Oeq is supposed to be zero according to definition, however Luz and Barkan 2000 determined this value as 16 ± 2 per meg. This was determined by air water equilibration in less than 24 hrs. By bubbling outside air into seawater at 25 °C In the later works the value of $\Delta^{17}O_{eq}$ is competing field among the researchers and which varies widely among different papers.

Table 1: Triple oxygen isotopic composition of dissolved oxygen in equilibrium with atmospheric air at 25°C. Uncertainties are indicated as ±1 standard error. Equilibration was carried out by stirring and bubbling for deionized water and seawater. In the table equilibration by bubbling shows large $\Delta^{17}O_{eq}$ than stirred ones.

Samples	Equilibration method	Temp. (°C)	n	δ^{17}O (‰)	δ^{18}O (‰)	$\Delta^{17}O_{eq}$ (per meg)
Deionized water						
Sarma et al. 2003	Bubbling	22	10	0.371	0.691	13 ± 5
Barkan and Luz 2003	Bubbling	25	7	0.390	0.720	17 ± 1
Sarma et al. 2006	Bubbling	24	10	0.390	0.717	18 ± 2
Stanley et al. 2010	Stirring	21	16	0.383	(0.722)	9 ± 2
Juranek and Quay 2005	Stirring	21	4	0.391	0.722	17 ± 3
Seawater						
Luz and Barkan 2000	Bubbling	25	N/A	0.382	(0.703)	18 ± 2
Reuer et al. 2007	Stirring	24.8	14	0.340	0.642	8 ± 3
Luz and Barkan 2009	Bubbling	25	5	0.391	0.722	17 ± 2

More recently, Luz and Barkan 2009 (Luz and Barkan 2009) reported a linear relationship between equilibration temperature and Δ^{17}Oeq.

$$\Delta^{17}O_{eq} = 0.5871\ t - 1.798$$

Where t is the temperature of equilibration system in degree Celsius. I have checked the value of $\Delta^{17}O_{eq}$ by bubbling and stirring for distilled and sea water at different temperature.

The Δ^{17}Omax is the maximum Δ^{17}O can be produced by photosynthesis only, and the value was estimated as 249 per meg in a terrarium experiment (Luz and Barkan 2000). Uncertainties of this method sharply increase when Δ^{17}O of dissolved oxygen in the water approaches $\Delta^{17}O_{max}$. Another source of error in this method is because of uncertainties associated with estimation of piston velocity from wind speed (Wanninkhof 1992; Nightingale et al. 2000; Sweeney et al. 2007; Bender et al. 2011).

This advanced method has wide application for the determination gross oxygen production, basin wide production measurement, better calculation of gas exchange coefficient and the method can be used for the determination of gross production by collection water samples underway of commercial ships (Angert et al. 2003; Sarma and Abe 2006; Sarma et al. 2006; Luz and Barkan 2009; Sarma et al. 2010; Stanley et al. 2010). A more generalized derivation of mass balance equation was made by Kaiser (Kaiser 2011).

1.11 The oxygen-argon ratio: its biological and physical significances

The atmospheric concentration of oxygen and argon is 20.946 % and 0.9340 % respectively. Oxygen concentration in the water is depends on biological physical processes, the physical processes include bubble injection, heat, water mixing and fresh water flux. However the argon concentration has no effect on biological processes. The saturation concentration of oxygen and argon can be calculated from salinity and temperature according to (Benson et al. 1979) and (Hamme and Emerson 2004). Argon in the ocean has similar properties like oxygen, thus argon can then use as a tracer of physical behavior of oxygen (Craig and Hayward 1987). However the solubility of nitrogen distinctly different from the oxygen, thus making it as a weaker choice as a physical parameter tracer. Argon saturation derives the contribution of air injection, which can be used to determine the net photosynthetic oxygen. Under steady state

condition the gas exchange balances production and respiration under negligible lateral mixing and vertical diffusion. A change of argon concentration in seawater depends on temperature change diffusive and bubble mediated gas exchange (Hamme and Emerson 2002). Thus the excess of oxygen in the seawater while comparing with argon is due to the production of O_2 by photosynthesis.

$$\Delta\,(O_2/Ar) = \left(\frac{C(O_2)}{C(Ar)}\right) / \left(\frac{C_{sat}(O_2)}{C_{sat}(Ar)}\right) - 1$$

This is also known as biological oxygen supersaturation, the denominator of this equation is simply a function of temperature and salinity. It is defined as the oxygen supersaturation in excess of argon supersaturation that is equal to biological oxygen saturation minus one (Hendricks et al. 2004). The oxygen to argon ratios in the ocean can be used to calculate biological oxygen saturation anomaly with respect to saturation concentration. F_{bio} is defining as the biological oxygen flux, the part of oxygen air sea gas exchange that is caused by biological activity (Kaiser et al. 2005).

A combination of triple oxygen isotope ratios and oxygen–argon ratios together can be used to determine both gross and net productivity in the study area. This combination can also give additional information like respiration rate. The calculation of G, R and N is valuable in terms of comparison with other methods is necessary to calculate CO_2 balance of the area (Quay et al. 2010; Robinson et al. 2009). The largest uncertainty associated with this method is the calculation gas exchange coefficient from with speed having an error of 30 % (Quay et al. 2010).

1.12 Noble gas supersaturation and water mass mixing

Distribution of dissolved gases in the ocean can give good information about physical and biological oceanic processes that play an important role in the global climate system. The studies on noble gas saturation was used to quantify air sea exchange, diaphycnal mixing and heat flux in the ocean (Gehrie et al. 2006; Ito and Deutsch 2006; Ito et al. 2007; Stanley et al. 2009; Ito et al. 2011; Emerson et al. 2012). It is important to study marine component of biogeochemical cycle of any gas including CO_2, Oxygen, nitrogen and noble gases one must be able to correctly quantify the air-sea gas exchange. In order to run the global climatic model it is necessary to determine the accurate air sea gas exchange. Studies on bubble dynamics in

the ocean have an important role to understand the noble gas supersaturation in ocean. One approach that has been used with success is to separate bubble flux into two component, fist component where bubble dissolve completely and thus inject gas with atmospheric abundance and other component where bubbles dissolves partially before emerging it to the surface and thus fractionate the gas.

Noble gases makes ideal for the determination of gas exchange because of its unique character is that, they are chemically and biologically in the ocean. Noble gas studies in ocean have been widely used to determine gas exchange processes and bubble injection (Emerson et al. 1995; Battle et al. 2003; Stanley et al. 2009). Another important parameter is significance of argon supersaturation in the ocean. Argon supersaturation in ocean is a measure in percent difference of gas concentration from the saturation value. Argon solubility in the seawater is a function temperature and salinity, which possess disequilibrium in the surface and interior. So that the saturated argon concentration (Ar_{sat}) is grater in the cold and fresh water than warm salty water. Solubility of argon is a function of temperature and salinity of seawater, it varies by 50 % over full range ocean temperature and 3 % over salinity variation (Hamme and Emerson 2004). The saturation state of argon is commonly expressed as

$$\Delta Ar = \delta Ar / Ar_{sat}$$

Where δAr is the difference between measured and saturated argon concentrations (δ Ar = [Ar] – $[A]_{sat}$). supersaturation and undersaturations were represented by positive and negative values respectively for both ΔAr and δAr. A nonlinear temperature dependency of argon solubility can also produce an argon supersaturation during water mass mixing, because of the mixing process of saturated water parcel effect linearly for both temperature and argon concentration as illustrated in the figure 1. Under normal conditions the oceanic argon concentrations were observed within few percent of their saturated values indicating that the temperature dependencies of argon solubility exert the primary influence on the oceanic argon distribution.

In the surface ocean mixed layer, the heat and argon content can be changed through interaction with the atmosphere. Since the solubility of argon in the ocean is a decreasing function of temperature, thus heating or cooling of a water parcel alter its argon content. Heating or cooling of a parcel of water can decrease or increase the saturation concentration of argon (Ar_{sat}) to produce a supersaturation (positive values for ΔAr) or undersaturation (negative values for ΔAr) respectively. In the absence of heating and cooling, argon can also be

transferred from atmosphere to ocean by bubble injection processes. Bubbles are produced in the ocean surface as a result of gentle breaking of surface waves, these bubbles can dissolves partially or fully under hydrostatic pressure excreted by the water column. This process can also increase the transfer of gases into the seawater, and this can created supersaturation of argon (Keeling 1993). Changes in the atmospheric pressure also can alter the value of argon anomaly. In contrast to argon concentration, the saturation state of δAr is not a conservative tracer in the interior ocean owing the nonlinear temperature dependence of argon solubility (Bieri et al. 1966). Mixing of saturated water parcel that affect both temperature and argon linearly will have an argon concentration that is supersaturated with respect to the temperature of the mixture. Because of the mixing of water parcel with different temperature rises the saturation state of argon, thus δAr can be used as a potential tracer of ocean mixing that occurs across isotherms.

Ito and Deutsch 2006 modelled the argon anomaly using one dimensional box model and then extended to three-dimensional GCM. That modelling study was considered the argon concentration before water mixing and surface water argon saturation is a function heat flux and gas exchange coefficient, for thermocline the model was considered water mixing with mixed layer, which is a bidirectional water mass fluxes were included to represent the mixing between warm surface and thermocline waters and Ekman ventilation at mid latitudes. And another important parameter is the meridional overturning, which ventilates the deep ocean from high latitudes and upwells into low latitude Surface Ocean through the thermocline, the model predicts the following points,

In the low latitude surface water is supersaturated with argon owing to local net heating, whereas undersaturation prevails at middle and high latitudes due to net heat loss. The stronger heat transport increase the surface ΔAr disequilibrium, whereas faster gas exchange brings surface water toward saturation (Ito and Deutsch 2006).

In the middle and high latitude the value of ΔAr at surface mixed layer will be negative because of net heat loss and is a decreasing function toward the water mixing ratios (Ito and Deutsch 2006).

In the thermocline the given Ar concentration, the mixing and performed components of ΔAr can be separately determined, provided the end member values for T and Ar are known.

$$\frac{D\delta Ar}{Dt} \approx \left(\frac{\partial^2 Ar\ sat}{\partial T^2}\right) k \left(\frac{\partial T}{\partial Z}\right)^2$$

$$\frac{D}{Dt} = \frac{\partial}{\partial t} + u_{res}.\nabla$$

Under typical ocean conditions, k = 10^{-5} m^2s^{-1} and $\frac{\partial T}{\partial Z}$ = 0.05 deg/m in the subtropical thermocline, modelling studies predicts an increase of argon saturation at a rates of 0.1 % per year, thus a decadal accumulation of ΔAr can be easily measured using present analytical methods (Ito and Deutsch 2006). In this article I were mainly focusing on the distribution of oxygen isotopes and argon saturation in the North Pacific Ocean, and results will be discussing on the basis of water mass formation and mixing. The modeled results predict a maximum argon supersaturation at low latitude thermocline was about +3.5 %, which decreases with depth, and below 450mthe ΔAr become zero and in the deep water the model predicts a ΔAr between -1 to -2 %. The distribution of δAr at KNOT, BATS and HOT stations were found to be negative with strong undersaturation in deep water and ventilated thermocline (Hamme and Emerson 2002). The deep water was formed through the sinking of surface water at polar region and thus causing the deep water was undersaturated with argon concentration.

The rate of mixing across density surface in the ocean thermocline is associated with the intensity of ocean overturning, and limits the supply of nutrients to the euphotic zone necessary to sustain ocean productivity.

The figure 1 illustrate the temperature dependency of argon solubility and effect of mixing of two equilibrated water parcels having different temperature mixing causes a supersaturation in the argon concentration. For example, predicted supersaturation of water masses mixing between end members of 30 °C and 0 °C, the maximum ΔAr would be about 8.5 %. However the measured argon saturation in the ocean was ranging between 3 to -2.5 in the thermocline of equatorial region and HOT station respectively (Gehrie et al. 2006). In this work I will be examining the mixing of Okhotsk seawater with Oyashio and Kuroshio water to form north pacific intermediate water and argon supersaturation associated with this phenomenon.

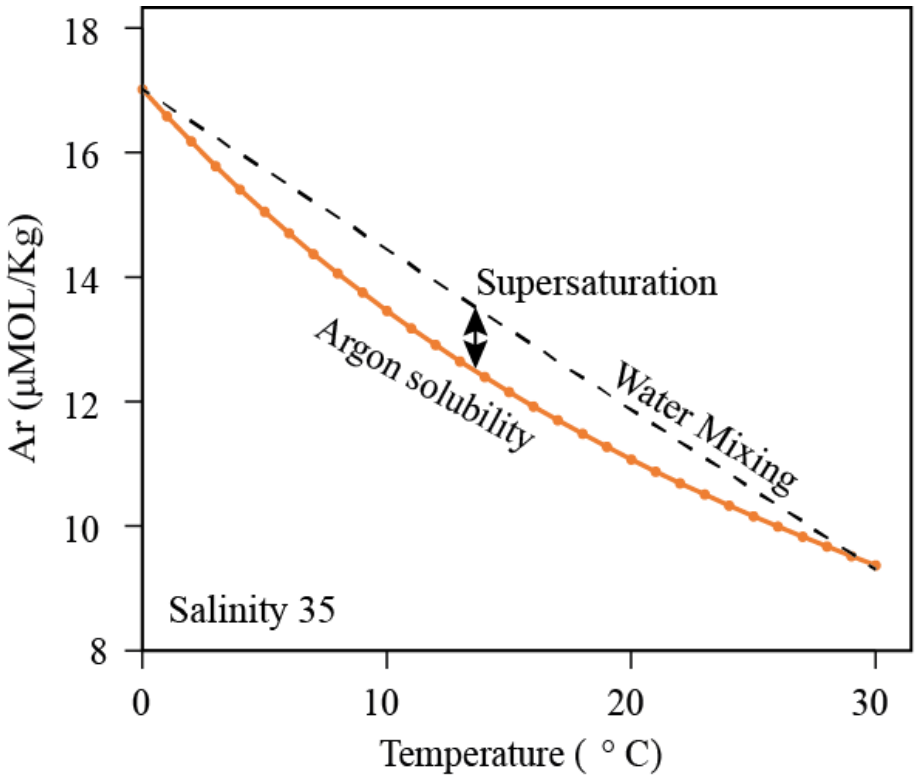

Figure 1: The figure 1 illustrate the temperature dependency of argon solubility and effect of mixing of two equilibrated water parcels having different temperature mixing causes a super-saturation in the argon concentration. The figure shows theoretical example when water masses mixing between end members of 30 °C and 0 °C, the maximum ΔAr would be about 8.5 %.

Chapter 2

Material and method

2.1 Study area: the northwest Pacific Ocean

Pacific Ocean is the largest of all ocean, it extent from Arctic Ocean to southern ocean. It covers 46 % of earth's water surface and an area of 165.25 million square kilometer. The volume of Pacific Ocean represents about 50.1 % of world ocean water, and is about 714 million cubic kilometer. The surface water temperature was varied from 30 to -1.4 °C at equator and polar region respectively. The maximum salinity of 37 was observed at southeastern area and minimum salinity was at the equator because of the high precipitation throughout the year. The motion of surface water in the northern hemisphere is clockwise direction, whereas in the southern hemispheres it is counter clockwise direction because of combined effect of coriolis force and wind stress. North equatorial current driven westward along 15 °N turn north near Philippines to become the warm Kuroshio Current. Which is then turn eastward around 45 °N known as kuroshio extension, which is then move southward to rejoin the north equatorial current.

In the study area there are several currents and water masses in having particular characters and unique properties. The important water masses circulation and currents are the north equatorial current, equatorial counter current, California current, Kuroshio current, Kuroshio extension, north pacific current, Oyashio current, subarctic current, Alaska gyre, north pacific intermediate water NPIW, north pacific mode water and oxygen minimum zone.

Water in motion is called a current, the direction toward which it moves is called set and its speed is known as drift. Currents are broadly divided to two classes, surface wind driven Ekman transport and density driven thermohaline circulation. Stress of wind blowing across the sea cause surface water to move, due to the low viscosity of water, this stress is not directly communicated to the ocean interior, balance by coriolis within a thin layer of surface water usually about 10 to 200 m thick. This layer is called Ekman layer and transportation is called Ekman transport. Because of the deflection by the coriolis force the Ekman transportation is not in the direction of wind, but it deflect 90° to the right angle in the northern hemisphere and 90° to the left in the southern hemisphere. The density of the water mainly drives Thermohaline circulation, which is associated with the salinity, temperature and pressure. These are produced

sinking of cold brine dense water at poles (Norwegian Sea and southern ocean) as result of sea ice formation. This water sinks deep into the ocean and triggers largest ocean circulation.

Equatorial Pacific Ocean has a unique characters in the ocean circulation, is equatorial water mass that extends over the entire Pacific Ocean from east to west. This equatorial water mass has its greatest wide spread along American cost, where it is present between 18 °S to 20 °N. Towards west it appears to be narrower towards west. The surface layer temperature is nearly constant to a depth that varies from as little as 10 or 15mup to nearly 100 m. the depth of thermocline is very small in the eastern side of pacific ocean, where sharp decrease of thermocline encountered at depths mostly less than 50 m. towards west the depth to the thermocline increases on western side of pacific ocean the minimum depths are between 150 and 200 m. Along equator the depth of thermocline is generally small, increasing from the 50moff the coast of Ecuador to about 200 m.

2.2 Water sampling location

The MR07-01 cruise was taken on *RV MIRAI* of JAMSTEC during 17 February 2007 to 26 march 2007 was conducted mainly to study biogeochemical processes along eastern North Pacific Ocean. Water samples were collected using 12 L Niskin bottles mounted on a conductivity temperature depth profiler. Subsampling was stated immediately to prevent any gas exchange, and also samples were collected for measuring hydrographical parameters. Water samples were collected by Dr. V.V.S.S Sarma (Scientist National institute of oceanography (NIO), Goa, India). The sampling was carried out from North Pacific Ocean from equator to north until 36°N at an interval of 2°along 155 °E. I sampled surface and subsurface water between 10m and 1000 m. for the present investigation I selectively picked samples from equator, 5°N, 10°N, 15°N, 20°N, 24°N 30°N and 36°N. Sampling locations were marked in the map given below.

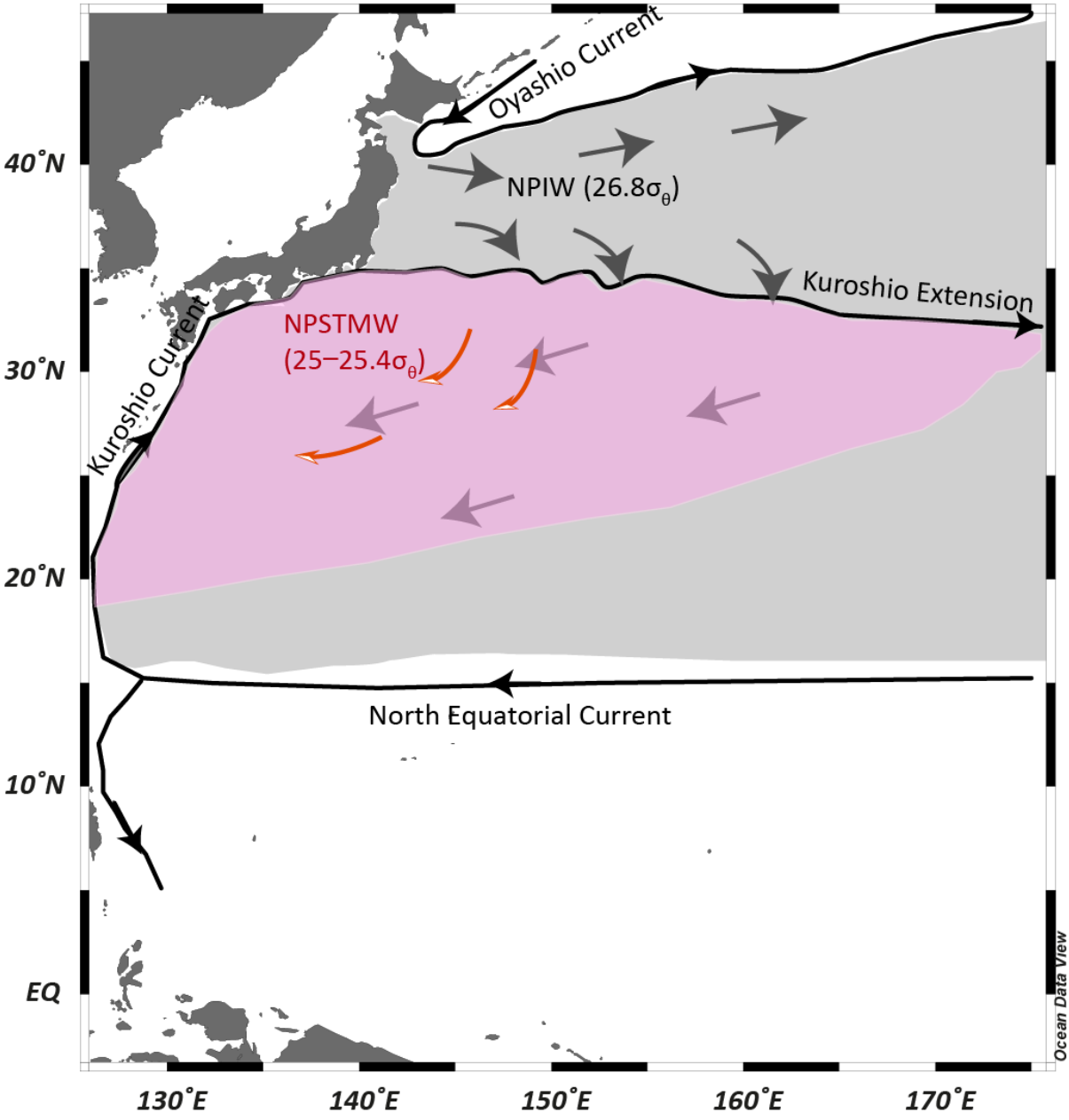

Figure 2: Seawater sampling location of North Western Pacific Ocean cruise MR07-01 along 155 °E for the hydrographical parameters along with dissolved oxygen isotope and molecular ratio analysis. Black dotes represents the sampling location for hydrographical parameters and circled black dotes represents

Ocean depth at study area varies between 2517mat equator and 5765 m at 30 °N. All the stations are full isolated from costal area and I am not expecting any properties of costal water. Sampling locations has a wide coverage of oceanographic properties of surface currents, water masses and oxygen minimum zones of North Pacific Ocean. The study area covers

surface currents like north equatorial current, Kuroshio Current and Kuroshio Oyashio mixing area and water masses like North Pacific Subtropical Mode Water (NPSTMW) and North Pacific Intermediate Water (NPIW) and north pacific oxygen minimum zone (OMZ). In order to prevent any gas exchange the subsampling was done priorly from the Niskin bottle of rosette sampler.

2.3 Water sampling method for dissolved oxygen purification and isotope ratio analysis.

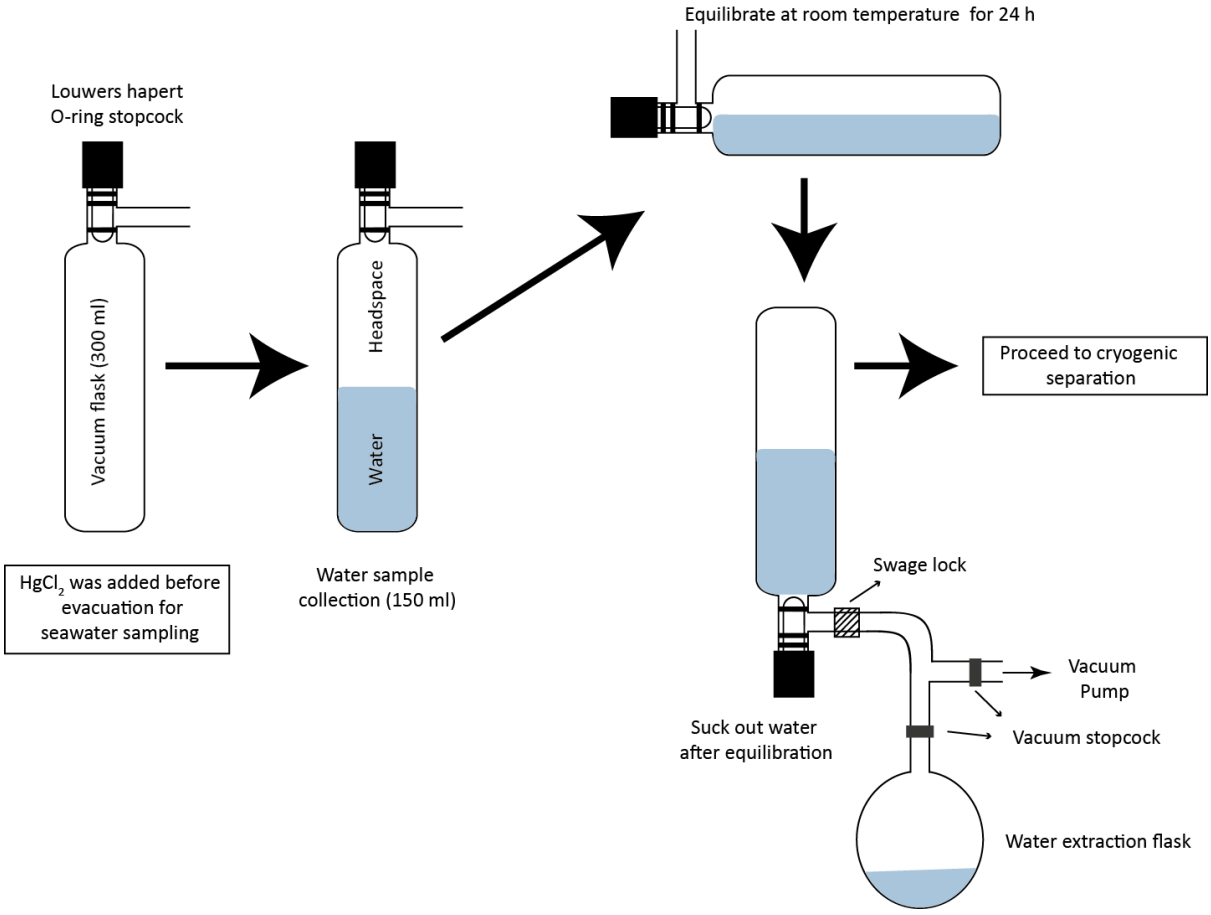

Figure 3: A 300 mL vacuum flask preparation for water sampling, the flask was then filled with about 150 mL of water by leaving another 150 mL headspace. The flask was then equilibrated for 24 h and then the water was sucked out. The flask containing dissolved gas was then cryogenically purified for oxygen-argon mixture.

Water sampling was carried out in a 300 mL glass flask, one side of this was fitted with a Louwers O-ring stopcock and I utilized headspace equilibration technique for the separation of dissolved gases in the water as shown in the figure 3. Prior to sampling, the 300 mL flask well evacuated using a rotary vacuum pump was containing 0.5 mL of $HgCl_2$ (Kirkwood 1992) saturated solution. After complete evacuation close the stopcock and put a rubber cap on the nozzle after filling it with water. Just before sampling, remove the rubber cap and water thoroughly and extend nozzle with a rubber tube (1/2", 3-4" long), another tube from niskin bottle put into the flask's nozzle and over it with water to be sampled. About half of the flask was filled with water sample and leaving 150 mL of headspace. Extreme care was taken to avoid the trapping of air bubbles during sampling and sampling was done slowly to prevent suction of atmospheric air. The stopcock was then closed, and the port (nozzle) was refilled with water and then sealed with a rubber cap to avoid any further leakage of Louwers Hapert O-ring stopcock. Each flask contains about 150 mL of water and another 150 mL vacuum headspace was then equilibrated at least for 24 h at room temperature (Luz et al. 2002; Barkan and Luz 2003; Sarma et al. 2003). The 300 mL flask was used to sample surface and bottom water samples which have sufficiently good amount of oxygen (oxygen saturation >20 %), at oxygen minimum zone the dissolved oxygen saturation was less than 20% were sampled using large flask 2 L to ensure the volume of dissolved oxygen sufficient enough to make m/z 32= 3 V for 100 cycles. Usually equilibration process would be taken place during the storage transportation of samples to laboratory, this time is usually more than 24 hours.

During the equilibration process all the dissolved gases will be degased to vacuum headspace. After equilibration the water in the flasks where then sucked out using a rotary pump by leaving dissolved gases in the vacuum headspace as shown in figure 3. The gases were then transferred quantitatively to a class tube containing preheated 13X molecular sieves (usually 3 pellet) cryogenically. These samples were stored for the isotopic and molecular sieve analysis. I have not performed any test to determine the duration of sample storage. Since we are not expecting any biological activity and isotope exchange in a sealed glass tube, the samples can be stored permanently. Hydrographical parameters Temperature, salinity, dissolved oxygen and nutrients of MR07-01 cruise were obtained from *R.V. MIRAI* data sheet. Expertized technicians in the ship analyzed all the parameters. Hydrographical profile of each location was also measured using CTD (Sea-Bird Electronics, Inc., USA) sensor attached to a rosette sampler. All hydrographical data are available in JAMSTEC website (http://www.godac.jamstec.go.jp/dataportal/viewer.htm)

2.4 Triple isotopic composition of dissolved oxygen at saturation with air (water and air equilibration experiment)

As explained in the section it is important to determine the $\Delta^{17}O_{eq}$ accurately to calculate gross oxygen production in World Ocean. A diagrammatic representation of air water equilibration system is shown in the figure 4. The experimental system contains water bath attached to thermostat, magnetic stirrer, aerator for bubbling and sensors. The temperature in the water bath was maintained by flowing water through a thermostat at a flow rate of 10 L per minute. The experiment was carried out in an open 2L flask immersed in a temperature controlled water bath. About $3/4^{th}$ of flask was filled with deionized water or $HgCl_2$ poisoned (to prevent biological activity) seawater. Bubbling or stirring using an aquarium aerator or magnetic stirrer respectively carried out the equilibration. Equilibration process was carried out for 48 hrs at water bath temperature 25 °C. Water dissolved oxygen, temperature and salinity was monitored using a calibrated conductivity and dissolved oxygen sensors respectively. The temperature of water bath was maintained 25±0.1 °C using a sophisticated thermostat. The temperature of water bath was monitored using the temperature sensors attached to DO and salinity sensors and also using a highly accurate mercury thermometer (precision 0.1 °C). Bubbling and stirring was stopped 30 minutes before sampling as suggested in literatures. At least 5 sub-samples (150 mL) were collected in pre-evacuated 300 mL flask, which was then equilibrated at room temperature for 24 hours and then preceded to gas extraction and purification. The equilibration was carried out using a shaker, after that the water was sucked out using rotary pump. The dissolved gases were directly purified for oxygen–argon mixture without storing it in glass tube containing molecular sieves.

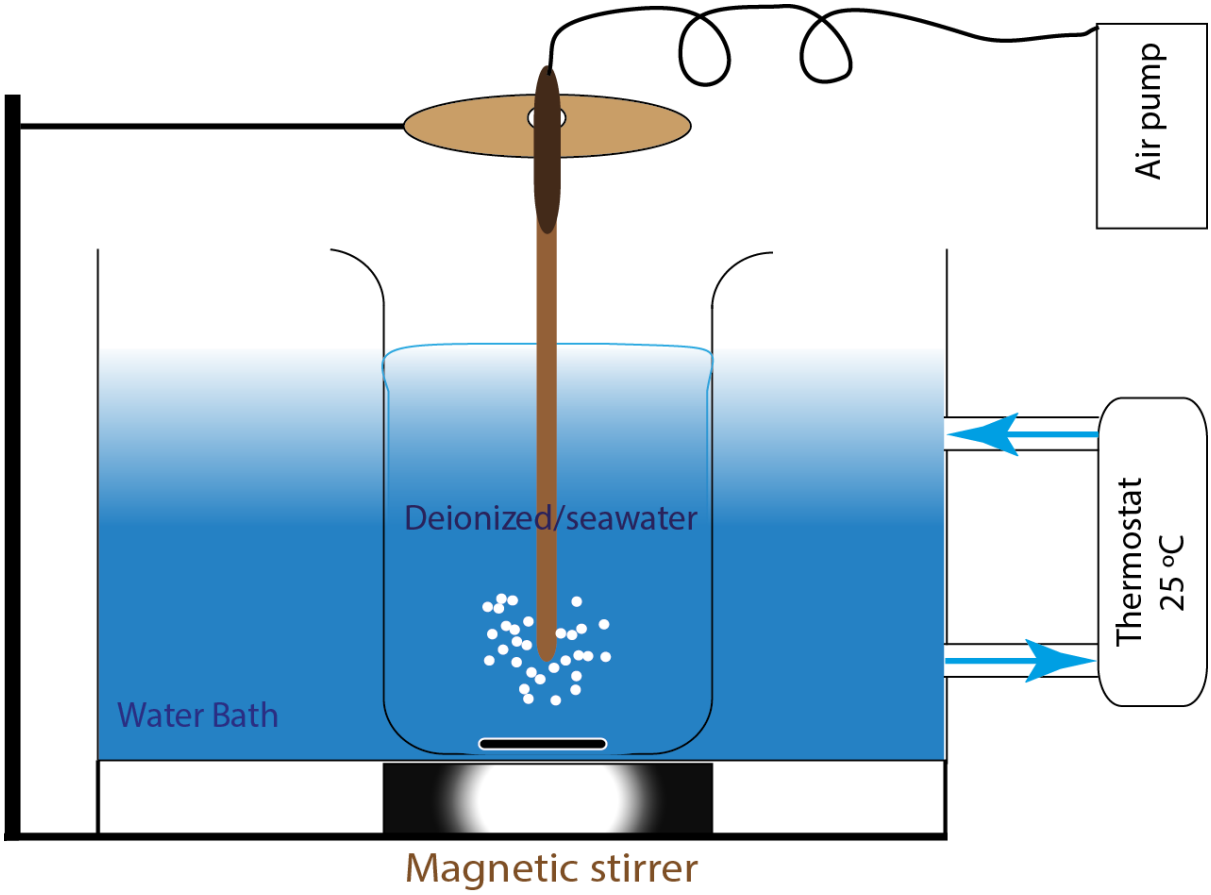

Figure 4: Schematic representation of equilibration system used for water air equilibration. In which a 2L beaker contain deionized or seawater immersed in temperature controlled water bath. Equilibration was carried out stirring and bubbling of fresh air, stirring was carried out magnetic stirrer and bubbling was using aquarium aerator.

2.5 Present strategy of gas purification method

Long time before the discovery mass independent isotopic fractionation in oxygen, scientists were measuring oxygen isotopic composition using mass spectrometer. Early analysis of oxygen isotopes were carried out by converting oxygen to carbon dioxide (Kroopnic.P and Craig 1972; Kroopnick and Craig 1976), and then analyze the ratio of $^{18}O/^{16}O$ as 46/44+45 mass ratios. This analytical method cannot yield $^{17}O/^{16}O$ directly and simultaneously because $^{13}C^{16}O^{16}O$ overlap the signal from the ionized molecule of $^{12}C^{17}O^{16}O$. Also isotopomers of N_2O can interfere to determine oxygen isotope ratios. Later in 1980 Epstein introduced a CO_2 water equilibration method to determine isotopic ratios of $^{17}O/^{16}O$.

However this method has a disadvantage that the precision of ^{17}O was ±0.5‰. In 1984 Thiemens and Meagher introduced a new method to purify oxygen–argon mixture from other gases like nitrogen, carbon dioxide and water. They introduced pure oxygen directly to mass spectrometer to analyze isotopic ratios. This bold step over took the disadvantages of previous method with sufficiently high precision of $1\sigma = 0.3‰$.

Thiemens and Meagher achieved this advances in oxygen isotopic ratio analysis was through a new cryogenic purification of oxygen–argon mixture. This method contains heating of oxygen with molecular sieve at 300°C may cause any reaction or fractionation. Moreover, the method was much complicated and time-consuming process. In 1999 Wassenaar and Koehler developed an on-line technique for the determination oxygen isotopic ratios of gaseous and dissolved O_2 using a continuous flow mass spectrometer by accounting bad analytical precision (±0.17‰ and ±0.5‰ in SD, for $\delta^{18}O$ and $\delta^{17}O$ respectively).

Later on Mark Thiemens discovered mass independent isotopic fractionation during the formation and dissociation of ozone in stratosphere. During early 21st century, Luz and Barkan applied mass independent oxygen isotopic fractionation to calculate biosphere and ocean productivity. In the past decade, the application of triple oxygen isotopes has served as a unique tracer to better understand geochemical cycles (Hendricks et al. 2005; Cepeda-Morales et al. 2013) and paleoenvironmental conditions (Blunier et al. 2002; Landais et al. 2007; Blunier et al. 2012). The oxygen isotope anomaly from the mass dependent fractionation line in dissolved oxygen has been used to estimate oceanic productivity (Luz and Barkan 2000; Hendricks et al. 2004) but this method requires a very precise analysis of oxygen isotope ratios ($\delta^{18}O$ and $\delta^{17}O$) as well as the isotope anomaly. The essential procedure for this precise analysis is to separate oxygen or oxygen–argon mixture from other gases present in natural air samples. Gas chromatography-based methods have been developed for the purification of oxygen (Sarma et al. 2003) or oxygen–argon mixtures (Barkan and Luz 2003) from natural air samples.

The analytical precision of Wassenaar and Koehler' method was not suitable for the calculation of oceanic productivity, this it leads to further modifications in the method for better precision. Recently 2003 Barkan and Luz published new automated chromatographic method for the purification of oxygen–argon mixture in natural air samples. This method used four stainless steel column packed with 5 Å molecular sieve, and GC column (0.2 m x 2mm) was held at -80 °C. This method requires a helium flow rate of 25 mL per minute and finally eluted oxygen–argon mixture was collected in a liquid helium manifold. Repeated measurements of

atmospheric oxygen yield the repeatability (±SE x t) of 0.004, 0.003 and 0.2% for $\delta^{18}O$, $\delta^{17}O$ and δ (O_2/Ar) respectively. This method was able to separate only oxygen and argon mixture in natural air samples, which leads to an argon interference correction for oxygen isotope ratios

Sarma et al 2003 introduced a more advanced method, a chromatographic method to separate nitrogen argon and oxygen in dissolved air samples for the analysis of triple oxygen isotope ratios. The separation system contains a stainless steel chromatographic column (8 m x 2 mm ID) packed with 45/60 mesh 5 A molecular sieve held at -90 °C during sample purification. This method requires ultra-pure helium flow of about 20 mL/ minute, and eluted oxygen was trapped cryogenically into a tube containing 13X molecular sieve. Repeated analysis of 3 mL atmospheric air over a 3 month yielded a reproducibility of 0.065 ‰ and 0.02 ‰ for $\delta^{17}O$ and $\delta^{18}O$ respectively. One of major disadvantage of these chromatographic methods requires high-purity helium as a carrier gas, and the depletion of helium reserves is a growing global concern. This motivated us to develop a new helium free method to purify oxygen–argon mixture or pure oxygen for isotope and molecular ratio analysis.

2.6 Development of new method for the purification oxygen-argon mixture in natural air samples

It was a great challenge to establish a new highly precise helium free cryogenic separation of oxygen–argon mixture in natural air samples. For the method proposed here, I tested various types of molecular sieve zeolite (MSZ) to determine their ability to separate oxygen or oxygen–argon from air samples, and the presence of isotopic or molecular fractionations during the adsorption and desorption processes. Although the method may not be as effective at separating oxygen and argon as other gases with similar physical properties, I confirmed that this method could be successfully used to separate oxygen–argon mixture. Subsequently, I determined equilibrium isotopic and molecular fractionations between the atmosphere and water, and compared our results with values reported elsewhere (Benson et al. 1979; Reuer et al. 2007; Luz and Barkan 2009; Stanley et al. 2009).

A schematic diagram of the cryogenic gas separation and purification system is shown in Figure 5. The experimental set up contains a rotary vacuum pump, which can produce a vacuum of $4x10^{-4}$ Torr. The entire purification system was built in ¼” stainless steel Swagelok pipes and fittings. The line section contain 4 needle valves, one cryogenic column containing molecular sieve, one sample injection finger and a sample collection ampule contain single 1/8”

pellet of 13X molecular sieve. I tested several methods and procedures before assigning final condition for high efficient separation of oxygen–argon mixture. The separation column is made of a Pyrex glass tube and two ends were fitted with stopcocks.

I have tested three different columns; first, one was identical to separation column used in the Thiemen's cryogenic purification setup (Thiemens and Meagher 1984). The second and final ones were like a "U" tubes having different dimensions, the second was characterised with an outer diameter of 10 mm and length of 27 cm was filled with 6.3 g of 5 A MSZ, and a third column, with an outer diameter of 6 mm and length of 17 cm, filled with 1.5 g of MSZ. Three types of MSZ (3 A, 4 A and 5 A) at different mesh were used in the performance test as shown in figure 5. I could not use the first column well, because of practical difficulties in maintaining column temperature and holding molecular sieve pellets in position.

A comparative study between second and third molecular sieve column for the selection of best column for efficient oxygen–argon mixture separation.

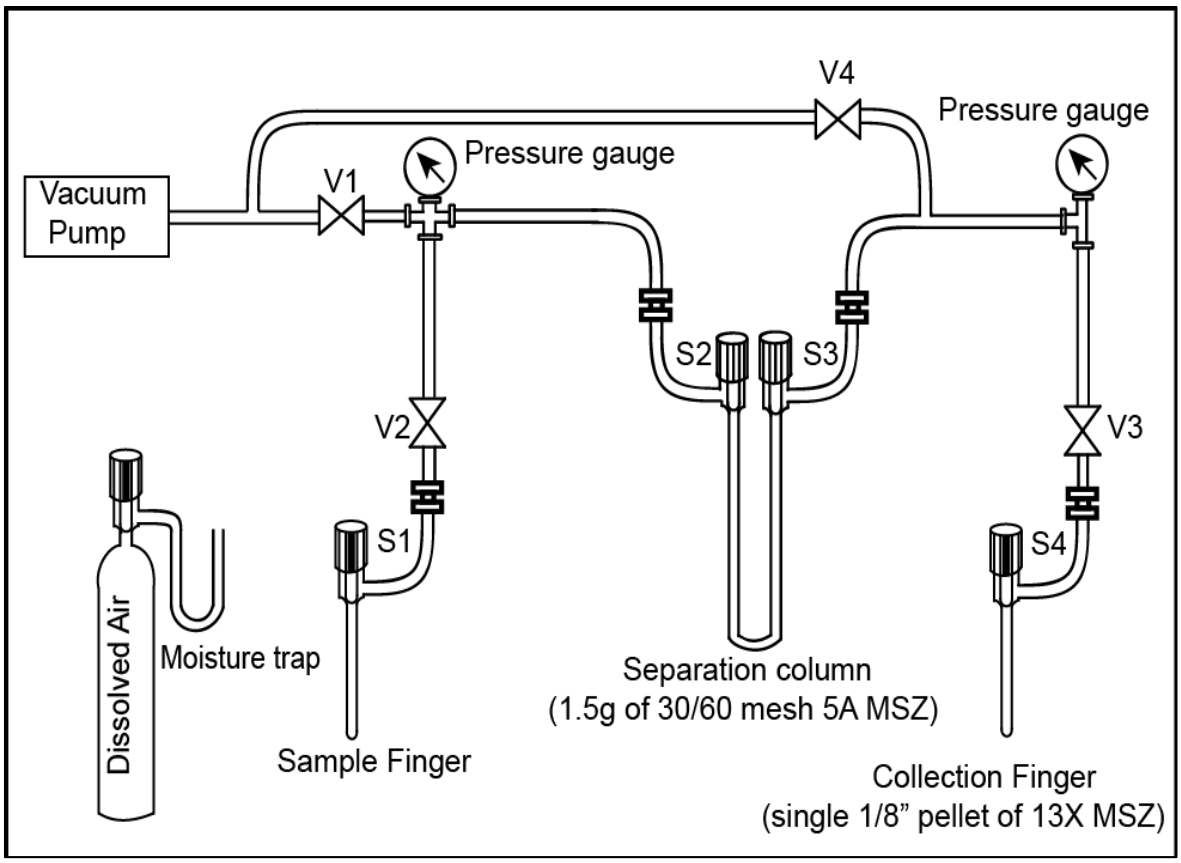

Figure 5: The vacuum line used for the cryogenic separation and purification of oxygen-argon mixture in atmospheric air. The raw sample finger, separation column and collection finger were replaced by oxygen-argon mixture cylinder, stainless steel union and ¼" glass tube containing molecular sieve respectively for the experiment to study the effect of molecular sieve on isotopic and molecular fractionation. V1, V2, V3 and V4 are the needle valves and S1, S2, S3 and S4 are Viton O ring stopcocks. An additional moisture trap was used for purifying dissolved gas samples, which is crucial for protecting separation column from moisture contamination and thus to save baking time.

Table 2: A test of the separation capacity using different amounts and types of MSZ and column temperature for an oxygen–argon mixture in air.

<table>
<tr><td rowspan="2">Slurry temperature (°C)</td><td colspan="4">Type of MSZ</td></tr>
<tr><td>5A (30/60 mesh) 1.5 g</td><td>5A (30/60 mesh) 6.3 g</td><td>4A (approx. 30/60 mesh) 1.5 g</td><td>3A (30/60 mesh) 1.5 g</td></tr>
<tr><td>–85</td><td>N_2 contamination (32 %)</td><td>N_2 contamination (7 %)</td><td colspan="2" rowspan="4">No significant separation of the oxygen–argon mixture occurred at these temperatures.</td></tr>
<tr><td>–92</td><td>Ideal temperature for oxygen–argon separation</td><td rowspan="2">Elution time was long (1 h) and sample was contaminated by N_2 (2 %) at these temperatures.</td></tr>
<tr><td>–105</td><td>Significant fractionation ($\delta^{17}O \approx 0.1$ ‰, $\delta^{18}O \approx 0.2$ ‰)</td></tr>
<tr><td><–130</td><td colspan="2">Elution time was more than 1 h</td></tr>
</table>

I tested the separation performance of these types of MSZ at four different column temperatures by introducing 6.6 mL of atmospheric air. The volume of the ampule was determined using the weight of the deionised water filled until the O-ring of the ampule just close. Initially experiment was carried out using the feasibility of nitrogen separation of columns using simple elution experiment. For this purpose, 6.6 mL of atmospheric air was trapped in the molecular sieve column at liquid nitrogen temperature and eluted out at room temperature. Connecting the output of Baratron gauge to a voltage recorder for an elution time of about 1 hour monitored the increase in pressure. The rate of change of pressure was plotted against elution time as shown in the figure 6, we can see two clear peaks, first one is oxygen–argon mixture and second one is prolonged nitrogen elution. It should be noted that, these two peaks were merged together and thus it must be mandatory to have a sufficient separation for an accurate analysis of oxygen isotopic ratios in the gas mixture. In order to achieve a sufficient separation I need to decrease column temperature from room temperature. A significantly good separation was observed when using 5 A MSZ at a temperature of –85 °C, however the separation of the oxygen–argon mixture was not fully successful due to significant nitrogen contamination in 30 % of the eluted oxygen which can easily alter oxygen isotope ratios. At a temperature below –130 °C, 5 A MSZ did not release any trapped gases within 1 h. Thus the column temperature should be fixed between these two extreme values for both the columns. Significant amounts of nitrogen

were also found in the separated oxygen–argon mixture when using 6.3 g of 5 A MSZ at temperatures of –92 °C and –105 °C. I did not find any nitrogen signal in the separated oxygen–argon mixture at these temperatures when using 1.5 g of MSZ; however, significant isotopic fractionation occurred at a temperature of –105 °C. Experiments using 3A and 4 A molecular sieves were mainly focussed to separate oxygen and argon in the eluted oxygen–argon mixture. The 3 A MSZ was 45/60 mesh, however the 4 A MSZ was 1/16" mesh, which was then powdered and sieved in to about 30/60 mesh. No significant separation of gases occurred when using the 3 A and 4 A MSZ at all temperatures. There was no significant separation of the oxygen–argon mixture occurred when using 4 A and 3 A MSZ at these temperatures. In addition I tested the fine powdered 3 A and 4 A MSZ, those molecular sieves were so fine which was not passing gas molecule through it and thus it was not giving a proper vacuum and full trapping of gas molecules even at liquid nitrogen temperature. Finally I confirmed that 1.5 g of 5 A (30/60 mesh) MSZ at a column temperature of –92 °C comprised the optimum conditions for separating oxygen–argon mixture from an air sample. The same results were obtained for a range of sample volumes (1.5–6.6 mL).

2.7 Separation and purification of oxygen–argon mixture

Oxygen–argon mixtures in atmospheric and dissolved air samples were separated under the optimum conditions described in the first Experimental section, and the uncertainties associated with isotope and molecular ratios were determined. The entire vacuum line was constructed using ¼" stainless steel tubes and fittings, except for the separation column. The cryogenic separation column was made of 17 cm long Pyrex gas tube was densely packed with 1.5 g of 5 A (30/60 mesh) MSZ. Both ends of the column were filtered with glass wool to prevent the extraction of molecular sieve granules under vacuum (Fig. 5). A freshly packed column was baked at 300 °C for more than 10 h, and the column was routinely baked at the same temperature for 10 min prior to each gas separation, until the vacuum level was below 4 x 10^{-3} Torr. During baking, all valves and stopcocks were open except S1. After the column was cooled to room temperature, V1, V4 and S3 were closed, and the column was then chilled using liquid nitrogen. Subsequently the sample gas was admitted, with sufficient time (approximately 5 min) allowed for it to transfer (trap) completely to the MSZ column. If sample volume is more than 3 mL, the trapping gas to the molecular sieve column should be slow down by opening S2 partially, otherwise the sample could pass through the small MSZ column

before it get fully trapped by molecular sieves. This will help us to achieve a good separation of nitrogen in the eluted gas mixture. After closing S2 and opening S3, the liquid nitrogen dewer was replaced with an alcohol slurry of –92 °C. The collection finger was simultaneously chilled by liquid nitrogen to trap the gases eluting from the separation column. The collection finger was containing single pellet of 13X molecular sieve at liquid nitrogen temperature. Twenty-five minutes was required for complete transfer of the oxygen–argon mixture, and the total experimental time was 40 min for single-sample preparation. Any moisture content in the molecular sieve column may cause a significant isotope and molecular fractionation and it will enhance baking time, thus an additional moisture trap (U trap in liquid nitrogen temperature) could be introduced before admitting sample to cryogenic column. I found the moisture trap was necessary for purifying dissolved gas samples.

2.8 Determination of isotopic and molecular fractionations during gas desorption from the molecular sieves

Our method involves the collection of eluted gases by MSZ at liquid nitrogen temperature (collection finger in Fig. 1). This process has confirmed the occurrence of isotopic fractionation during gas desorption from the MSZ surface (Abe 2008). Abe 2008 confirmed the magnitude of this isotopic fractionation and suggested that it could be minimised by gently baking the collected gases at a temperature of 60 °C (Abe and Yoshida 2003). However, he only tested for isotopic fractionation during these processes using pure oxygen. Since I are dealing with oxygen–argon mixture, it is important to test the magnitude of isotopic and molecular fractionations in oxygen–argon mixture. The experiment was thus conducted using oxygen–argon mixture (4.48 % in volume) packed in a cylinder, with different amounts of 5A and 13 X MSZ (1/8" pellet) in a Pyrex glass tube. I have maintained the same length of column throughout the experiment. These MSZ pellets were preheated under vacuum using a spirit lamp (ethanol) for approximately 5 min. An aliquot of 1.2 mL gas was trapped completely in a ¼" Pyrex tube with MSZ at liquid nitrogen temperature. After flame sealing, the tube was heated at 60 °C for 10 min, and then gas was admitted into a dual-inlet mass spectrometer. Isotopic and molecular ratios were measured with respect to identical oxygen–argon gas mixture (4.48 % in volume) in reference side of duel inlet mass spectrometer.

The amount and type of molecular sieves were changed, and the isotopic and molecular fractionations were studied for the same amount (volume) of gas. The experiment was repeated for one, two and three pellets of 5 A and 13 X MSZ. The weight of a single pellet was

approximately 70 mg, and the same experimental conditions and same volume of gas were maintained in all cases. A triplicate analysis was conducted in each case, and data were corrected for corresponding zero enrichment. All oxygen isotope ratios were corrected with corresponding zeroenrichment values.

2.9 Analysis of isotope and molecular ratios of oxygen–argon mixture: Isotope ratio mass spectrometer- brief introduction

Oxygen isotope and molecular ratios of purified oxygen–argon mixture was carried out using an isotope ratio mass spectrometer (Delta plus; Thermo Fisher Inc., Waltham, MA, USA). Isotope ratio mass spectrometer is a gas source mass spectrometer used to measure relative abundance of isotopes in a given samples. A. O. Nier pioneered the basic design of IRMS in 1947. Early 1960s the instrument was used only by a small group of scientist, having very limited publications. The recent statistic shows the abundance a study using IRMS was up to 150 publications per year and different modifications and peripherals was introduced with time. IRMS has a wide range of applications in environmental, biological, health,

Basic diagrammatic sketch of IRMS was shown in figure 6, consist of inlet system, source, magnetic analyzer and collector.

Inlet system of an IRMS is B.F Murphey first introduced the changeover valve in 1947, which allows inlet system to switch sample and reference gas alternatively to mass spectrometer under high vacuum.

The source of IRMS is an electron gun typically heated tungsten filament producing a small current of electrons with an energy of 50 to 150 eV, which is sufficient enough for ionizing gas molecules like O_2, Ar, CO_2, H_2 etc. the ionized molecules are then accelerated by an high voltage of 10-50 KV to a magnetic analyzer. The efficiency of ionization is the sensitivity of mass spectrometer, which is about 1000 to 2000 molecules per ion, however advanced instruments have better sensitivity around 500 molecules per ion.

An electromagnet having a magnetic field of 100 to 500 Gauss used to keep accelerated ions in a spiral path. This magnetic field separates charged ions according to their m/z values. When a charged particle enters to the magnetic field, its path deflects to an angle 60 °C, then it strike on an ion detector.

Ion detector of IRMS usually is a grounded faraday cup. When a charged ion hit on a faraday cup, it produces electric impulses. It is very common to use an array of faraday cups corresponding to each ion (eg. 3 cups for m/z=32, 33 and 34) for precise analysis simultaneously without any mass jumping. These small ion currents were then amplified several times over a large resistors ($10^{11}\Omega$), and then the measured current will be converted to isotopic ratios.

The isotope and molecular ratios of the oxygen–argon mixture were analysed using a mass spectrometer (Delta plus; Thermo Fisher Inc., Waltham, MA, USA) relative to a reference oxygen–argon mixture and the output voltage of the major signal (m/z 32) were arranged to be equal to 3V. The signals at *m/z* 28, 32 and 40 were measured dynamically to determine the oxygen to argon ratio as well as to check for nitrogen contamination. Each sample was analyzed in mass spectrometer consists of four separate runs during which the ratio of sample to reference is determined 25 times to obtain greater analytical precision.

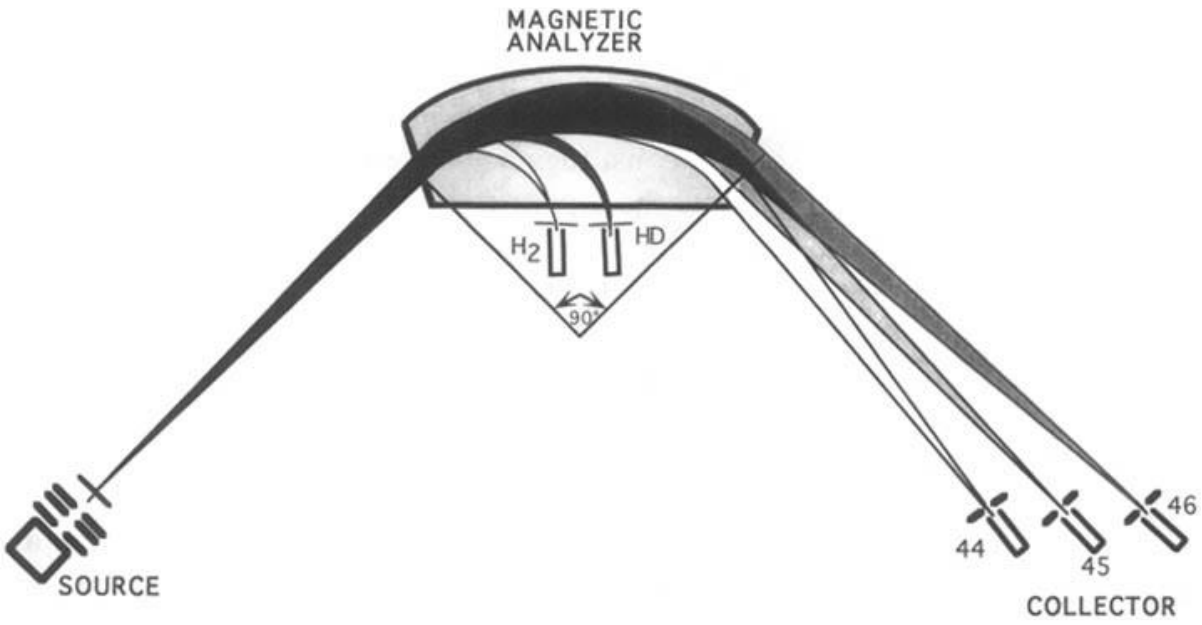

Figure 6: Diagrammatic representation of isotope ratio mass spectrometer showing source, analyzer and collector. Collector is a faraday cup corresponding to masses 44, 45, and 46, and of H_2 and HD, are shown. (Source: PRINCIPLES of STABLE ISOTOPE DISTRIBUTION: Robert E. Criss)

2.10 Units and notations

All oxygen isotope ratios were reported as δ relative difference to a standard material. The representation of isotope ratios of an element and units were standardized with time by (Friedman and O'Neil 1977; Gonfiantini1978, 1984; Coplenet al. 1983; Coplen 1996; Coplen et al. 2006) and recently IUPAC has organized notation representation and standard values internationally (Brand et al. 2014).

In this manuscript I have used following definitions and units,

Oxygen isotope ratios were reported as δ relative to atmospheric oxygen as standard reference material.

$$\delta^{18}O = \left(\frac{R_{sample} - R_{\text{standard}}}{R_{\text{standard}}} \right)$$

Where R is the ratio of heavy/light isotope. Unit of δ is ‰.

The ^{17}O excess (Δ^{17}O) was defined as

$$\Delta^{17}O = \ln\left(\delta^{17}O + 1\right) - \lambda \ln\left(\delta^{18}O + 1\right)$$

Where I adopted $\lambda = 0.518$ (Reuer et al. 2007; Stanley et al. 2009), and unit of Δ^{17}O is per meg (parts per million)

The oxygen–argon ratio was expressed as

$$\delta\left(\frac{O_2}{Ar}\right) = \left(\frac{\left(\frac{O_2}{Ar}\right)_{samp}}{\left(\frac{O_2}{Ar}\right)_{ref}} - 1 \right)$$

Argon supersaturation is defined as,

$$\Delta Ar = \left\{ \frac{[Ar]}{[Ar_{sat}]} - 1 \right\} x100$$

Where [Ar] was calculated from measured $\delta(O_2/Ar)$ and [Ar_{sat}] is the concentration argon at saturation and is theoretically calculated according to (Hamme and Emerson 2004), the argon anomaly ΔAr is expressed in %.

2.11 Argon interference in oxygen isotope ratio analysis

Kroopnick started analysis of oxygen isotope ratios since 1972 and Craig (Craig and Kroopnic.P 1970; Kroopnic.P and Craig 1972; Kroopnick and Craig 1976), later on their method was modified by several researchers. In 1984 Mark Thiemens (Thiemens and Meagher 1984) introduced a new method for analyzing oxygen isotope ratios by introducing pure oxygen (oxygen–argon mixture) to mass spectrometer. In 2003 Abe and Yoshida (Abe and Yoshida 2003) found a linear correlation between oxygen isotope ratios and partial pressure of other gases in the samples. The speculations of the partial pressure dependent isotope ratio fractionations are the interference of oxygen isotope ionization by argon in the ionization chamber. Presence of argon in the ionization chamber, the mean free path of ionized oxygen may be reduced and thus it fractionate during the admission to flight tube (Abe and Yoshida 2003). The effect of argon interference on oxygen isotope is greater than the interference by nitrogen contaminations in the sample. So both should be separated for high precise analysis of oxygen isotope ratios. However our cryogenic separation technique could be useful only for removing nitrogen not argon in sample. Our Pacific Ocean dissolved gas samples were containing a wide range of oxygen–argon ratios. The calculated oxygen to argon ratio was varied between 20.3 and 2.45, and oxygen to argon ratio in the standard atmospheric air was 22.4. Thus it demands an argon interference correction.

I have studied effect of argon interference on oxygen isotopic ratio measurement for a wide range of samples contains different concentrations of argon in the argon oxygen mixture.

2.12 Preparation of oxygen–argon mixture for argon interference correction

I prepared oxygen–argon mixture by mixing pure cylinder oxygen (99.9%) and argon (9.9999%) at desired ratios. This oxygen–argon gas mixtures were then analyzed against reference gas mixture to produce calibration curve in each group of samples. A schematic diagrammatic representation of oxygen–argon gas mixture preparation was shown in figure 7. Which contains pure gases, gas mixing unit and a 300 mL double stopcock ampule. Prior to preparation flow rates of individual gases were adjusted using control valves for a maximum

flow of 1 L per minute for safe preparation. These gases were then connected to input side of mixing unit and the output of mixing unit was connected to an ampule. Open both stopcocks of ampule, allowing a free flow of gases through the ampule. The mixing ratios of oxygen and argon can be adjusted by controlling the flow rate through the gas-mixing unit. The table 3 below is showing detailed flow rates of individual gases. After setting the flow rate, allow the mixture to flush ampule for 3 minute and then close stopcock 2 and then detach the output tube from ampule and close stopcock 1. The ratios of individual gas mixtures were corrected using IRMS by measuring m/z = 32 and 40.

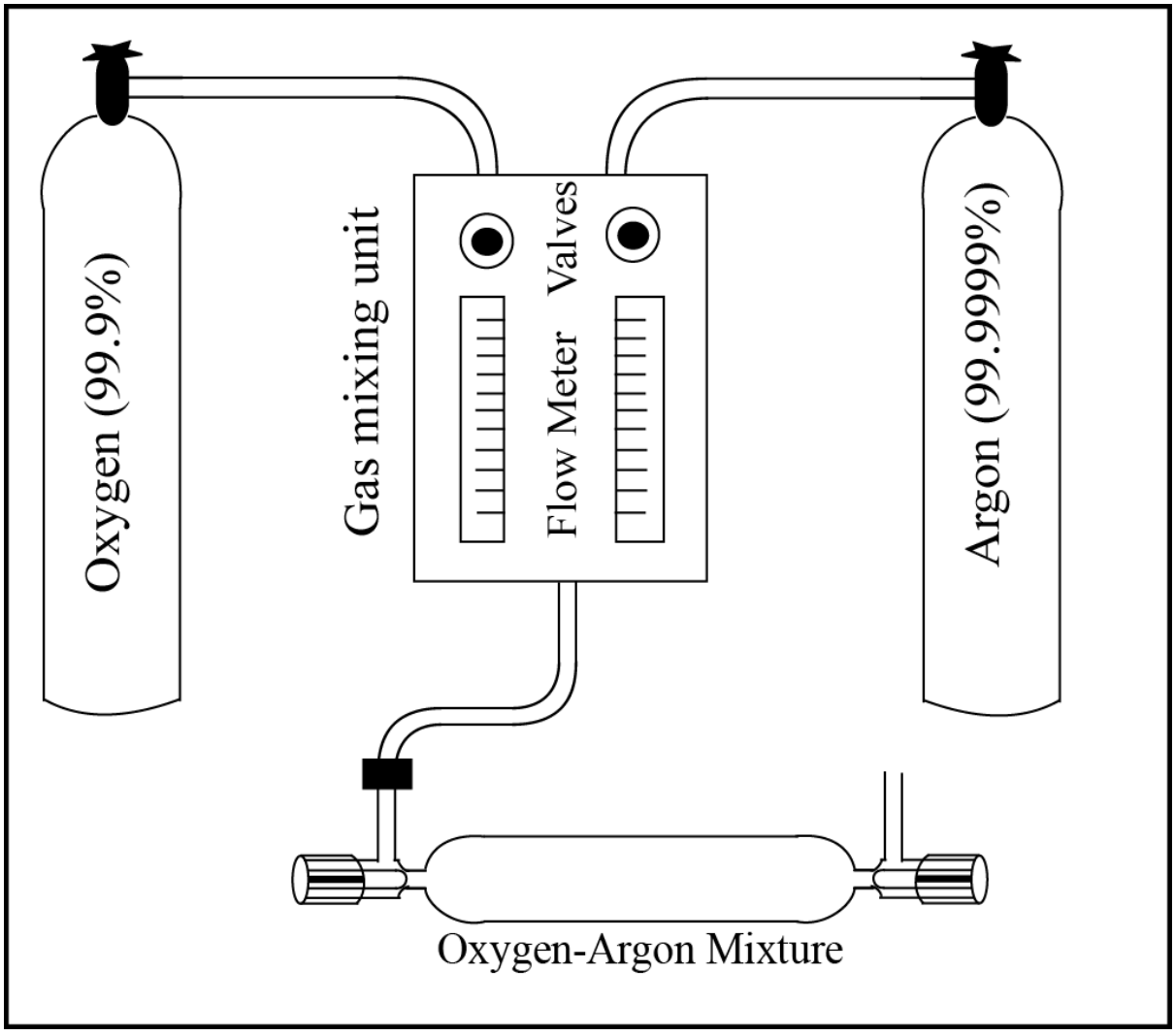

Figure 7: Schematic representation of oxygen–argon mixture preparation system, which contain pure oxygen (99.9%) and argon (99.9999 %) gases, gas mixing unit, and a 300 mL flask to collect prepared gas mixture. The flask was dried in vacuum, and it was flushed with gas mixture for at least 3 minutes at a flow rate of 1 L/ min.

Table 3: Showing the flow rate of pure oxygen and argon to prepared desired oxygen–argon mixture. Total flow rate was maintained at 1 L per minute.

O_2/Ar	Flow rate of O_2 (mL/min)	Flow rate of Ar (mL/min)
21	0.96	0.04
18	0.95	0.05
15	0.94	0.06
12	0.92	0.08
10	0.91	0.09
7	0.88	0.12
5	0.83	0.17
3	0.75	0.25
2.5	0.71	0.29

2.13 Correction for argon interference in oxygen isotope ratios

The cryogenic separation technique can be used only for removing nitrogen, but not for argon in sample. The presence of argon in the purified samples can interfere the analysis of oxygen isotope ratios in the mass spectrometer, and the interference is linearly correlated with partial pressure of argon in the sample (Luz et al. 2002; Abe and Yoshida 2003; Barkan and Luz 2003; Sarma et al. 2003). Our Pacific Ocean dissolved gas samples were containing a wide range of oxygen–argon ratios, which were varied between 20.3 and 2.45. Thus it demands an accurate and wide range of argon interference correction.

During the field sample analysis period, which was between January and February in 2015, air and prepared oxygen-argon mixtures were frequently inserted for molecular and isotopic determination. The observed results of $\delta^{17}O$ and $\Delta^{17}O$ showed a strong polynomial dependency to argon to oxygen ratio (Fig. 9), whereas $\delta^{18}O$ result indicated less dependency ($\delta^{18}O = 3.782\ 10^{-9}\ (\delta(Ar/O_2))^2 - 5.738\ 10^{-5}\ \delta(Ar/O_2) - 5.790$, $R^2 = 0.7665$). Therefore, it can be said that observed argon dependency on $\Delta^{17}O$ was derived not by $\delta^{18}O$, but by $\delta^{17}O$ change.

It should be noted that the above-mentioned regression equations for argon dependency on isotopic composition are limited only for the samples determined with a constant signal

height of m/z 32 = 3 V. Some samples having low oxygen amount (approximately less than 20 % in saturation) were analysed at lower signal height as minimum as 1.2 V and required additional correction described next.

Figure 10 indicates the relationship between sensitivity of $\Delta^{17}O$ to signal height and mixing ratio of argon. Vertical axis of Fig. 10 represents the slope of regression for the $\Delta^{17}O$ values and those signal heights changing from 1.0 to 3.0 V at a certain argon-oxygen ratio. This figure clearly demonstrates that the measured $\Delta^{17}O$ value in oxygen-argon mixture is affected by signal height and argon concentration. For numerical calibration of measured $\Delta^{17}O$ and $\delta^{17}O$ values, following equations obtained from the multiple non-linear regressions were applied.

$$Corrected\ \Delta^{17}O = mesured\Delta^{17}O - \left(-2.725\ 10^{-6} \times \left(\delta\left(\frac{Ar}{O_2}\right)\right)^2 + 2.143 \times \delta\left(\frac{Ar}{O_2}\right) - 2.249\ 10^{-4} \times ([32]sa)^2 + 1.102 \times [32]sa - 1.282 \times 10^3\right)$$

$$Corrected\ \delta^{17}O = mesured\ \delta^{17}O - \left(1.739\ 10^{-8} \times \left(\delta\left(\frac{Ar}{O_2}\right)\right)^2 + 1.298\ 10^{-4} \times \delta\left(\frac{Ar}{O_2}\right) - 1.744\ 10^{-4} \times [32]sa - 1.282\ 10^3\right)$$

For $\delta^{18}O$, no distinct regression was obtained. Therefore post-calibrated $\delta^{18}O$ values were calculated from post-calibrated $\Delta^{17}O$ and $\delta^{17}O$ values.

2.14 Evaluation of propagating errors on isotope ratios due to argon and signal height corrections

The above mentioned corrections relating to argon concentration and measured signal height generate additional uncertainties on isotope ratios of samples. Here the total propagating errors are evaluated. For each isotope ratio, following equation was defined to obtain propagating error;

$$\sigma_{total} = \sigma_{conv} + \sigma_{ar} + \sigma_{32},$$

where σ_{total}, σ_{conv} ,σ_{ar}, and σ_{32} represent total error, error due to conversion of standard from reference gas to air, error due to argon dependency, and error due to signal height variation. The value of σ_{conv} was obtained by the standard deviation of repeated analyses of air during analytical period, which was concerned to analytical precision of single gas analysis. Values of σ_{ar} and σ_{32} were obtained by the RMSE (root mean square error) of each regression, and σ_{32} concerns only to samples measured below 3 V, as mentioned above.

Table 4. Summary of individual error components for each isotope ratio. The value of σ_{ar+32} represents the error concerning to argon concentration as well as signal height variation. Values of σ_{total1} and σ_{total2} represent errors for 3 V and < 3 V, respectively.

Isotope ratio	σ_{conv}	σ_{ar}	**σ_{total1}**	σ_{ar+32}	**σ_{total2}**
$\delta^{17}O$	0.05	0.02	**0.07**	0.19	**0.24**
$\delta^{18}O$	0.10	0.04	**0.14**	0.38	**0.48**
$\Delta^{17}O$	11	11	**22**	39	**50**

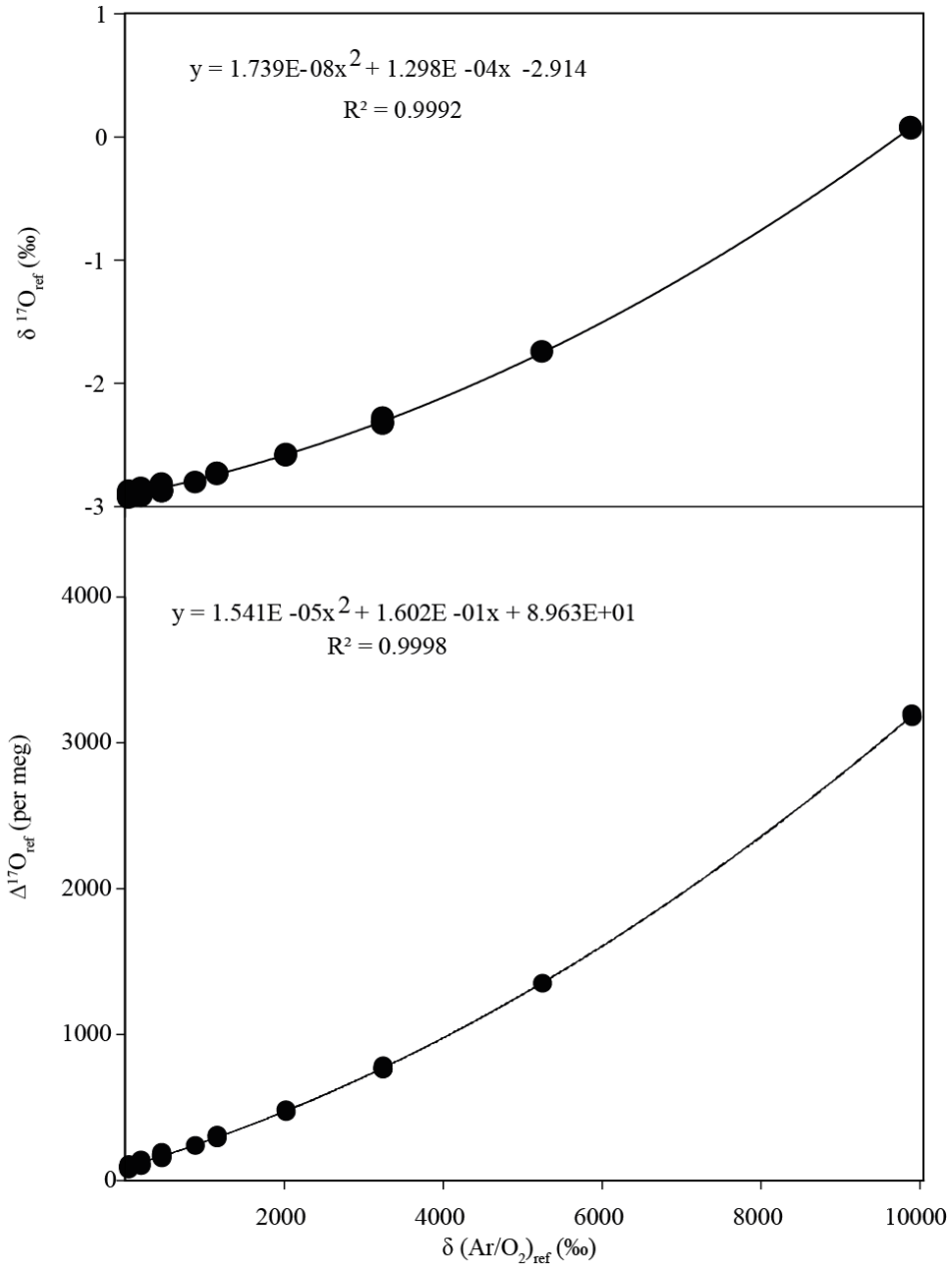

Figure 8: Figure shows the responds of $\delta^{17}O$ and $\Delta^{17}O$ towards partial pressure argon in the sample. Both $\delta^{17}O$ and $\Delta^{17}O$ showed an increasing trend along with amount of the argon in the sample.

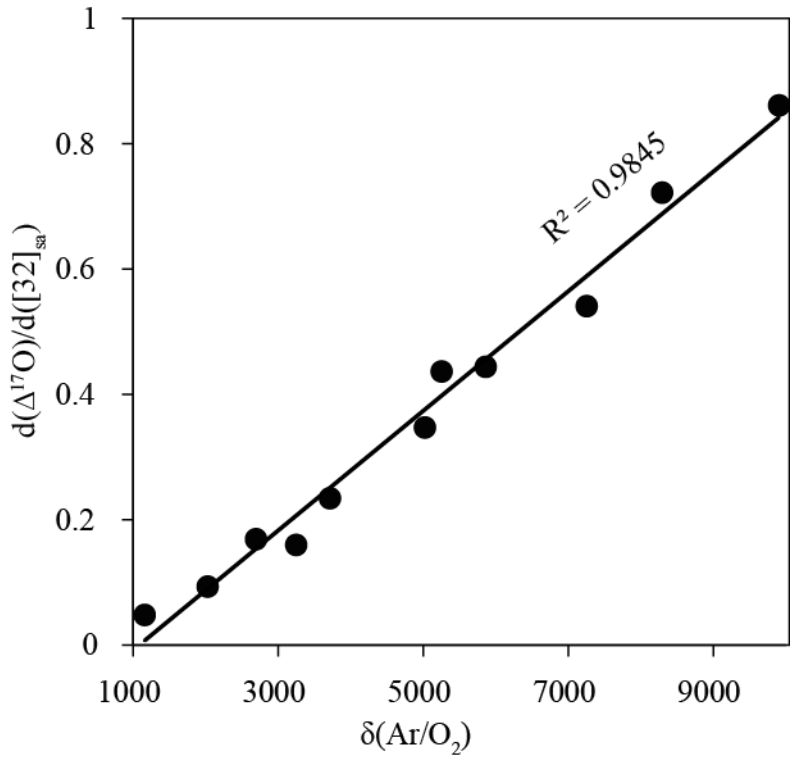

Figure 9: The figure shows the interference of both argon concentration and analytical voltage on $\Delta^{17}O$. The y axis is the slope of a plot between analytical voltage and $\Delta^{17}O$.

Chapter 3

Results

3.1 The efficiency of cryogenic separation of oxygen–argon mixture

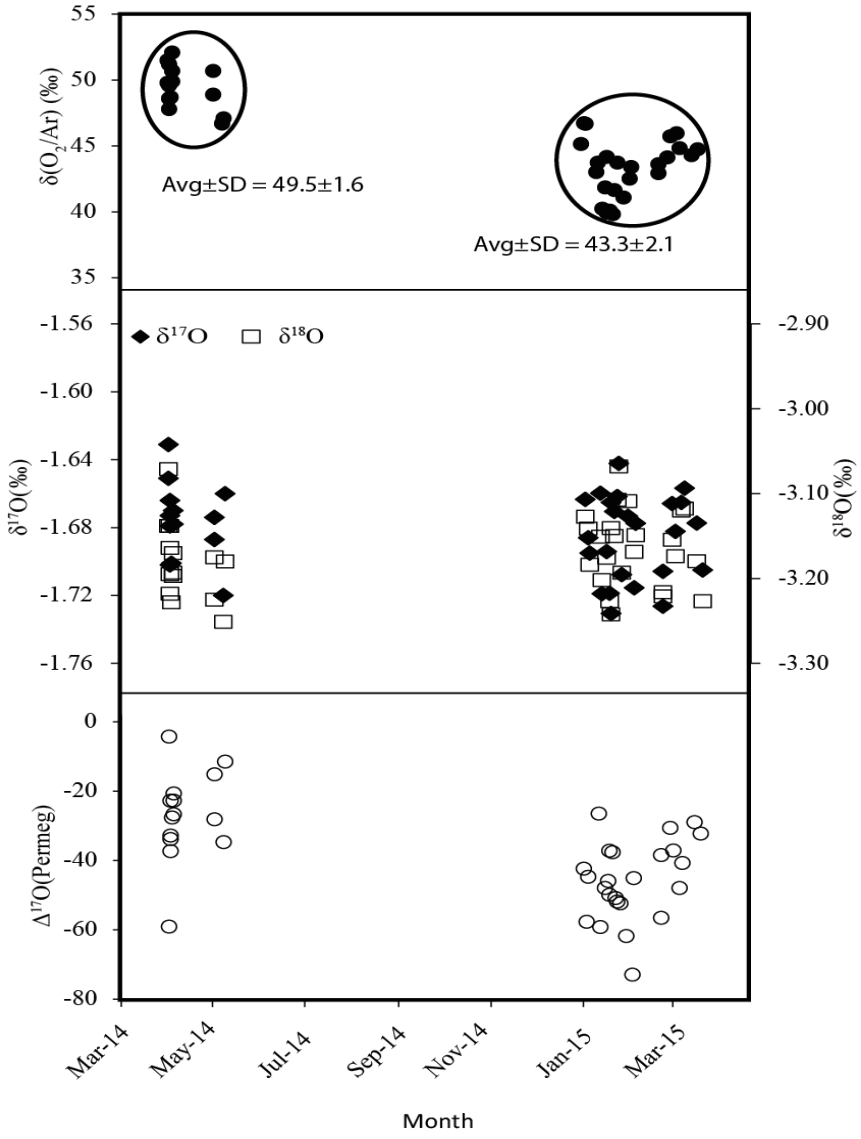

Figure 10: The figure shows the reproducibility of cryogenic purification method for the determination of triple oxygen isotope ratios and oxygen to argon ratio. The $\delta^{17}O$, $\delta^{18}O$ and $\Delta^{17}O$ was varied within the analytical precision, however $\delta(O_2/Ar)$ show two significantly different sets depending on analytical time. This significant difference in $\delta(O_2/Ar)$ could be generated by mass spectrometer.

Repeated analysis of air samples collected in laboratory over 5 months was purified cryogenically was tabulated in table 5. Using 1.5 g of 5 A MSZ in the separation column at –

92 °C, more than 99.9 % of the nitrogen could be removed, and the recovery of an oxygen–argon mixture was found to be better than 99.2 %. The $\delta^{17}O$, $\delta^{18}O$, $\Delta^{17}O$ and δ (O_2/Ar) results for 38 repeated analyses are shown in Table 5. The reproducibility (±1 SD) was 0.024 ‰ for $\delta^{17}O$, 0.045 ‰ for $\delta^{18}O$, 15 per meg for $\Delta^{17}O$ and 3.5‰ for δ (O_2/Ar). Sarma et al. (Sarma et al. 2003) reported values of 0.01, 0.02 and 15 for $\delta^{17}O$, $\delta^{18}O$ and $\Delta^{17}O$, respectively, for a chromatographic separation of pure oxygen, while Barkan and Luz (Barkan and Luz 2003) indicated values of 0.01 ‰, 0.02 ‰, 4 ‰ and 0.4 ‰ for $\delta^{17}O$, $\delta^{18}O$, $\Delta^{17}O$ and δ(O_2/Ar), respectively. The uncertainties in our present method were slightly higher, but were comparable to the methods used in previous studies (Angert et al. 2003; Juranek and Quay 2005; Juranek and Quay 2010; Juranek et al. 2012; Juranek and Quay 2013). The δ (O_2/Ar) in the table 5 shows two distinct groups which was having an average of 49.5±1.6 (April to May 2014) and 43.3 ± 2.1 (January to March 2015), shows a clear dependency of δ (O_2/Ar) on IRMS condition and the parameter is not stable over the study period. However the isotopic rations and oxygen anomaly has no significant difference within analytical period. Even though the extraction procedure for oxygen–argon mixture was same during the study period, the observed significant difference in δ(O_2/Ar) could be generated from the mass spectrometer condition. All of the samples of this study was analyzed during January 2015 to March 2015, thus the results will not be affected by this large variation observed in the δ(O_2/Ar).

The bottom two rows in Table 5 show the results of shared air samples for an inter-laboratory calibration exercise conducted in 2012 (provided by R. Stanley, Woods Hole Oceanographic Institution, USA), using a modified chromatographic separation technique originally given by Sarma et al. (Sarma et al. 2003).

The preparation system was same, except for the column temperature which was set to -40 °C instead of -90 °C. The $\delta^{17}O$, $\delta^{18}O$ and $\Delta^{17}O$ values were consistent and agreed well; δ (O_2/Ar) value given by the cryogenic method was not significantly different from the value using chromatographic method, although the latter uncertainty was very large. The standard deviation of new cryogenic method was compared with previous studies shows sufficient analytical precision (Table 6) .

In summary, the cryogenic separation method presented here had a sufficiently good performance in terms of its precision and accuracy for the determination of oxygen isotope ratios and the oxygen to argon ratio.

Table 5: Results of repeated analyses for 4 mL atmospheric air samples. All values are expressed relative to laboratory standard oxygen–argon mixture. The $\Delta^{17}O$ was calculated according to the equation $\Delta^{17}O = \ln(\delta^{17}O + 1) - \lambda\ln(\delta^{18}O + 1)$, where I adopted $\lambda = 0.518$. A correction with a constant zero enrichment factors on the isotope ratios (0.028 for $\delta^{17}O$ and 0.010 for $\delta^{18}O$) was applied. The bottom two rows are values determined using a gas chromatographic method (see text in detail).

date	$\delta^{17}O$(‰)	$\delta^{18}O$(‰)	$\Delta^{17}O$ (per meg)	$\Delta(O_2/Ar)$ (‰)
14-Apr-14	-1.631	-3.138	-4	51.5
14-Apr-14	-1.651	-3.071	-59	49.8
15-Apr-14	-1.664	-3.138	-37	49.6
15-Apr-14	-1.679	-3.195	-23	51.2
15-Apr-14	-1.673	-3.164	-33	47.8
15-Apr-14	-1.702	-3.218	-34	48.6
16-Apr-14	-1.701	-3.228	-28	48.7
17-Apr-14	-1.678	-3.197	-21	52.1
17-Apr-14	-1.670	-3.170	-27	50.7
17-Apr-14	-1.678	-3.193	-23	49.9
14-May-14	-1.674	-3.175	-28	48.9
14-May-14	-1.687	-3.225	-15	50.7
20-May-14	-1.720	-3.251	-35	46.7
21-May-14	-1.660	-3.180	-12	47.1
12-Jan-15	-1.663	-3.127	-42	45.1
14-Jan-15	-1.686	-3.141	-58	46.7
15-Jan-15	-1.695	-3.184	-45	46.7
22-Jan-15	-1.660	-3.151	-27	43.0
23-Jan-15	-1.719	-3.202	-59	43.7
26-Jan-15	-1.694	-3.176	-48	40.3
28-Jan-15	-1.719	-3.227	-46	41.9
29-Jan-15	-1.665	-3.141	-37	39.9
31-Jan-15	-1.670	-3.150	-38	40.1
2-Feb-15	-1.662	-3.107	-51	39.8
5-Feb-15	-1.708	-3.193	-52	43.7
9-Feb-15	-1.673	-3.109	-62	41.1
13-Feb-15	-1.715	-3.169	-73	42.5
14-Feb-15	-1.677	-3.149	-45	43.4
29-Jan-15	-1.731	-3.242	-50	44.2
3-Feb-15	-1.642	-3.068	-52	41.7
10-Mar-15	-1.666	-3.154	-31	44.1
12-Mar-15	-1.682	-3.174	-37	45.7
16-Mar-15	-1.665	-3.120	-48	46.0
18-Mar-15	-1.657	-3.118	-41	44.8
26-Mar-15	-1.677	-3.180	-29	44.3
30-Mar-15	-1.705	-3.227	-32	44.8
4-Mar-15	-1.726	-3.221	-57	43.6
4-Mar-15	-1.706	-3.216	-38	42.9
Average	**-1.682**	**-3.171**	**-39**	**45.6**
SD	**0.024**	**0.045**	**15**	**3.6**
Assigned value	**–1.689**	**–3.210**	**–25**	**63**
SD	**0.039**	**0.064**	**17**	**15**

Table 6: Comparison of 1 SD values with previous studies

Reference	$\delta^{17}O$ (‰)	$\delta^{18}O$ (‰)	$\Delta^{17}O$ (per meg)
Angert et al. 2003	NA	0.02	5
Barkan and Luz 2003	0.056	0.028	N/A
Hendricks et al. 2004	NA	0.06	9
Helman et al. 2005	0.056	0.028	N/A
Eisenstadt et al. 2010	0.056	0.028	N/A
Juranek and Quay 2010	0.06	0.025	60
Quay et al. 2010	0.01	0.05	43
This study	**0.021**	**0.044**	**15**

3.2 Isotopic and molecular fractionations during gas desorption from the MSZ

The magnitudes of isotopic and molecular fractionations with different amounts of MSZ are plotted in Fig. 12. The average isotopic fractionation by one, two and 3 pellets 1/8" mesh 5A was 0.025±0.007 ‰, -0.153±0.006 ‰ and -0.167±0.006 respectively. In the case of 13X shows less fractionation and one, two and three pellets have an average values -0.022±0.006 ‰, -0.014±0.006 ‰ and -0.064±0.006 ‰ respectively. In the case of a single MSZ pellet (70 mg), the use of both 5 A and 13 X MSZ resulted in insignificant isotopic fractionations in oxygen isotopes. Significantly lower values of $\delta^{17}O$ and $\delta^{18}O$ were found when using 140 and 210 mg of 5 A, while for 13X, the isotopic values were significantly lower than the original value only when 210 mg was used. The $\Delta^{17}O$ values were not dependent on the amount and type of MSZ, which confirmed the results of a previous study (Abe 2008; Luz and Barkan 2000; Luz et al. 1999; Thiemens 2002; Thiemens and Heidenreich 1983). These results confirm that the isotopic fractionation process during gas desorption from the MSZ is mass dependent.

The molecular fractionation results for the oxygen–argon mixture were linearly correlated with the amount of MSZ (Fig. 2C). The average isotopic fractionation by one, two and three pellets of 13X molecular sieve was -2.9±1.7 ‰ (SD), -8.7±1.3 ‰ and -14.8±1.6 ‰ respectively. Similarly in the case of 5 A shows more fractionation and the average values are -11±1.7 ‰ (SD), -20.6±1.4 ‰ and -24.7±1.5 ‰. The use of 5A MSZ induced a larger molecular fractionation than the use of 13X, but the slope of the linear regression indicated similar values:

For 13X MSZ,

$\delta(O_2/Ar) = -0.090\ MSZ + 2.8,\ R^2 = 0.99;$

For 5A MSZ,

$\delta(O_2/Ar) = -0.10\ MSZ - 5.4,\ R^2 = 0.94.$

Based on these results, the use of the least amount of MSZ is recommended to minimise isotopic and molecular fractionations. For oxygen–argon mixtures greater than 1.2 mL STP, equivalent to 6 mL of atmospheric air, insignificant isotopic fractionation was achieved with the use of a single pellet (70 mg) of 13X MSZ, although slight fractionation was found in molecular composition. However, this was negated if the sample and air standards were prepared in the same manner.

3.3 Application of this method to determine equilibrium isotope fractionation during gas exchange between air and water

The equilibration experiment was conducted by bubbling and stirring of seawater and deionised water at a constant water temperature of 25°C. The results of the equilibrium isotope fractionation between air and water are summarised in Table 7. The average (average ± SE) oxygen isotope ratios ($\delta^{17}O$ and $\delta^{18}O$) of deionised water bubbling was 0.335 ± 0.013 ‰ and 0.637± 0.021 ‰ respectively, and stirring was yielded an oxygen isotopic fractionation of 0.369± 0.009 ‰ and 0.702 ± 0.017 ‰. However the equilibration of seawater yielded a slightly different fractionation while compared with deionised water equilibration. The average dissolved oxygen isotopic fractionation at equilibrium with atmospheric air was significantly lower than deionised water, the average ± SE of $\delta^{17}O$ and $\delta^{18}O$ was measured as 0.319± 0.012 ‰ and 0.603± 0.021 ‰ for stirring and the average ± SE of $\delta^{17}O$ and $\delta^{18}O$ was measured as 0.305± 0.006 ‰ and 0.579 ± 0.011 ‰ respectively.

Table 7. Isotopic and molecular fractionations that occurred during the use of MSZ at liquid nitrogen temperature during the trapping and transfer of eluted gases. The $\delta^{17}O$ and $\delta^{18}O$ values are corrected for average zero enrichment values

Amount of MSZ (mg)	Difference from original composition using 5A				Difference from original composition using 13X			
	$\delta^{17}O$ (‰)	$\delta^{18}O$ (‰)	$\Delta^{17}O$ (per meg)	$\delta(O_2/Ar)$ (‰)	$\delta^{17}O$ (‰)	$\delta^{18}O$ (‰)	$\Delta^{17}O$ (per meg)	$\delta(O_2/Ar)$ (‰)
70	0.03 ± 0.08	0.00 ± 0.03	27 ± 74	–11.0 ± 2.3	–0.02 ± 0.01	–0.01 ± 0.06	–16 ± 18	–2.9 ± 1.8
140	–0.07±0.04	–0.11 ± 0.09	–20 ± 10	–20.6 ± 2.1	–0.01 ± 0.03	0.00 ± 0.06	–14 ± 11	–8.8 ± 1.8
210	–0.13± 0.04	–0.23 ± 0.02	–10 ± 50	–24.7 ± 4.3	–0.06 ± 0.11	–0.10 ± 0.15	33 ± 61	–14.8 ± 4.1

I also measured oxygen to argon molecular ratios of equilibrated water samples at 25 °C by bubbling and stirring. Seawater stirring and bubbling produced an average ± SE of δ (O_2/Ar) was -86±2 ‰ and -87±3 ‰ respectively. Deionised water stirring and bubbling produced an average ± SE of δ (O_2/Ar) was -87±1 ‰ and -89±3 ‰ respectively. The water equilibration at 25 °C yielded an average value of δ (O_2/Ar) of dissolved gas at saturation with atmospheric air was -87±2 ‰. Neither the method of equilibration nor the water salinity does not have a large significant effect on molecular fractionation.

The difference in $\delta^{18}O$ of 0.702 ‰ for stirred DW was consistent with the results of previous studies that ranged from 0.691 ‰ to 0.722 ‰. Furthermore, our value was identical to the result given by Benson and Krause (Benson et al. 1979), which was obtained by a polynomial regression of data observed between 0 and 60 °C. Stanley et al. (Stanley et al. 2010) and Kaiser (Kaiser 2011) suggested that the choice of equilibration method might influence the fractionation factor. For both DW and SW, the δ values were slightly higher when stirring than bubbling, but the $\Delta^{17}O$ values were similar. Our $\Delta^{17}O$ values were closer to those reported by Stanley et al. (Stanley et al. 2010) for DW and Reuer et al. (Reuer et al. 2007) for SW, which were obtained by the stirring method, and significantly different from other results produced using the bubbling method.

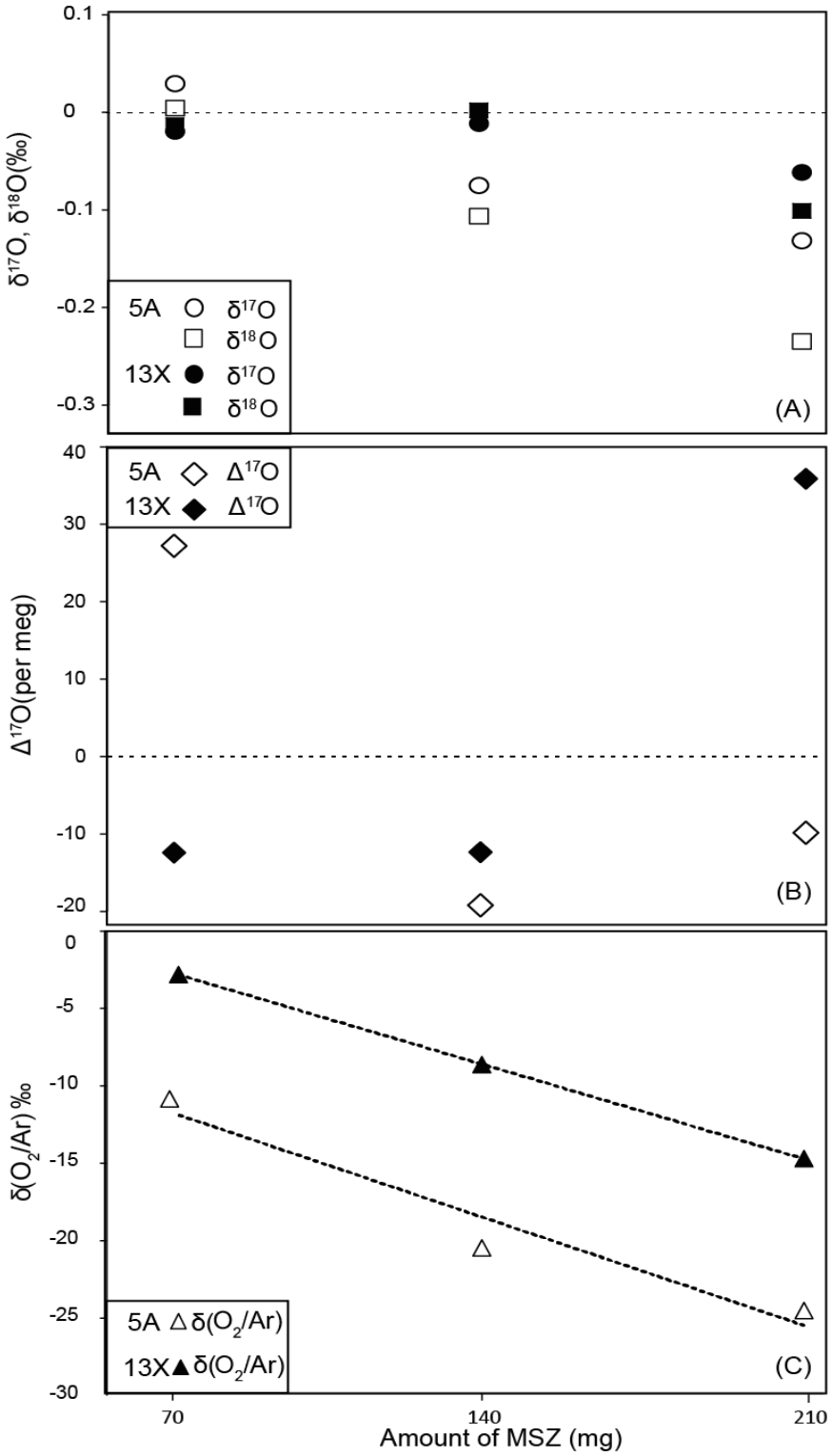

Figure 11: Isotopic and molecular fractionations that occurred during the use of MSZ at liquid nitrogen temperature for trapping and transfer of eluted gas. (A) Shows the isotopic fraction is insignificant while using single pellet of 5A and one or two pellets of 13X MSZ. (B) $\Delta^{17}O$ was unaffected during this adsorption and desorption process of gases on MSZ. (C) Molecular fractionation is linearly correlated with amount MSZ, and the trend is identical for both 5A and 13X MSZ.

3.4 Hydrographical parameters

Hydrographical parameters Temperature, salinity, dissolved oxygen and nutrients of MR07-01 cruise were obtained from *R.V. MIRAI* data sheet. Expertized technicians in the ship analyzed all the parameters. Hydrographical profile of each location was measured using CTD (Sea-Bird Electronics, Inc., USA) sensor attached to a rosette sampler.

3.5 Temperature (Potential temperature), salinity and dissolved oxygen

In situ CTD temperature along with salinity and water column pressure were used to calculate potential temperature at each depth of sampling location. I used potential temperature to perform the calculation of argon concentration at each sampling depth. Salinity of subsampled water was measured using high accuracy salinometer (Model 8400B "AUTOSAL" ; Guildline Instruments Ltd.) the salinometer had a measurement range of 0.005 to 42 (PSU) with an accuracy better than ±0.002. The instrument was standardized using IAPSO Standard Seawater with a standard deviation of 0.0004 in salinity.

Station 1 (EQ, 155 °E)

The salinity and temperature profile of this station has plotted in figure12. This station was characterized with shallow mixed layer ~50 m, surface salinity minimum layer and salinity maximum layer just below and then constant salinity water. The highest temperature at this station 29.8 °C was recorded at surface layer up to a depth 50 m and then it decreased to 1.68 °C at the bottom at 2400 m. At thermocline the temperature drop was very sharp, within 350 m temperature was decreased by 20 °C to 9.5 °C at 400 m.

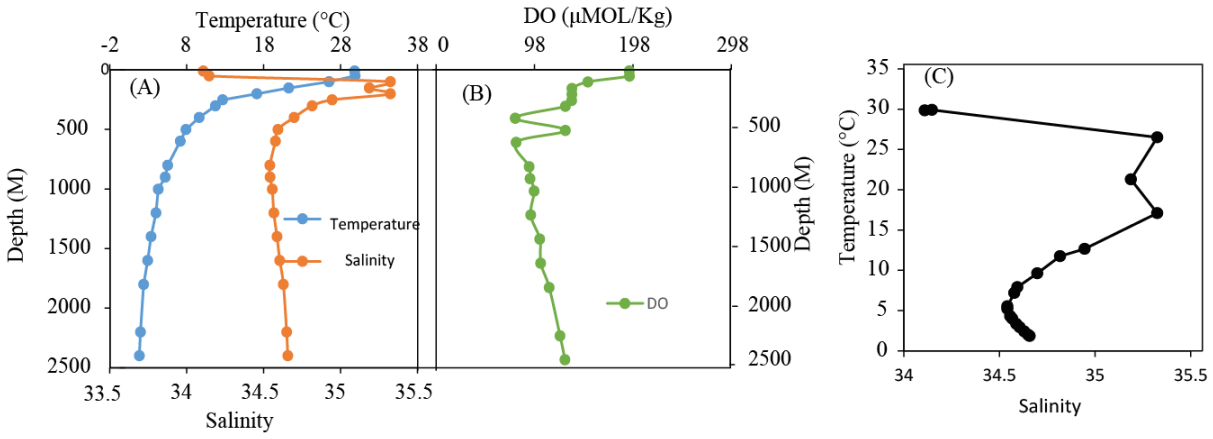

Figure 12: Distribution of temperature, salinity, dissolved oxygen T-S diagram at equator.

A very normal salinity pattern was observed at this station, at surface salinity was minimum 34.1 PSU that was highly dependent on local weather condition at each location. At a depth of 100 and 200 meters I observed two salinity maxima of 35.32 PSU, in between these two depths, at 150 there was a slight salinity minimum of 35.18 PSU. Equatorial salinity minimum of 32.5 PSU was observed a depth of 800 to 1000 m, however at this station the salinity minimum depth was broad and deep, after this salinity minimum zone the values were started increasing gradually towards bottom. At this station deep water was having a constant salinity below 500 m. The T- S diagram of this station was plotted in figure 12 C the pattern different water bodies, surface low salinity- high temperature (mixed layer), subsurface high salinity and low salinity-temperature at 800 m having a density of 27.3 σ_θ. The distribution of dissolved oxygen was plotted in figure 12B. At surface the dissolve oxygen was supersaturated by 1.5 % having a corresponding DO concentration of 194.7 µmol/ Kg that was then decreased towards bottom. The DO shows unique pattern at this station, the concentration was a constant 136 µmol/ Kg from 150 m to 250 m, and the DO minimum was observed at depth of 400 m and 600 m, where the concentration was 78.6 µmol/ Kg and 79.4 µmol/ Kg, however an abnormal DO maxima was observed between those DO minimum depth at 500 m, that depth DO was 129.4 µmol/ Kg, below 600 m the DO was increasing with depth and reached a bottom maximum of 129 µmol/ Kg at 2400 m.

Station 2 (5 °N, 155 °E)

Hydrographic parameters of this station were plotted in figure 13. Mixed layer depth at this station was also ~50 m, and a similar standard temperature salinity profile were observed however the dissolved oxygen profile was slightly different from previous station. At surface the temperature was maximum and salinity was minimum.

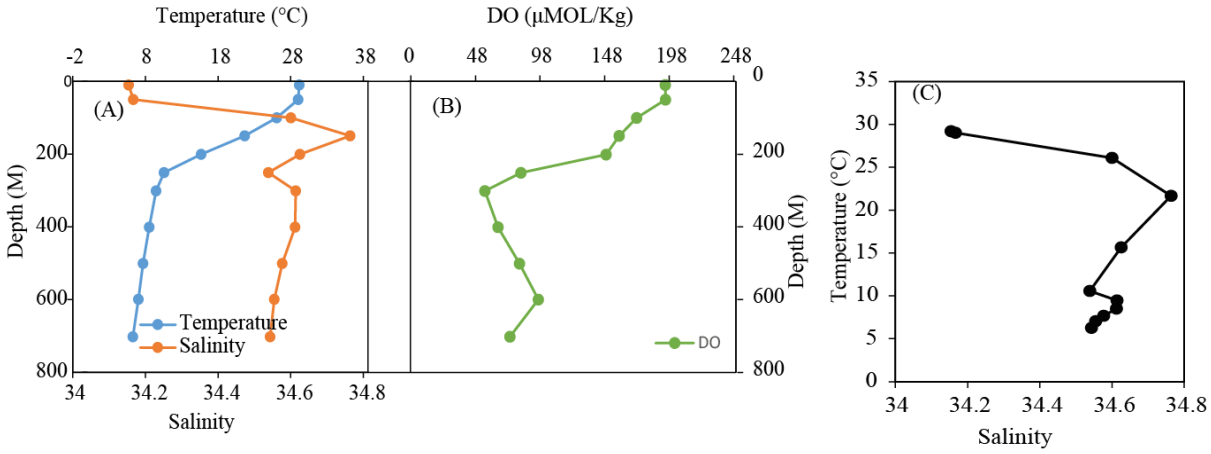

Figure 13: Distribution of temperature, salinity, dissolved oxygen T-S diagram at station 5 °N.

A maximum surface temperature of 29.2 °C was reduced sharply to 10.5 °C at 250 m through the shallow thermocline. Deepest sample was collected at 700M was having lowest temperature of 6.2 °C. Surface sample was having lowest salinity at this station, below the mixed layer salinity was increased to a maximum value of 34.76 PSU at 150 m and then it decreased to a salinity minimum at 250 m, and then increased to another salinity maximum. At this station two clear distinct salinity maxima were observed at 150 m and 300-400 m. after the two salinity maxima, it was started decreasing gradually in deep water without any significant change in its pattern. These two salinity maxima was clearly observed in T-S diagram of this station (21.6, 34.7) and (9.4, 34.6) having a corresponding density of 24.18 σ_θ and 26.75 σ_θ respectively and the salinity minimum water was observed at density of 26.5 σ_θ, the salinity minimum was too sharp, that means very thin salinity minimum water layer. The depth profile of dissolved oxygen was plotted in the figure 13 B. Dissolved oxygen concentration at this station was varied between 100.6 and 19.7 corresponding to a concentration of 195.1 and 55.2 µmol/ Kg. At surface the DO was supersaturated by 0.6 % and surface DO concentration was 195 µmol/ Kg. which was then decreased steadily to a minimum of 55.2 µmol/ Kg at 300 m, which was then increased to 96.7 at 600 m, however at 700 m the DO was 74.6 µmol/ Kg.

Station 3 (10 °N, 155 °E)

Mixed layer depth at this station was started deepening as a result of surface water-cooling, the depth was approximately 50 m. The temperature was maximum 27.9 °C at surface and started decreasing drastically in thermocline. A temperature change of 14 °C was observed in the thermocline of this station within a change of 100 m, below the thermocline water was gradually cools down and reached a temperature of 4.5 °C at 1000 m.

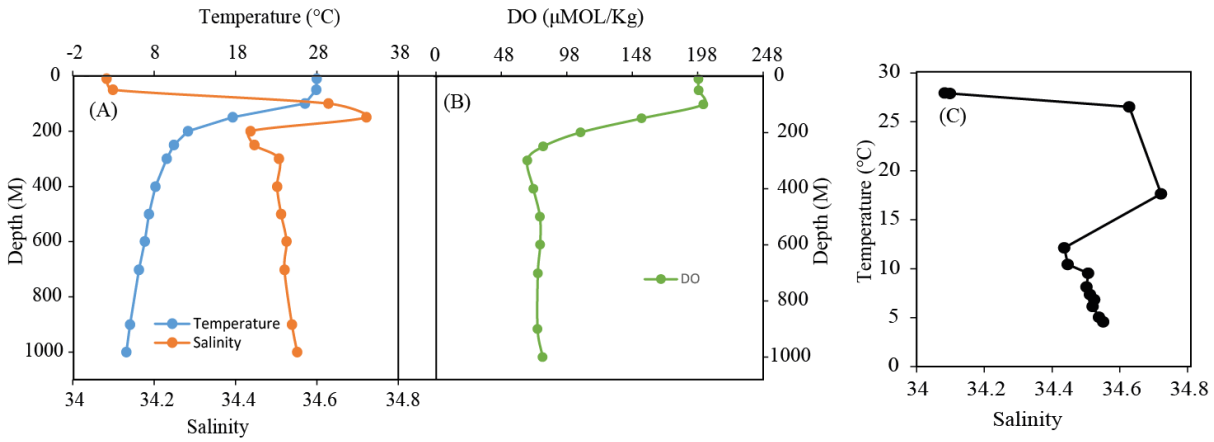

Figure 14: Distribution of temperature, salinity, dissolved oxygen T-S diagram at station 10 °N.

The salinity was minimum 34.08 PSU at surface mixed layer and the value was increased along the thermocline and reached a salinity maximum layer at 150 m. Immediately after this maxima salinity decreased rapidly to a salinity minimum (34.4 PSU) layer at 200 m. there was a small salinity hike at 300 m and then salinity was increasing slightly until 1000 m. T-S diagram shows a salinity maximum (17.6, 34.7) and salinity minimum (12.1, 34.4) corresponding to a depth of 150 and 200 m respectively. The effect NPIW was not so strong at this station. The profile of dissolved oxygen concentration was potted in figure 14 C. At surface dissolved oxygen was saturated, and it was varied between 100.4 % at the surface and 24.3 % at 300 m with a corresponding DO concentration of 198.6 µmol/ Kg and 67.9 µmol/ Kg respectively. Below 500 m, the DO concentration was constant until deepest sampling depth of 1000 m. Mixed layer depth started deepening as a result of cold surface water, at this location depth of mixed layer was ~100 m. The depth profile of salinity and temperature was plotted in figure 14. At the surface water temperature was maximum 27.2 °C was decreased rapidly through thermocline until 400 m, the temperature decrease was slow in deep water. About 18 °C temperature change occurred between a depth of 100 and 400 m (change was 0.06 °C/M).

Station 4 (15 °N, 155 °E)

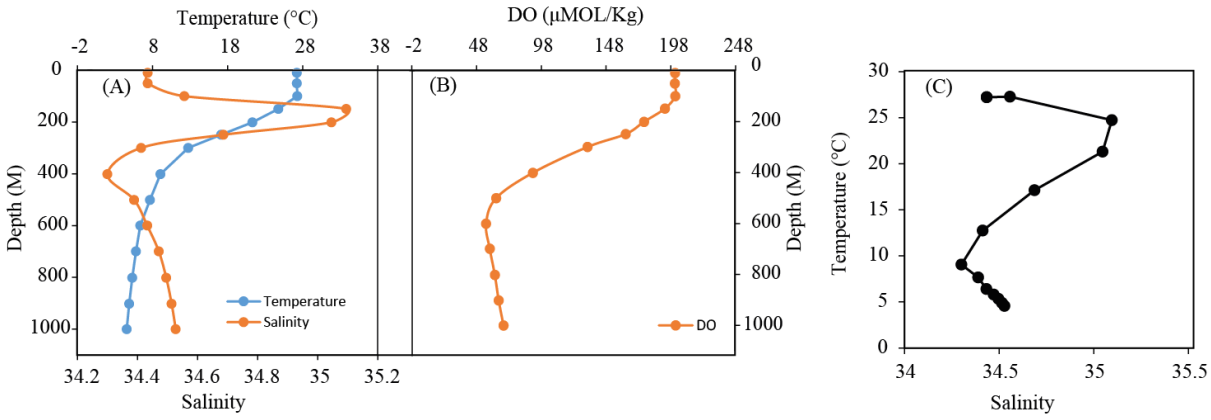

Figure 15: Distribution of temperature, salinity, dissolved oxygen T-S diagram at station 15 °N.

At this station salinity profile was showing very distinct salinity maximum and minimum layers. At surface salinity were 34.4 that increased sharply in thermocline to a salinity maximum of 35.09 at 150 m, after this salinity maximum it reduced drastically to a salinity minimum of 34.3 at 400 m. at this station salinity minimum layer was comparatively thin. Below salinity minimum layer its value increases towards bottom of the station. T-S diagram of this station shows clear water masses namely north pacific surface water, north pacific intermediate water and deep water. However that does not satisfy the minimum conditions of the NPIW. The density of water at this salinity minimum zone was 26.5 σ_θ. Dissolved oxygen profile was plotted in the figure 15 B. The dissolved oxygen saturation was varied between 100.7 % and 18.4 % at depth of surface and 700 m respectively corresponding to a 201.2 % and 55.4 %. Below 600 m the DO was increased gradually towards bottom.

Station 5 (20 °N, 155 °E)

Mixed layer depth at this station was ~50 m. The depth profile of salinity and temperature was plotted in figure 16. Surface and thermocline salinity was distinguished by a salinity maximum at 150 m. Lowest temperature at this station was 3.95 °C recorded at 1000 m. At the surface water temperature was maximum 26.4 °C was decreased rapidly through thermocline until 600 m, the temperature decrease was slow in deep water. About 20 °C temperature change occurred between a depth of 100 and 600 m, however temperature change per meter was reduced than previous station and it is about 0.04 °C/M. This was the last station where salinity profile was showing very distinct salinity maximum and minimum layers. At surface salinity was 34.8 which increased sharply in thermocline to a salinity maximum of 35.0 at 150 m, after this salinity maximum it reduced drastically to a salinity minimum of 34.1 at 600 m. at this station salinity minimum layer was started thickening. Below salinity minimum layer its value increases towards bottom of the station. T-S diagram of this station shows clear water masses namely north pacific surface water, north pacific intermediate water and deep water. However that does not satisfy the minimum salinity potential density anomaly conditions of the NPIW. Dissolved oxygen profile was plotted in the figure 16 B. The dissolved oxygen saturation was varied between 100.7 % and 18.4 % at depth of surface and 700 m respectively corresponding to a 202.8 % and 49.5 %. Below 800 m the DO was increased gradually towards bottom. Another notable point was the depth of DO minimum was increasing while moving from equator to northern most stations, at this station the increase in DO minimum zone was about 200.

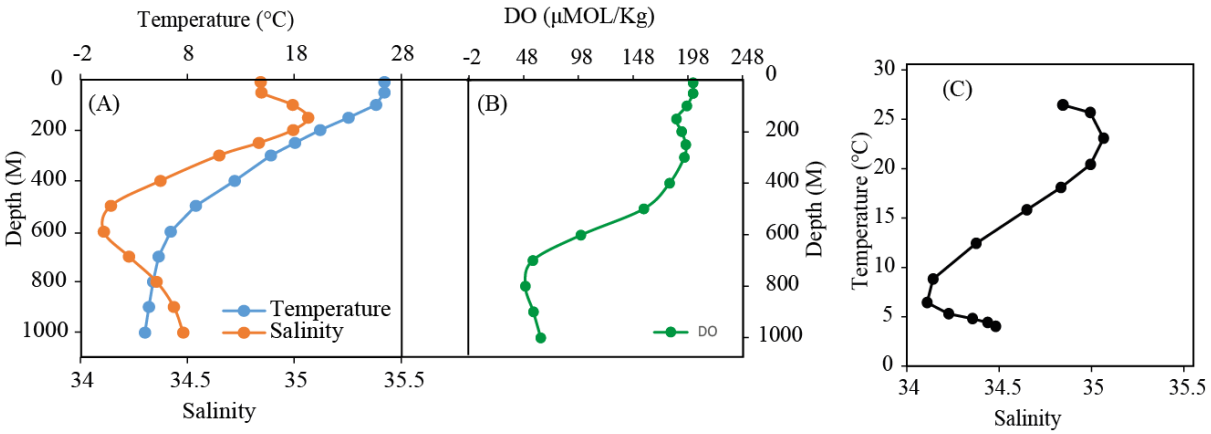

Figure 16: Distribution of temperature, salinity, dissolved oxygen T-S diagram at station 20 °N.

Station 6 (24 °N, 155 °E)

Mixed layer depth of this station was very thin, and the depth was around 10 m even though the water temperature was lower than previous stations. . At the surface water temperature was maximum 23.7 °C was decreased rapidly through thermocline until 800 m. At this there was no subsurface salinity maximum like previous stations. At surface salinity was 35.0 which increased reduced drastically to a salinity minimum of 34.0 at 700 m. at this station salinity minimum layer was started thickening. Below salinity minimum layer its value increases towards bottom of the station. T-S diagram of this station shows clear water masses namely north pacific surface water, north pacific intermediate water and deep water. At this station the water at 700 m satisfies the minimum salinity potential density anomaly conditions of the NPIW. The T-S diagram shows different pattern from the previous station having no subsurface maximum peak. However the Dissolved oxygen profile was plotted in the figure 17B. The dissolved oxygen saturation was varied between 100 % and 183 % at depth of surface and 1000 m respectively corresponding to a 208.5 % and 50.4 %. Another notable point was the depth of DO minimum was increasing while moving from equator to northern most stations, the deepest sampling location was identified as DO minimum zone of this station and no data available below this depth.

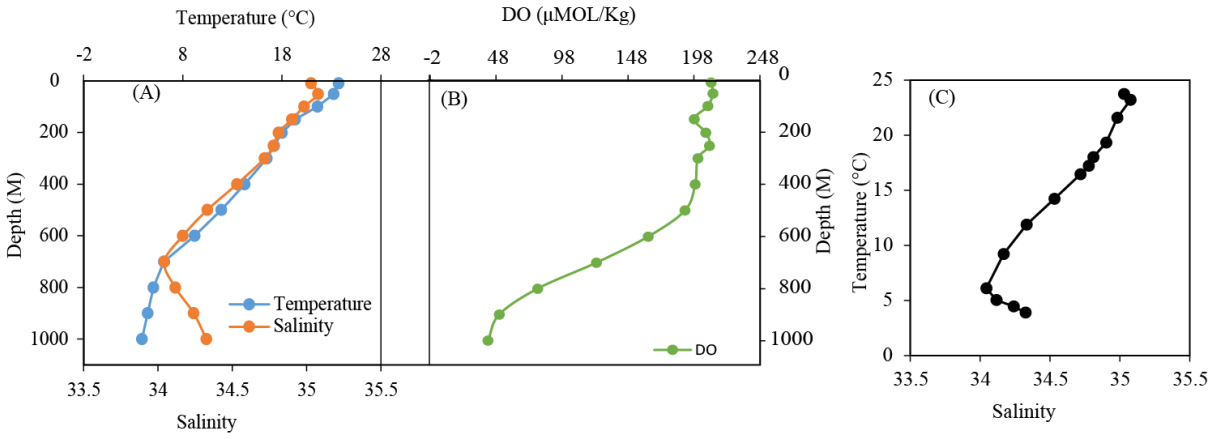

Figure 17: Distribution of temperature, salinity, dissolved oxygen T-S diagram at station 24 °N.

Station 7 (30 °N, 155 °E)

Mixed layer depth of this station was found maximum thick, and the depth was around 200 m because of the cold surface water and the station was characterized by north pacific mode water and Kuroshio Current start flowing eastward. At the surface water temperature was maximum 18.2 °C was decreased rapidly through thermocline to 3.9 °C at 1000 m. At this there was no subsurface salinity maximum like previous stations. At surface salinity was 34.7 which increased reduced drastically to a salinity minimum of 34.0 at 700 m. at this station salinity minimum layer was started thickening. Below salinity minimum layer its value increases towards bottom of the station. T-S diagram of this station shows clear water masses namely north pacific surface water, north pacific intermediate water and deep water. At this station the water at 700 m satisfies the minimum salinity potential density anomaly conditions of the NPIW. The T-S diagram shows different pattern from the previous station having no subsurface maximum peak. However the Dissolved oxygen profile was plotted in the figure 18 B. Dissolve oxygen concentrations was found constant in the mixed layer. The dissolved oxygen saturation was varied between 99 % and 16 % at depth of surface and 1000 m respectively corresponding to a 230.5 % and 53.5 %. Another notable point was the depth of DO minimum was increasing while moving from equator to northern most stations, the deepest sampling location was identified as DO minimum zone of this station and no data available below this depth.

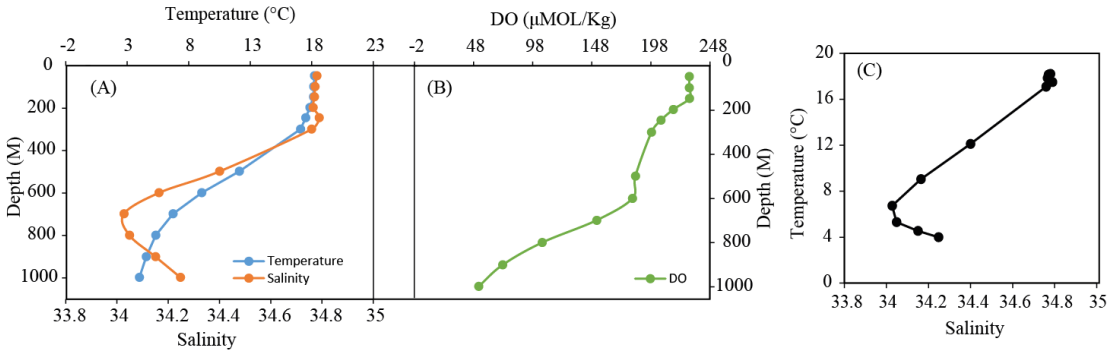

Figure 18: Distribution of temperature, salinity, dissolved oxygen T-S diagram at station 30 °N.

Station 8 (36 °N, 155 °E)

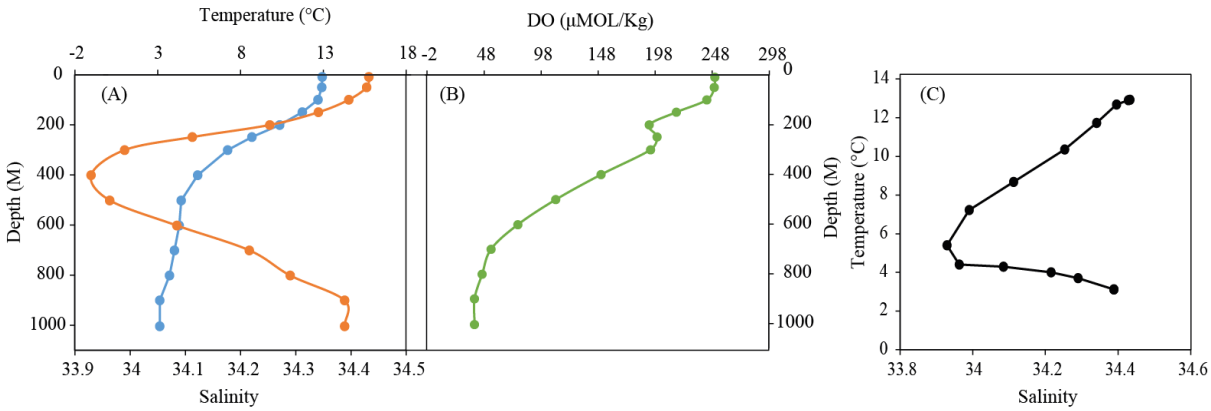

Figure 19: Distribution of temperature, salinity, dissolved oxygen T-S diagram at station 36 °N.

Mixed layer depth of this station was found thick, and the depth was around 100 m because of the cold surface water and the station was characterized by mixing zone of Kuroshio extension and Oyashio current. At the surface water temperature was maximum 12.9 °C was decreased rapidly through thermocline to 3.0 °C at 1000 m. At this there was no subsurface salinity maximum like previous stations. At surface salinity was 34.4 which increased reduced drastically to a salinity minimum of 33.9 at 400 m. at this station salinity minimum layer was maximum thick. Below salinity minimum layer its value increases towards bottom of the station. T-S diagram of this station shows clear water masses namely north pacific surface water, north pacific intermediate water and deep water. At this station the water at 700 m satisfies the minimum salinity potential density anomaly conditions of the NPIW. The T-S diagram shows different pattern from the previous station having no subsurface maximum peak. The shape t-s diagram was like a “C”. The dissolved oxygen profile was plotted in the figure 19B. Dissolve oxygen concentration was found constant in the mixed layer. The dissolved oxygen saturation was varied between 97 % and 12 % at depth of surface and 1000 m

respectively corresponding to a 250.3 % and 39.6 %. The deepest sampling location was identified as DO minimum zone of this station and no data available below this depth. This station was characterized by lowest oxygen saturation at both surface and bottom.

A conclusion of the distribution of hydrographical pattern was given below. The section diagram of hydrographical parameters salinity, dissolved oxygen and potential temperature were plotted in the figure 20, 21 and 22 respectively. The sampling depths for hydrographical parameters were marked in the figure 6. The water salinity along the study area was varied between 33.93 (400 m, 36 °N) and 35.32 (100 m, equator). The surface water salinity was minimum at equator to 20 °N than the thermocline at those stations, however equator to 10 °N the lowest salinity 34.12±0.03 was recorded at the surface. This surface salinity minimum was due to the local rainfall at the equatorial region which belongs to ITCZ (Maes et al. 2002). Equatorial and subtropical regions are the highly evaporative areas and thus below the subsurface minimum the salinity was increased to a maximum up to 35.32 (Figure 20). Below subsurface salinity maximum, it was decreases smoothly towards bottom, this unique character was observed between equator and 10°N. The highest surface water temperature of 29.8 °C was recorded at equator and the lowest temperature was recorded at high latitude stations. The water temperature was decreased drastically below the mixed layer through the thermocline. The temperature – salinity (T–S) diagram shows two distinct pattern for low (EQ, 5 °N, 10 °N and 15 °N) and high (20 °N, 24 °N, 30 °N and 36 °N) latitude stations. The low latitude stations were characterized by low salinity high temperature surface water, this low salinity surface water was almost diminished the stations north of 20 °N, however the high latitude stations were characterized by low salinity cold water at an intermediate depth is known as NPIW. The T–S diagram for low latitude stations were much scattered than the high latitude station. The core of NPIW is characterized by potential density around 26.8 σ_θ and salinity is lower than 34.25. This water originate from cold low saline water of sub polar region specifically Okhotsk sea around Kuril island (Talley 1991; Talley 1993; Yasuda 1997). Dissolved oxygen concentration in the study area was measured using Winkler titration method. The analytical precision of the Winkler method was within 0.05 μmol/Kg during MR07-01 cruise, however some studies shows the precision of Winkler method was within few μmol/Kg at oxygen minimum zones (Morrison et al. 1999; Paulmier and Ruiz-Pino 2009). At the surface all the stations, the surface water was saturated or slightly super saturated with oxygen. Towards north the surface water oxygen saturation was decreased. The lowest oxygen super saturation of 12 %

was recorded in the North Pacific Ocean the oxygen minimum zone (OMZ) was recorded between 900 to 1300 m (27.2 to 27.4σ_θ).

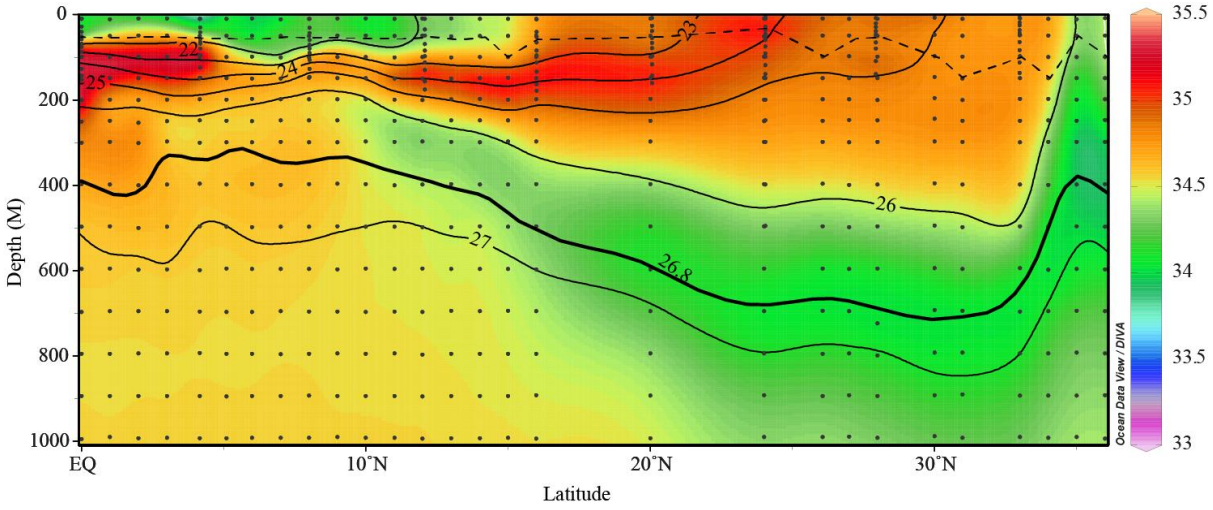

Figure 20: Section diagram of salinity long with overlaying potential density anomaly σ_θ along the study area showing the location of North Pacific intermediate water. As a result of local weather condition associated ITCZ in the equatorial region; the surface water was less saline than subsurface water. Core of NPIW has a salinity less than 34.25 and density around 26.8 σ_θ, a bold density isoline (26.8 σ_θ) represent the core of NPIW. The dotted line on the top of the figure represents the mixed layer depth along the study area.

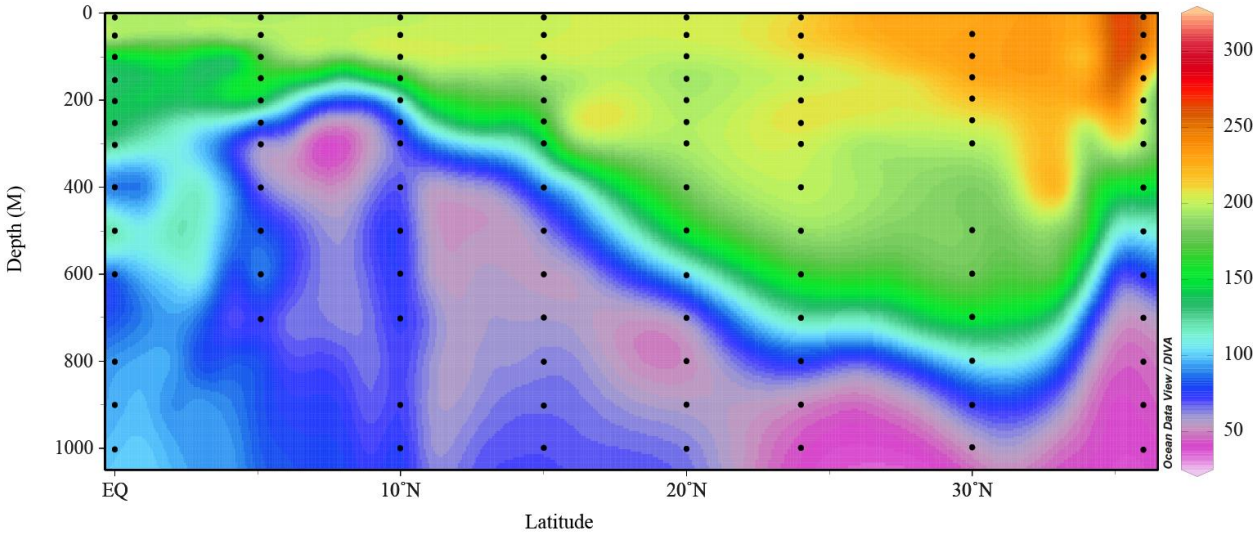

Figure 21: The section diagram of dissolved oxygen concentration along the study area. The doted points in the figure represent the depth of water sampling for the determination of dissolved oxygen isotope and molecular ratios.

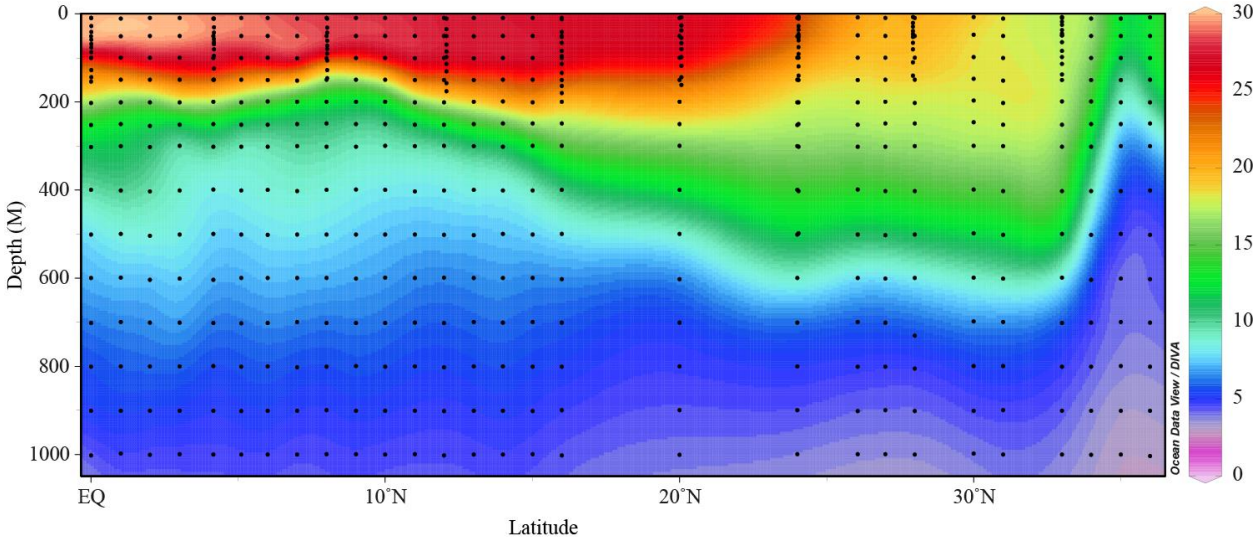

Figure 22: The section diagram of potential temperature along the study area. The doted point in the figure represent the depth of water sampling the determination of hydrographical parameters.

3.6 Dissolved oxygen isotope ratios, oxygen isotope anomaly and argon saturation

All oxygen isotope ratios and oxygen isotope anomaly were subjected for argon interference correction and the data were expressed in delta relative to atmospheric oxygen. The ^{17}O excess ($\Delta^{17}O$) was defined as $\Delta^{17}O = \ln(\delta^{17}O + 1) - \lambda \ln(\delta^{18}O + 1)$, where I adopted $\lambda = 0.518$ (Luz and Barkan 2009; Reuer et al. 2007; Sarma et al. 2006; Stanley et al. 2010). The oxygen to argon ratio was expressed as $\delta(O_2/Ar) = (O_2/Ar)_{sam}/(O_2/Ar)_{ref} - 1$. Argon saturation is defined as $\Delta Ar = [Ar] / [Ar]_{sat} - 1 \times 100$. Where [Ar] was calculated from the measured $\delta(O_2/Ar)$ and [Ar_{sat}] was the saturation concentration of argon and is theoretically calculated from temperature and salinity according to Hamme and Emerson 2004 (Hamme and Emerson 2004).

The uncertainties associated with the cryogenic purification were being monitored for last a year, the results of repeated analysis of atmospheric air was plotted in the figure 11. The analytical precision of our new method was consistent for $\delta^{17}O$, $\delta^{18}O$ and $\Delta^{17}O$, the average values were -1.68±0.02 ‰ (SD), -3.17±0.05 ‰ (SD) and -39±15 per meg (SD). However the analytical precision of $\delta(O_2/Ar)$ was significantly different between two sets of analysis, the

average value for April-2014 to May 2014 was 49.5±1.6 ‰ (SD) and for January 2015 to March 2015 the average was 43.3±2.1 ‰ (SD). Even though the extraction procedure for oxygen–argon mixture was same during the study period, the observed significant difference in $\delta(O_2/Ar)$ could be generated from the mass spectrometer condition. All of the samples of this study was analyzed during January 2015 to March 2015, thus the results will not be affected by this large variation observed in the $\delta(O_2/Ar)$.

Station 1 (EQ, 155 °E)

At equator the surface mixed layer value of oxygen isotopes $\delta^{17}O$ and $\delta^{18}O$ were negative, the values were -0.442 ‰ and -1.049 ‰ respectively (Figure 23A). In the mixed layer of this station all the $\delta^{17}O$ and $\delta^{18}O$ were negative and below mixed layer it increased to maxima. In the thermocline as a result of respiration and less photosynthesis the $\delta^{17}O$ and $\delta^{18}O$ were increased and values are 4.645 ‰ and 8.799 ‰ respectively at 400 m. in this station the $\delta^{17}O$ and $\delta^{18}O$ was showing two maxima and minima at depth around 200, 400 m and 250 and 500 m respectively.

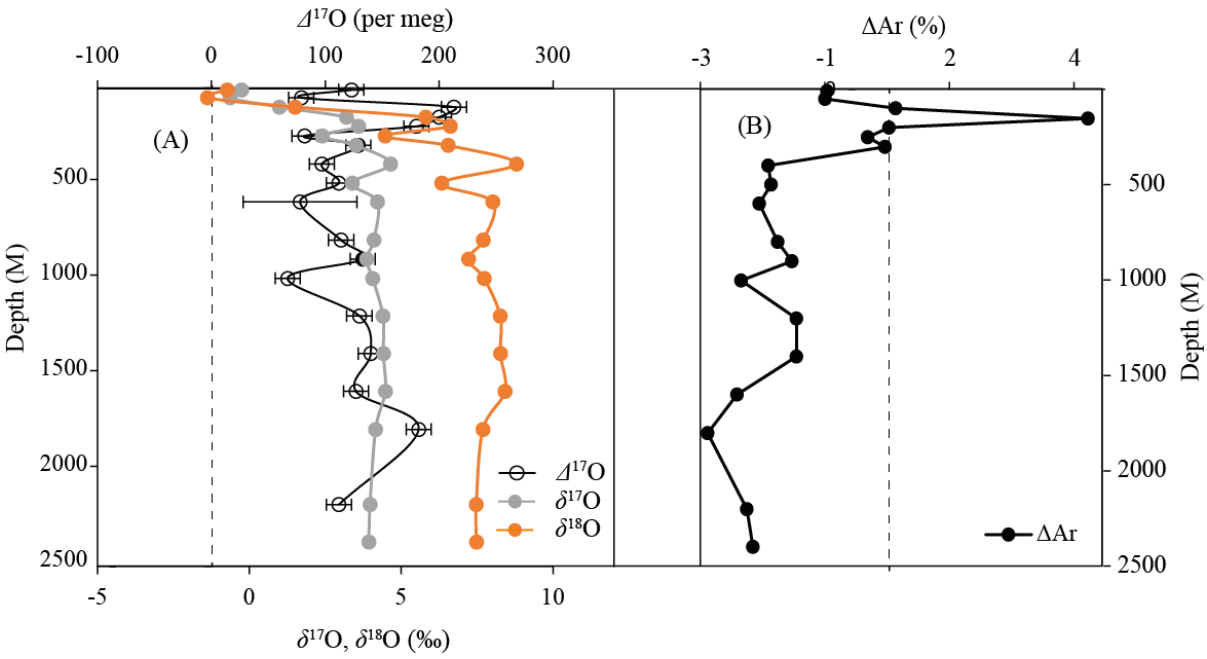

Figure 23: Distribution of dissolved oxygen isotope ratios, dissolved oxygen isotope anomaly and argon anomaly at equator.

The minimum peak at 500 meter was corresponding to maximum oxygen water at this station. Below 600 m the oxygen isotope ratios were almost constant. Oxygen isotope anomaly $\Delta^{17}O$ of dissolved oxygen at the surface was 123 per meg and which was increased to 200 per meg in the thermocline (Figure 23A). The average mixed layer $\Delta^{17}O$ was 101 per meg. The $\Delta^{17}O$ was almost constant varing below 300 m, having an average value of 104±21 per meg, however at 1000 m the lowest value of 67 was recorded. At the surface the water, the argon concentration was at slightly undersaturation with atmospheric air and ΔAr values are close to zero (Figure 23B). The ΔAr was varied between 3.5% and -2.6 %. At all the stations mixed layer sample shows same results, that means the measured argon concentration was more close to calculated saturation value, this also validate the method and the calculations are appropriate. In the thermocline at 150 m the ΔAr shows maximum value of 4.2% and the depth is characterized by maximum salinity and $\Delta^{17}O$. Below 300 m all the ΔAr shows negative.

Station 2 (5 °N, 155 °E)

At the station 5 °N the surface value of oxygen isotopes $\delta^{17}O$ and $\delta^{18}O$ were negative, the values were -0.696 ‰ and -1.47 ‰ respectively (Figure 24A). In the mixed layer of this station all the $\delta^{17}O$ and $\delta^{18}O$ were negative and below mixed layer it increased to maxima. In the thermocline as a result of respiration and less photosynthesis the $\delta^{17}O$ and $\delta^{18}O$ were increased and values were 5.689 ‰ and 10.925 ‰ respectively at 300 m. in this station the $\delta^{17}O$ and $\delta^{18}O$ was showing only one maxima at 300 m, below that it was decreasing smoothly towards bottom. The minimum peak at 500 meter was corresponding to maximum oxygen water at this station.

Oxygen isotope anomaly $\Delta^{17}O$ of dissolved oxygen at the surface was 66 per meg and which was increased to 166 per meg in the thermocline (Figure 24A). The average mixed layer $\Delta^{17}O$ was 55 per meg. A constant $\Delta^{17}O$ was recorded between a depth of 250 m and 600m. The minimum $\Delta^{17}O$ value was obtained at 700 meters.

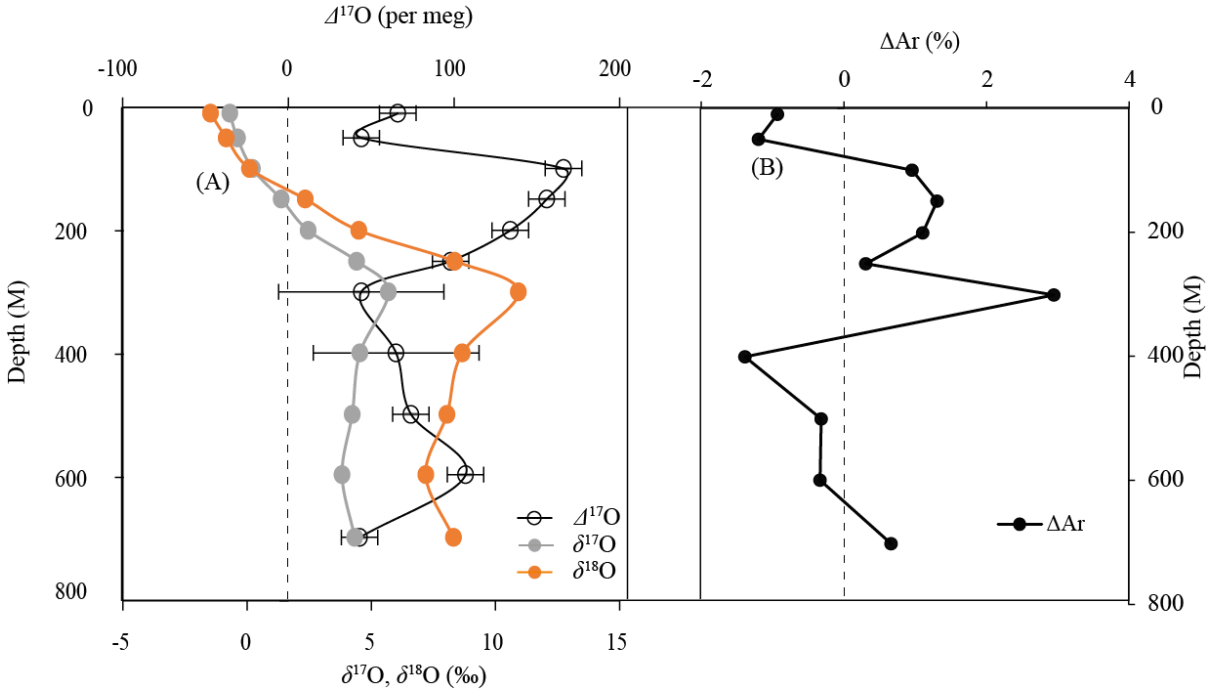

Figure 24: Distribution of dissolved oxygen isotope ratios, dissolved oxygen isotope anomaly and argon anomaly at station 5 °N.

At the surface the water, the argon concentration was at slightly undersaturation with atmospheric air and ΔAr values are close to zero (Figure 24B). The ΔAr was varied between 2.9 % and -1.4 %. At all the stations mixed layer sample shows same results, that means the measured argon concentration was more close to calculated saturation value, this also validate the method and the calculations are appropriate. In the thermocline at 150 m the ΔAr shows maximum value of 2.9 %, below thermocline the ΔAr was showing negative at only one depth of 400 m, and then it was started increasing towards bottom.

Station 3 (10 °N, 155 °E)

At the station 10 °N the surface value of oxygen isotopes $\delta^{17}O$ and $\delta^{18}O$ were very small, the values were 0.20 ‰ and 0.09 ‰ respectively (Figure 25A). Below 10 m the oxygen isotope ratios were decreasing until 200 m up to a value of -0.31 and -0.81. In the mixed layer of this station all the $\delta^{17}O$ and $\delta^{18}O$ were negative and below mixed layer it increased to maxima because of respiration and less photosynthesis the $\delta^{17}O$ and $\delta^{18}O$ were increased and values were 4.97 ‰ and 9.46 ‰ respectively at 300 m. below that it was decreasing smoothly towards bottom.

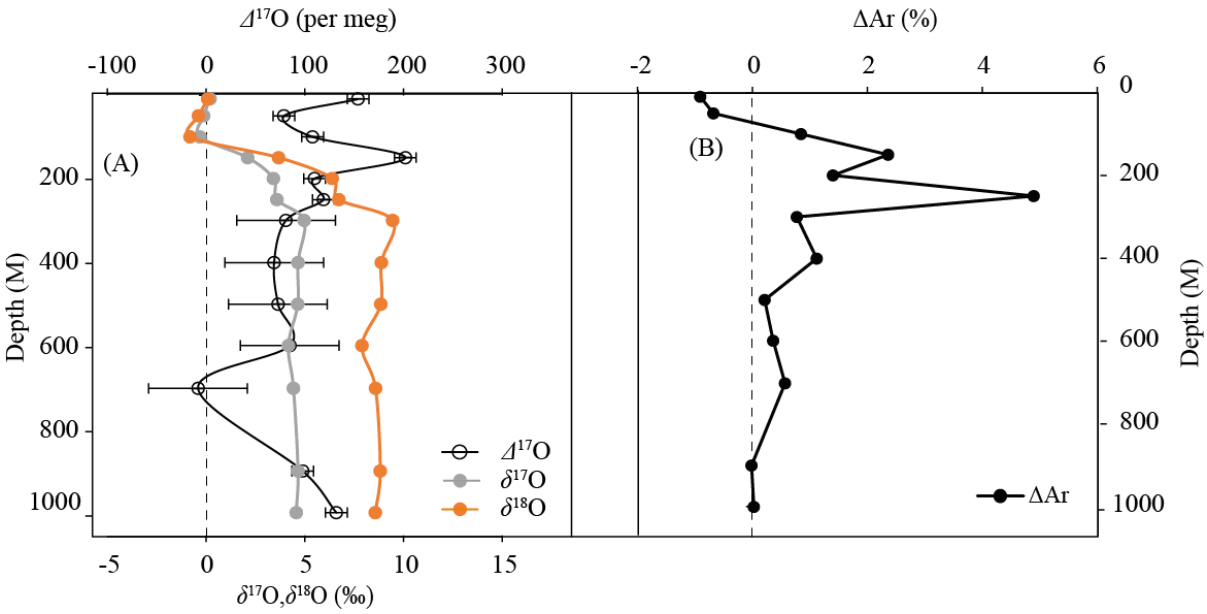

Figure 25: Distribution of dissolved oxygen isotope ratios, dissolved oxygen isotope anomaly and argon anomaly at station 10 °N.

Oxygen isotope anomaly $\Delta^{17}O$ of dissolved oxygen at the surface was 154 per meg and which was increased to 202 per meg in the thermocline at 150 m (Figure 25A). The average mixed layer $\Delta^{17}O$ was 116 per meg. The $\Delta^{17}O$ was almost constant between 300 and 1000 m.

At the surface the water, the argon concentration was at slightly undersaturation with atmospheric air and ΔAr value, which was significantly different from zero (Figure 25B). The ΔAr was varied between 4.9 % and -0.6 %. Below the mixed layer the ΔAr in all the sampling depth of this station shows positive. In the thermocline at 150 m the ΔAr shows small than the peak at 250M the corresponding values are 2.2 %, and 4.9 % respectively. Below 250 m the ΔAr was very small, the values at 900 and 100 meter it was not significantly different from zero

Station 4 (15 °N, 155 °E)

At the station 15 °N the surface value of oxygen isotopes $\delta^{17}O$ and $\delta^{18}O$ were negative, the values were -0.06 ‰ and -0.36 ‰ respectively (Figure 26A). In the mixed layer of this station all the $\delta^{17}O$ and $\delta^{18}O$ were negative and which was then decreased to a lowest value of -0.49 ‰ and -1.1 ‰ observed at 150 m. below the mixed layer as a result of respiration and less photosynthesis the $\delta^{17}O$ and $\delta^{18}O$ were increased and values were 5.27 ‰ and 10.18 ‰

respectively at 600 m. Below 600 m it was decreasing smoothly towards bottom. Another interesting point of this station was the oxygen isotope maximum depth was increased about 300 m to 600 m while comparing with previous station, Oxygen isotope anomaly $\Delta^{17}O$ of dissolved oxygen in the surface was 131 per meg and which was increased to 171 per meg in the thermocline (Figure 26A). The average mixed layer $\Delta^{17}O$ was 91 per meg. The $\Delta^{17}O$ was almost constant until the deep sample at 1000 m, the negative values for $\Delta^{17}O$ was mainly because high analytical uncertainty associated with those samples.At the surface the water, the argon concentration was at slightly undersaturation with atmospheric air and ΔAr values are close to zero (Figure 26B). The ΔAr was varied between 2.3 % and -0.8 %. At all the stations below mixed layer sample shows argon supersaturation except a single depth at 800 m. at this station the maximum ΔAr was observed at 1000 m not at thermocline, However at this station also ΔAr was showing a peak at 150 m like previous station. Below mixed layer the ΔAr was showing peaks at 150 m, 300 m, 700 m and 100 m.

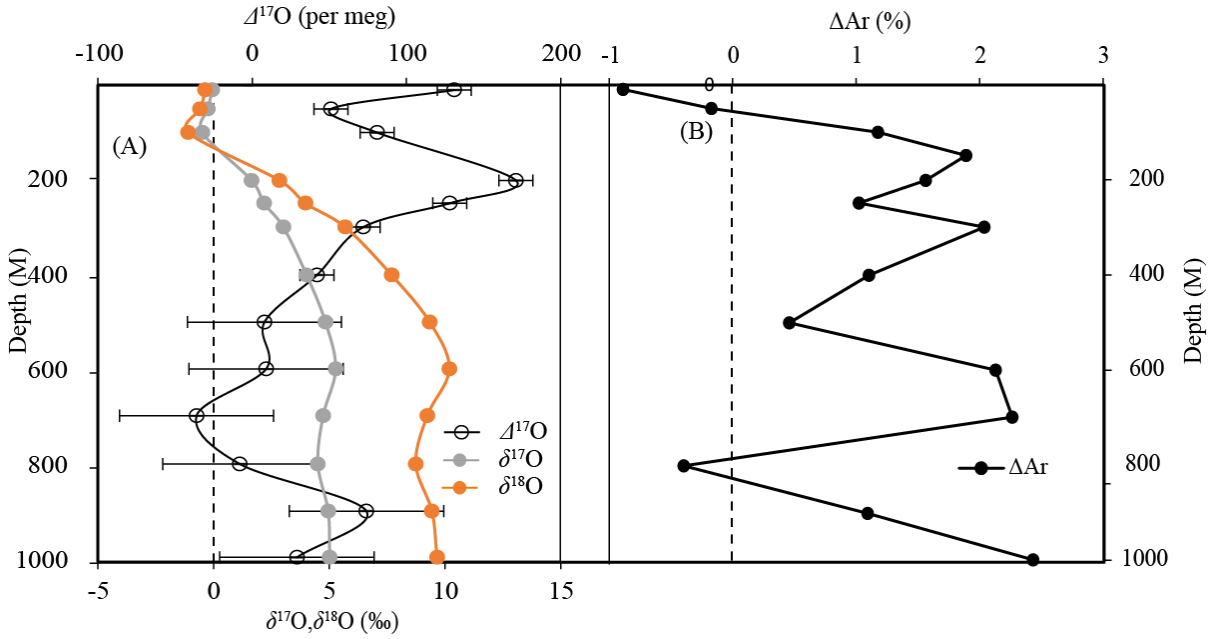

Figure 26: Distribution of dissolved oxygen isotope ratios, dissolved oxygen isotope anomaly and argon anomaly at station 15 °N.

Station 5 (20 °N, 155 °E)

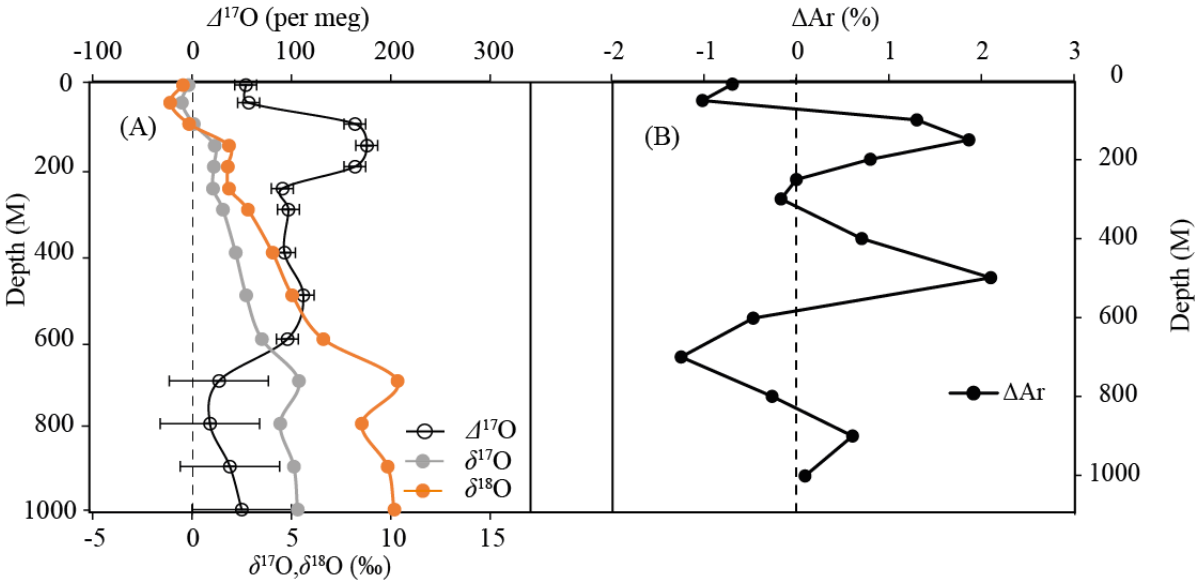

Figure 27: Distribution of dissolved oxygen isotope ratios, dissolved oxygen isotope anomaly and argon anomaly at station 20 °N.

At the station 20 °N the surface value of oxygen isotopes $\delta^{17}O$ and $\delta^{18}O$ were negative, the values were -0.18 ‰ and -0.45 ‰ respectively (Figure 27A). In the mixed layer of this station all the $\delta^{17}O$ and $\delta^{18}O$ were negative and which was then decreased to a smallest value of -0.51 ‰ and -1.1 ‰ observed at 50 m. below the mixed layer as a result of respiration and less photosynthesis the $\delta^{17}O$ and $\delta^{18}O$ were increased and values were 5.37 ‰ and 10.35 ‰ respectively at 700 m. Below 700 m it was decreasing smoothly towards bottom. Another interesting point of this station was the oxygen isotope ratios were increasing very gradually up 400 m, and then it was increased drastically to a maximum at 700M. The $\delta^{17}O$ and $\delta^{18}O$ were almost constant at a depth from 150 to 250 m. Oxygen isotope anomaly $\Delta^{17}O$ of dissolved oxygen in the surface water was 54 per meg and which was increased to 176 per meg below the mixed layer (Figure 27A). The average mixed layer $\Delta^{17}O$ was 56 per meg. The peculiarity of this station was only one $\Delta^{17}O$ maximum peak, which consist of three consecutive sampling depth from 100 m to 200 m, the difference in $\Delta^{17}O$ within those sampling was not significant and the average value was 168±7 per meg. The $\Delta^{17}O$ was almost constant below 600 m until

the deep sample at 1000 m. At the surface the water, the argon concentration was at lightly undersaturation with atmospheric air and ΔAr values are close to zero (Figure 27B). The ΔAr was varied between 2.2 % and -1.3 %. At this below mixed layer sample shows argon undersaturation at depths 300 m and in between 600 m and 800 m. At this station the maximum ΔAr was observed at 500 m not at thermocline, however at this station also ΔAr was showing a peak at 150 m like previous station. Below mixed layer the ΔAr was showing peaks at 150 m, 500 m and 900 m.

Station 6 (24 °N, 155 °E)

At the station 24 °N the surface value of oxygen isotopes $\delta^{17}O$ and $\delta^{18}O$ were positive unlike previous stations, the values were 0.25 ‰ and 0.38 ‰ respectively (Figure 28A). In the mixed layer of this station all the $\delta^{17}O$ and $\delta^{18}O$ were positive and which was then increased as a result of respiration and less photosynthesis, the $\delta^{17}O$ and $\delta^{18}O$ values were 6.47 ‰ and 12.47 ‰ respectively at 1000 m. there was no sample and data were available below the 1000 m to know the trend oxygen isotope ratios. Another interesting point of this station was the oxygen isotope ratios were negative at a depth of 200 m, and the values were -0.47 ‰ and -1.04 ‰ respectively. Oxygen isotope anomaly $\Delta^{17}O$ of dissolved oxygen in the mixed layer was 58 per meg and which was increased to 139 per meg below the mixed layer (Figure 28A). The average mixed layer $\Delta^{17}O$ was 59 per meg. Below $\Delta^{17}O$ maximum, it was decreased irregularly, and the $\Delta^{17}O$ almost constant below 400 m until the deep sample at 1000 m. At the surface the water, the argon concentration was at lightly undersaturation with atmospheric air and ΔAr values are close to zero (Figure 28B). The ΔAr was varied between 6.0 % and -0.4 %. At this below mixed layer sample shows argon undersaturation at depths 200 m. At this station the maximum ΔAr was observed at 1000 m not at thermocline, however at this station also ΔAr was showing a peak at 150 m like previous station. Another notable point was the intensity of ΔAr peak at 150 m started reducing, and it was further decreasing towards northern most

stations.

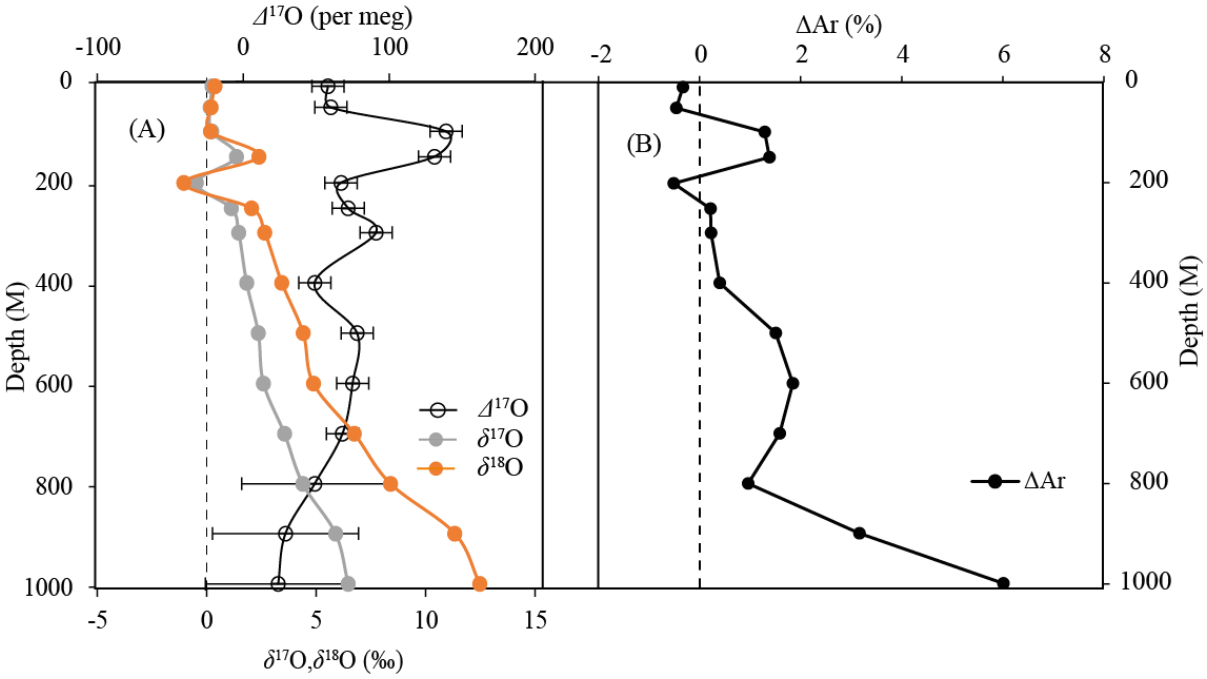

Figure 28: Distribution of dissolved oxygen isotope ratios, dissolved oxygen isotope anomaly and argon anomaly at station 24 °N.

Station 7 (30 °N, 155 °E)

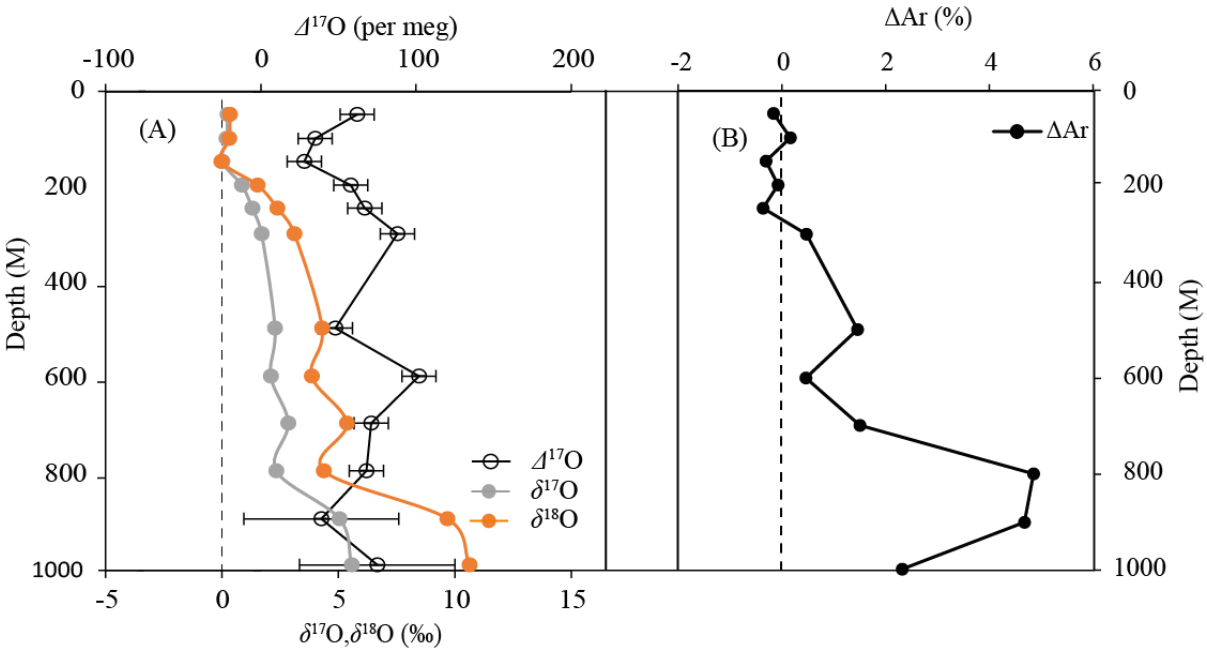

Figure 29: Distribution of dissolved oxygen isotope ratios, dissolved oxygen isotope anomaly and argon anomaly at station 30 °N.

This station was characterized the most thickly mixed layer among all the other stations, and the thickness of mixed layer depth at this station was 200 m. At the station 30 °N the surface value of oxygen isotopes $\delta^{17}O$ and $\delta^{18}O$ were positive unlike previous stations, the values were 0.24 ‰ and 0.34 ‰ respectively (Figure 29A). In the mixed layer of this station all the $\delta^{17}O$ and $\delta^{18}O$ were positive and which was then increased as a result of respiration and less photosynthesis, the $\delta^{17}O$ and $\delta^{18}O$ values were 5.57 ‰ and 10.64 ‰ respectively at 1000 m. there was no sample and data were available below the 1000 m to know the trend oxygen isotope ratios. Another interesting point of this station was the oxygen isotope ratios were increasing gradually until a depth of 800 m, below that depth it was increased drastically from 4.37 ‰ to 9.68 ‰ for $\delta^{18}O$. Oxygen isotope anomaly $\Delta^{17}O$ of dissolved oxygen in the surface was 62 per meg and which was increased to 100 per meg below the mixed layer (Figure 29A). The average mixed layer $\Delta^{17}O$ was 46 per meg. Below 700 m the $\Delta^{17}O$ was found constant until 1000 m. At the surface the water, the argon concentration was at lightly undersaturation with atmospheric air and ΔAr values are close to zero (Figure 29B).

The ΔAr was varied between 4.8 % and -0.3 %. At this station below mixed layer sample shows argon undersaturation at depths 200 m. At this station the maximum ΔAr was observed at 1000 m not at thermocline, however at this station also ΔAr was showing a peak at 150 m like previous station. Another notable point was the intensity of ΔAr peak at 150 m started reducing, and it was further decreasing towards northern most stations. The ΔAr was increasing below 600 m and reached a maximum of 4.8 % and 4.7 % at 800 and 900 m respectively, and then decreased at 1000 M

Station 8 (36 °N, 155 °E)

This station was characterized the thick mixed layer depth at this station was 100 m. At the station 36 °N the surface value of oxygen isotopes $\delta^{17}O$ and $\delta^{18}O$ were positive unlike low latitude stations, the values were 0.41 ‰ and 0.68 ‰ respectively (Figure 30A). In the mixed layer of this station all the $\delta^{17}O$ and $\delta^{18}O$ were positive and which was then increased as a result of respiration and less photosynthesis, the $\delta^{17}O$ and $\delta^{18}O$ values were 6.07 ‰ and 11.65 ‰ respectively at 1000 m. there was no sample and data were available below the 1000 m to know the trend oxygen isotope ratios. Another interesting point of this station was the oxygen isotope ratios were increasing gradually until 1000 m.

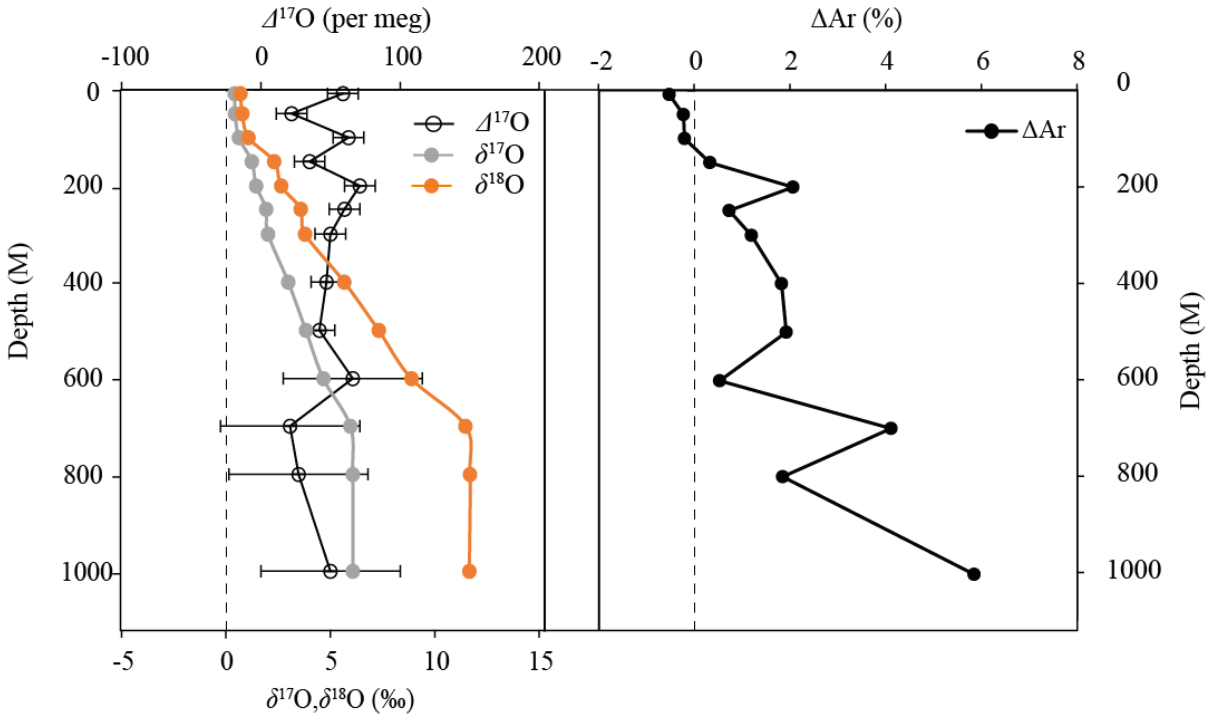

Figure 30: Distribution of dissolved oxygen isotope ratios, dissolved oxygen isotope anomaly and argon anomaly at station 36 °N.

Oxygen isotope anomaly $\Delta^{17}O$ of dissolved oxygen in the surface water was 97 per meg (Figure 30A). The average mixed layer $\Delta^{17}O$ was 95 per meg. Below $\Delta^{17}O$ maximum, it was decreased irregularly. At the surface the water, the argon concentration was at lightly undersaturation with atmospheric air and ΔAr values are close to zero (Figure 30B). The ΔAr was varied between 5.8 % and -0.7 %. At this station below mixed layer all depths shows argon supersaturation. At this station the maximum ΔAr was observed at 1000 m not at thermocline, however at this station also ΔAr was showing a peak at 200 m like previous station.

Combined and common features of oxygen isotope composition, oxygen isotope anomaly and argon saturation was given below. For simplicity in compilation the sampling stations were grouped into two groups, (1) Low latitude stations (EQ, 5 °N, 10 °N and 15 °N) and (2) high latitude stations (20 °N, 24 °N, 30 °N and 36 °N).

3.7 The $\delta^{18}O$

The dissolved oxygen isotope ratio is a measure of gas exchange, photosynthesis and respiration in the open ocean, which always have an inverse relationship with oxygen saturation. In the study area the $\delta^{18}O$ was varied from -1.47 ‰ to +12.47 ‰ in all the depths. In the mixed layer the $\delta^{18}O$ was varied between -1.49 and 1.53, more notably the surface dissolved oxygen

isotope ratios were negative from equator to 20 °N and at all other stations the $\delta^{18}O$ was positive and close to zero. Moving from equator to northern most sampling station, the mixed layer $\delta^{18}O$ increases and reached close to equilibrium value at 36 °N. The $\delta^{18}O$ was observed a maximum below photic zone having dominant microbial respiration. All the low latitude stations (EQ, 5 °N, 10 °N and 15 °N) show a distinct $\delta^{18}O$ maximum at a depth between 250 m and 600 m, however $\delta^{18}O$ maxima of subtropical stations (20 °N, 24 °N, 30 °N and 36 °N) seems to be below 1000 m (deepest sampling depth). Below mixed layer the $\delta^{18}O$ increases with depth along with decrease in oxygen saturation and reached a maximum value of +12.47 ‰ at 1000 m of 24 °N at which the oxygen saturation was 13.1 % (figure 32).

At equator below mixed layer the $\delta^{18}O$ increased as like a general pattern, however it was observed two minima at a depth of 250 m and 500 m, out of that peaks at 500 m corresponds to a high oxygen concentration while comparing with nearby sampling depths. This indicates some particular source of high oxygen water at that depth. A similar observation was noticed at 200 m of station 30 °N, where the $\delta^{18}O$ was minimum and the dissolved oxygen concentration at that station was 207 μmol/Kg. At 5 °N and 10 °N the distribution of $\delta^{18}O$ was similar, the $\delta^{18}O$ maximum was observed at 300 m for both stations.

At the boundary between the mixed layer and thermocline the $\delta^{18}O$ was close to $\delta^{18}O_{eq}$ or higher. The shallowest $\delta^{18}O$ maximum was observed at equatorial stations, this is because of the strong stratification and upwelling of high oxygen deep water. Below mixed layer the $\delta^{18}O$ was increased linearly from 0.7 ‰ to 12.4 ‰ along with a sharp decrease of oxygen saturation. The northern most stations were characterized with highest $\delta^{18}O$ in the study area, which are associated with low oxygen saturated water. This feature is because of respiration fractionate dissolved oxygen by selective utilization of light isotopes (Kroopnick and Craig 1976; Levine et al. 2009; Quay 1997). Our measurements of dissolved oxygen isotope ratios were within the published results from the same study region (Bender 1990; Hendricks et al. 2005). As result of gas exchange the surface dissolved oxygen isotopic composition will move towards an equilibrium value at respective water temperature (Benson et al. 1979; Keedakkadan and Abe 2015; Luz and Barkan 2009; Sarma et al. 2003). However the most of the measured values in the mixed layer were negative, especially in the surface mixed layer from equator to 20 °N and less than equilibrium ($\delta^{18}O_{eq} \approx$ 0.7 ‰) in other stations. Negative values of oxygen isotope ratios are because of the addition of photosynthetically produced oxygen, which has an oxygen isotope ratio of -22.96 ‰ for $\delta^{18}O$ (Guy et al. 1993) under slow wind and gas exchange. Figure 32 shows at equatorial region the mixed layer oxygen saturation

has little influence on $\delta^{18}O$, implying the dominance of photosynthesis over respiration. Thermocline at these stations can vary between 200 and 400 m depth (Lysne and Deser 2002). Oxygen isotopic fractionation in the oxygen minimum zone has a significantly different pattern from the overlaying water (figure 35). In the North Pacific Ocean there are two source of water, one is from NPIW and other one is high oxygen water from south pacific enters north pacific at a depth near oxygen minimum at north of 25 °N. Thus the mixing of newly ventilated NPIW water and old might produce a different pattern for fractionation line.

3.8 Dissolved oxygen isotope anomaly ($\Delta^{17}O$)

The dissolved oxygen isotope anomaly was determined along the study area and data were potted in figure 31. The measured range of oxygen isotope anomaly ($\Delta^{17}O$) was varied from -36 to 213 per meg at all depth of north western Pacific Ocean (Figure 31). The expected values for the $\Delta^{17}O$ in the oceanic environment must be within highest (+249 per meg) and lowest (+5 per meg) (Keedakkadan and Abe 2015; Luz and Barkan 2000). The maximum value for $\Delta^{17}O$ was observed well within the expected value, however the negative values are associated with highest analytical uncertainty. In the mixed layer the $\Delta^{17}O$ was varied between 22 and 154 per meg at 36 °N and 10 °N respectively. At the surface, the $\Delta^{17}O$ values were controlled by photosynthesis and gas exchange, photosynthesis increases the $\Delta^{17}O$ and gas exchange bring back it to an equilibrium value. All the mixed layer $\Delta^{17}O$ was within the literature values (Hendricks et al. 2005; Juranek and Quay 2010; Munro et al. 2013) except a single value at the surface of station 10 °N. The measured $\Delta^{17}O$ at surface (10 M) was always higher than 50 m. A peak $\Delta^{17}O$ area was observed just below the mixed layer at all stations at a depth between 150 m and 200 m, however going towards north this maxima was decreased from 190 per meg at 10 °N and this subsurface maximum was almost diminished north of 30 °N. Thin mixed layer through which light can penetrate into thermocline and thus producing significant photosynthetic oxygen characterized the equatorial region. Thus the subsurface $\Delta^{17}O$ maxima were due to the accumulation of photosynthetically produced oxygen in the stratified area below mixed layer. Below $\Delta^{17}O$ maximum zone, the $\Delta^{17}O$ was showing a unique pattern consist of two maxima and minima at all stations except 20 °N and 36 °N, where this pattern was not so clear. The equatorial station was showing opposite pattern to nearby sampling stations, the maxima was observed at 300 m and 900 m, and the minima was observed at 250 m. At higher latitudes (20 °N to 36 °N) the deep-water $\Delta^{17}O$ was found consistent at a depth between 700 m to 800M, which were characterized by core of the recently ventilated NPIW.

3.9 Argon anomaly (ΔAr)

Argon anomaly in ocean water is a measure of diaphicnal mixing, bubble injection, water mass cooling and heating. I have determined ΔAr in North Pacific Ocean along 155 °E, from equator to 36 °N by measuring $\delta(O_2/Ar)$ and solubility of argon at equilibrium at a particular temperature and salinity (Hamme and Emerson 2004) and the results were plotted in the figure 31 and 34. I compared our data with published (Emerson et al. 2012) data from same location, most of them were within the analytical precision. The observed ΔAr in the North Pacific Ocean was varied between -1.8 % and 6.0 %. Other studies observed a similar ΔAr in the equatorial Pacific Ocean and it was varied between 3 to -2.5 %, and maximum values were observed in the equatorial subsurface water and minimum was in the abyssal areas of Pacific Ocean (Gehrie et al. 2006). Along the study area the ΔAr minimum value of -1.8 % was observed at equator at depth of 1000 m and maximum value of 6.0 % was recorded at 1000 m of station 6 (24°N). Along the study area the mixed layer ΔAr was mostly negative and the values were varied from -1.2% to 1.2 %. A subsurface maximum ΔAr zone was observed below the mixed layer at a depth of around 150 m. In addition to that, the low latitude stations were characterized by another positive peak at a depth around 250 – 300 m. At equator the ΔAr was negative below 300 m the water was undersaturated with argon until bottom (2372 M). The GCM model predicted argon anomaly (Ito and Deutsch 2006) in the subsurface waters of low and middle latitude stations was showing similar trend with determined ΔAr along the study area. This consistent argon undersaturation below 300 m can be a representative of column of water produced at high latitude where ΔAr can easily be negative due to water mass cooling. Similar negative values were observed at 5 °N and 10 °N at a depth between 400 m to 600 m and 600 m to 800 m respectively. Deep water was formed as result of subduction surface water in the Polar and sub Polar Regions and will be exploring the possible source this argon undersatuated water mass.

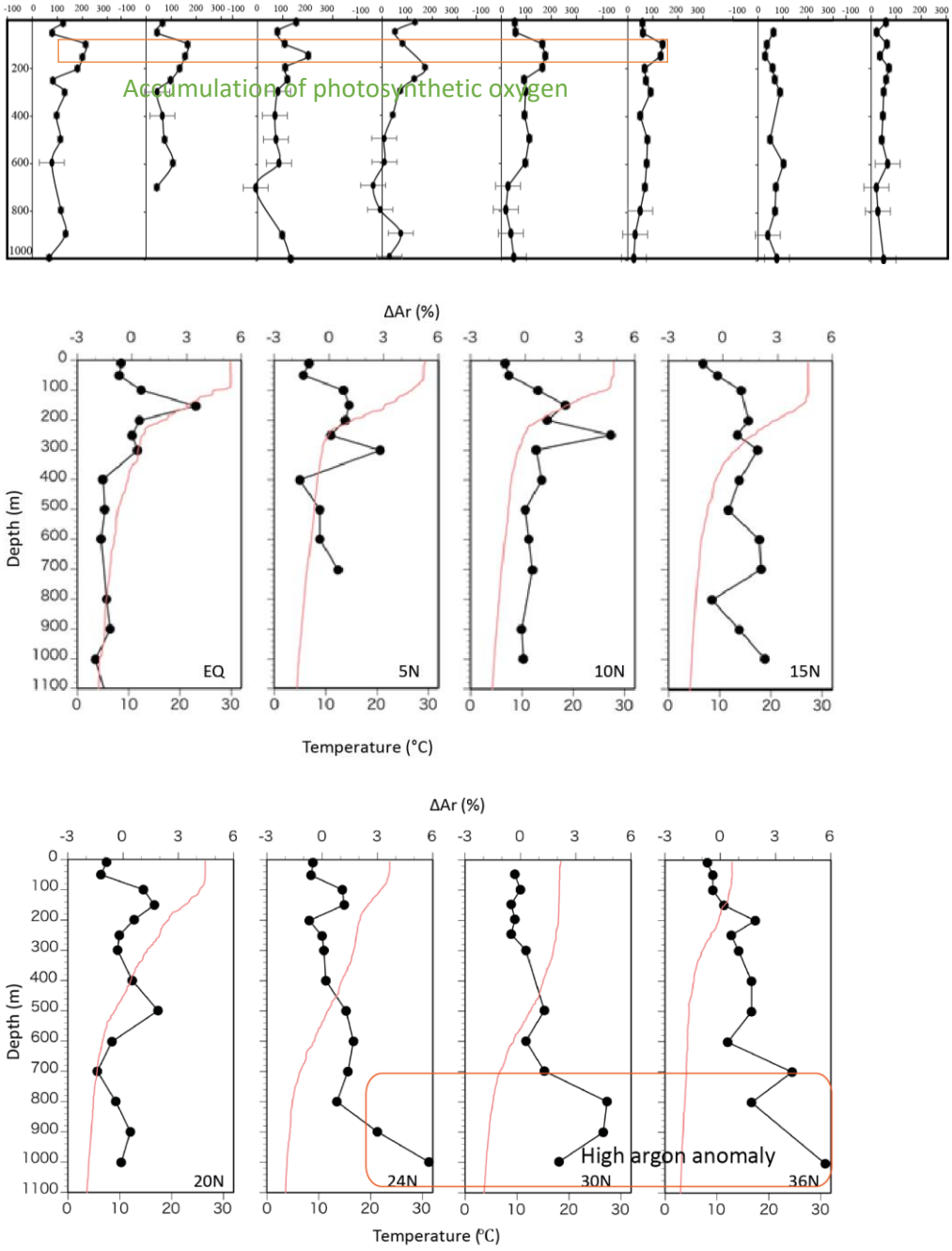

Figure 31: Results of triple oxygen isotope ratios ($\delta^{18}O$ and $\Delta^{17}O$) and argon saturation (ΔAr) along the North Pacific Ocean. Separate plots were made for results of equatorial stations (EQ – 15 °N) and northern most stations (20 °N to 36 °N).

I have determined ^{18}O respiration fractionation (α^{18}_R) for the mixed layer community along the study area as 0.982 using equation 10, which agrees well with other published values ranging from 0.977 to 0.985 (Guy et al. 1993; Kiddon et al. 1993; Quay et al. 1993; Helman et al. 2005).

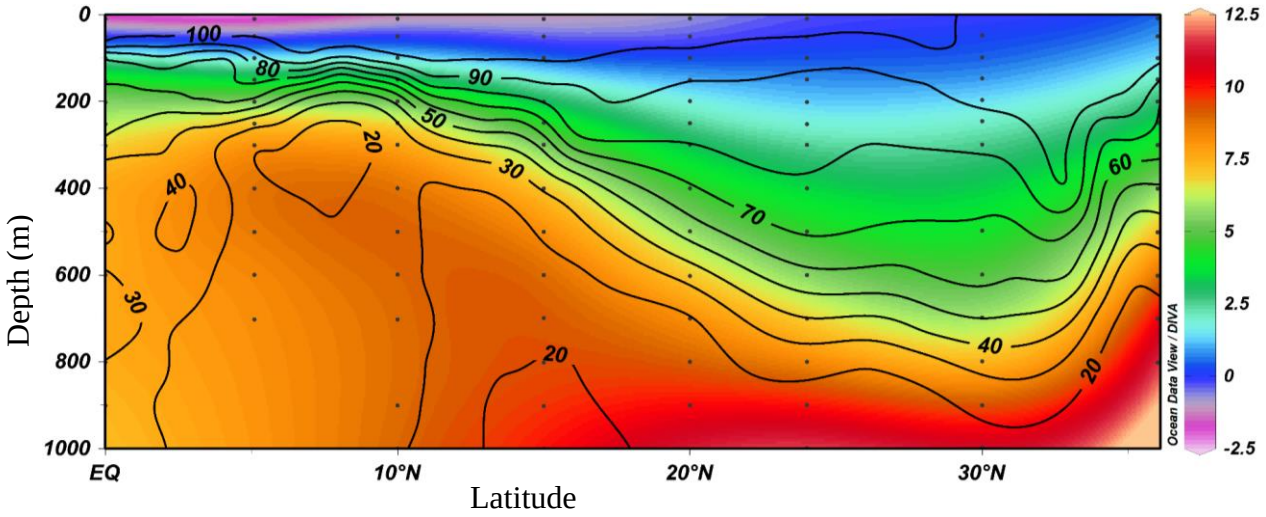

Figure 32: The section diagram of dissolved oxygen isotope ratio ($\delta^{18}O$) along with overlaying oxygen saturation degree in the northwestern Pacific Ocean. The black dots represent the water sampling depth for the measurements of dissolved oxygen isotope ratios. The dashed oxygen saturation isoline represents the area of oxygen minimum zone in the study area. The dashed line on the tope represents the approximate depth at which the measured $\delta^{18}O$ was equal to its equilibrium value at that water temperature (Benson et al. 1979).

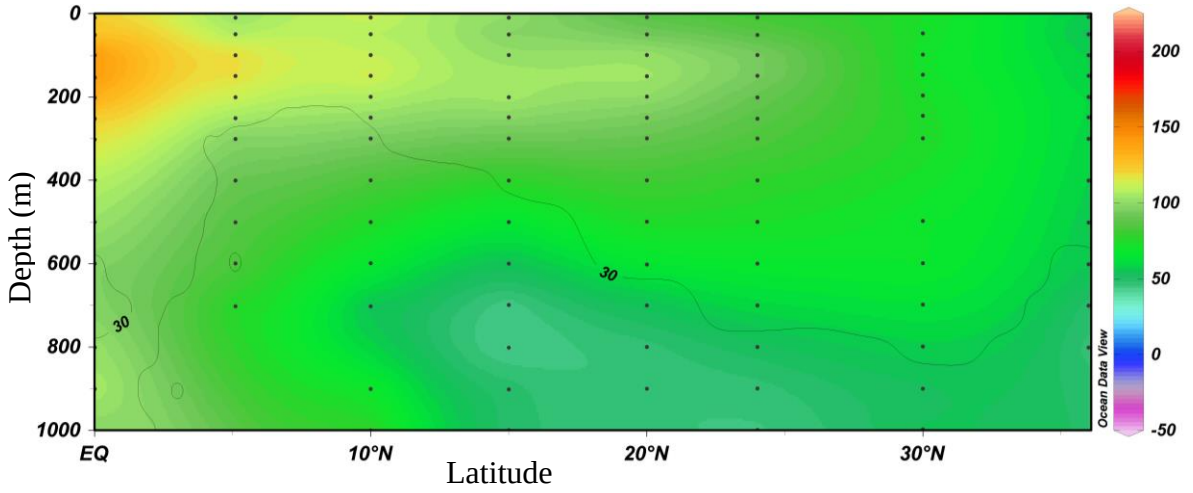

Figure 33: The section diagram of dissolved oxygen isotope anomaly ($\Delta^{17}O$) in the northwestern Pacific Ocean. An isoline represent 30% oxygen saturation zone, in which sample analysis containing an uncertainty of 50 per meg.

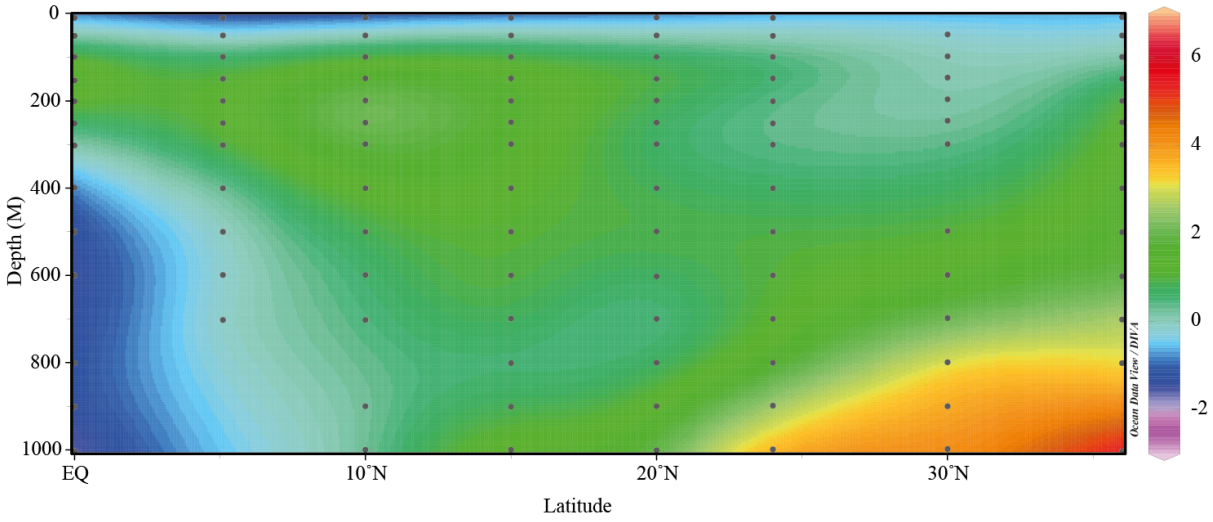

Figure 34: The section diagram of argon saturation (ΔAr) in the northwestern Pacific Ocean.

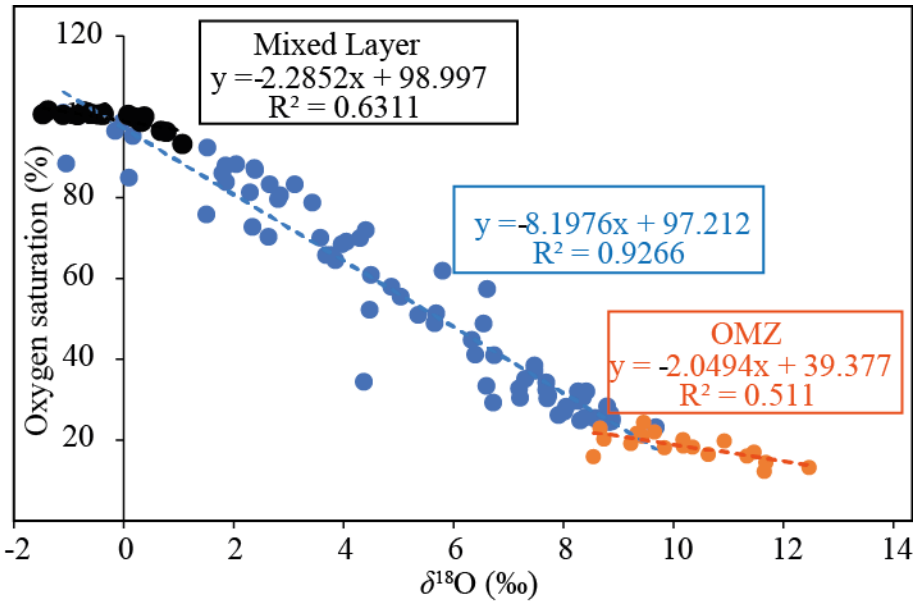

Figure 35: The dissolved oxygen saturation versus $\delta^{18}O$ for mixed layer, oxygen minimum zone and samples in between them. Dissolved oxygen concentration at mixed layer was mainly controlled by the photosynthesis and gas exchange. The most of the mixed layer $\delta^{18}O$ was less than the equilibrium value of 0.75‰; this is mainly because of the addition of photosynthetic oxygen, which has a large negative value relative to atmospheric oxygen. Bellow the mixed layer the $\delta^{18}O$ was mainly controlled by biological respiration and thus the relationship between oxygen saturation and $\delta^{18}O$ was strong.

Chapter 4

Discussion

4.1 Application of this method to determine equilibrium isotope fractionation during gas exchange between air and water

The results of the equilibrium isotope fractionation between air and water are summarised in Table 8. The difference in $\delta^{18}O$ of 0.702 ‰ for stirred DW was consistent with the results of previous studies that ranged from 0.691 ‰ to 0.722 ‰. Furthermore, our value was identical to the result given by Benson and Krause (Benson and Krause 1980; Benson and Krause 1984), which was obtained by a polynomial regression of data observed between 0 and 60 °C. Stanley et al. (Stanley et al. 2010) and Kaiser (Kaiser 2011) suggested that the choice of equilibration method might influence the fractionation factor. For both DW and SW, the δ values were slightly higher when stirring than bubbling, but the $\Delta^{17}O$ values were similar. Our $\Delta^{17}O$ values were closer to those reported by Stanley (Stanley et al. 2010) for DW and Reuer (Reuer et al. 2007) for SW, which were obtained by the stirring method, and significantly different from other results, produced using the bubbling method.

One possible reason for the observed differences in δ values between equilibration methods is a bubble-mediated supersaturation that occurred only in bubbled water. Because small bubbles injected into water dissolve completely, bubbled water could result in oxygen supersaturation (Hamme and Emerson 2006). If this applied to our DW results, 7–8 % supersaturation of the oxygen concentration should have been observed by the O_2 sensor [(0.702 – 0.637)/0.702]. I confirmed that no significant difference existed in the O_2 concentration between the two methods, and collected aliquots at the equilibrium concentration. Therefore, an isotope disequilibrium (i.e. insufficient time for isotope equilibration when the concentration equilibrium is achieved) was then considered. I attempted to calculate the residual fraction of bubble-injected air from a simple mass balance equation, although the calculation was unsuccessful. For the isotope disequilibrium, diffusive input O_2 had 2.8 ‰ lower isotopic composition relative to the atmosphere, whereas bubble-injected O_2 had an identical isotopic composition to the atmosphere. Thus, the overall isotopic composition of input O_2 must have been higher than for diffusive transport only, and the disequilibrium isotopic composition of dissolved oxygen must also be higher than that in isotopic equilibrium.

Further detailed investigations, such as changing the bubble size and relaxation time, and investigating the temperature dependency of each fractionation factor, are required.

With regard to the inconsistent $\Delta^{17}O$ values reported previously, our results suggest that the lower values may be correct (Luz et al. 2002; Stanley et al. 2009). However, the choice of equilibration method might not be the reason for this. The difference between two research groups was extremely small (0.01 ‰), and I could not clarify the exact reasons in this study. The accumulation of more data through inter-laboratory comparisons might solve this issue. Another interesting result was the difference in δ values between DW and SW (Table 4), when the DW results were lower than the SW. The differences were 0.99 and 0.58 ‰ respectively for $\delta^{18}O$ and $\delta^{17}O$ when using stirred water and similar to those for DW reported by Stanley (Stanley et al. 2010) and SW reported by Reuer (Reuer et al. 2007) at 0.80 and 0.43 ‰, respectively.

The difference of isotope fractionation of oxygen between freshwater and SW should be investigated to find a significant difference in δ values. Benson and Krause (Benson and Krause 1984) investigated the temperature dependency of equilibrium $\delta^{18}O$ values in freshwater and reported that the effect of salinity on fractionation was undetectable in the range from 0 to 40 °C, based on a comparison with the salinity dependency of helium isotope fractionation. At a temperature of 25 °C, oxygen solubility decreases by 20 % when salinity increases from 0 to 35 (Knox et al. 1992). If this magnitude of decrease in solubility were converted to a temperature change, the 20 % decrease corresponds to a temperature difference of 15–25 °C, increasing to 25–40 °C. In this case, the difference in equilibrium $\delta^{18}O$ values would be 0.07 ‰ (Kaiser 2011), which is similar to our result of 0.10 ‰ between DW and SW.

Finally, I used this method to determine equilibrium isotope fractionation during gas exchange between air and water. For the stirring of equilibrated DW, the difference in $\delta^{18}O$ values was within the range previously reported, and the difference in $\Delta^{17}O$ was consistent with recent studies and lower than earlier ones. I found a slight difference in $\delta^{18}O$ values between equilibration methods, but no significant difference in $\Delta^{17}O$ values. In addition, a difference in the $\delta^{18}O$ values of DW and SW occurred at 25 °C.

Table 8: Triple oxygen isotopic composition of dissolved oxygen in equilibrium with atmospheric air at 25°C. Uncertainties are indicated as ±1 standard error. Stirring or bubbling for deionised water and seawater, respectively, achieved equilibration. Reported values were labelled as follows; Sarma et al. as Sa03 (Sarma et al. 2003), Barkan and Luz as BL03 (Barkan and Luz 2003), Juranek and Quay (Juranek and Quay 2005) as JQ05, Sarma et al. as Sa06 (Sarma et al. 2006), Stanley et al. as St10 (Stanley et al. 2010), Luz and Barkan as LB00 (Luz and Barkan 2000), Reuer et al.(Reuer et al. 2007) as R07 and Luz and Barkan (Luz and Barkan 2009) as LB09. The samples from Sa03, Sa06 and St10 corresponded to distilled water. These values are from the study by Kaiser (Kaiser 2011), except for BL03. The B and S symbols in each label represent bubbling and stirring, respectively. The number in each label represents the reaction temperature. Values in parenthesis were not specified in each paper, but could be calculated from $\delta^{17}O$ and $\Delta^{17}O$ results according to Kaiser (Kaiser 2011). The water used in the study by Reuer (Reuer et al. 2007) et al. was not natural seawater, but had an equivalent salinity created by adding sodium chloride.

Samples	*n*	$\delta^{17}O$ (‰)	$\delta^{18}O$ (‰)	$\Delta^{17}O$ (per meg)
Deionised water (DW)				
This study				
by stirring, 25	5	0.369 ± 0.009	0.702 ± 0.017	5 ± 3
by bubbling, 25	8	0.335 ± 0.013	0.637 ± 0.021	5 ± 5
Sa03, B, 22	10	0.371	0.691	13 ± 5
BL03, B, 25	7	0.390	0.720	17 ± 1
JQ05, S, 21	4	0.391	(0.722)	17 ± 3
Sa06, B, 24	10	0.390	0.717	18 ± 2
St10, S, 21	16	0.383	(0.722)	9 ± 2
Seawater (SW)				
This study				
by stirring, 25	5	0.319 ± 0.012	0.603 ± 0.021	6 ± 5
by bubbling, 25	5	0.305 ± 0.006	0.579 ± 0.011	5 ± 5
LB00, B, 25		0.382	(0.703)	18 ± 2
R07, S, 24.8	14	0.340	0.642	8 ± 3
LB09, B, 25	5	0.391	0.722	17 ± 3

I propose that the cryogenic separation presented here is an alternative analytical method for determining the triple isotopes of oxygen and the oxygen to argon ratio with sufficiently high precision. The device used for sample preparation is much simpler than in the conventional chromatographic method, with less risk of air contamination for the samples because switching between a vacuum and helium flow system is not necessary. Since the devices used in this method was much simple, and thus the preparation system can be carried on-board very conveniently. The main limitation of this method was that I could not separate

oxygen from argon under any of the conditions described in this manuscript. The present method has been calibrated for a range of sample volumes (2–6.6 mL), the samples having a volume beyond this range may require some slight modification in experimental conditions like elution time and/or column temperature.

4.2 Gross Oxygen Production in Northwestern Pacific Ocean

Using above explained mass balance of dissolved oxygen isotope ratios in ocean, it very simple to estimate gross oxygen production in the ocean by measuring triple oxygen isotope ratios and calculating piston velocity from 10 days averaged wind speed. The estimation of variability of photosynthetic production of oxygen in ocean is important to understand global carbon and oxygen cycles and ultimately carbon fixing and responds to future climate forcing. Initially scientists were using in vitro determination methods like ^{14}C labeled incubation, ^{18}O incubation, dissolved oxygen methods has very large uncertainty. There are many studies compared in vitro and in situ estimates of marine production indicate that marine productivity are underestimated by bottle rate approaches (Juranek and Quay 2005; Karl et al. 2003; Williams et al. 2004). The table 9 below showing the average mixed layer $\Delta^{17}O$, 10 days average wind speed and calculated GOP using averaged $\Delta^{17}O$. Along the study area the GOP was varied from 135 $mmolO_2m^{-2}d^{-1}$ to 422 $mmolO_2m^{-2}d^{-1}$eat equator and 10 °N respectively. A general trend of gross production was, at equator the productivity was less then increased maxima at 10 °N which was then decreased towards high latitude stations. It was been noted that at equator the measured primary production was less than expected because of the equatorial region was highly upwelling area, this water in the mixed layer have not reached true steady state. This observation can be easily understand by comparing $\Delta^{17}O$ of equator at two depths, at surface water the $\Delta^{17}O$ was 123 per meg, just below 50 m the $\Delta^{17}O$ was 79 per meg and both of these sampling depths were in mixed layer. This huge difference in the value of $\Delta^{17}O$ within the mixed layer depths was because of insufficient time to achieve steady state condition which was assumed in the derivation of the mass balance of dissolved oxygen isotope in the mixed layer. Once the upwelled water having rich in nutrient comes out to the surface at equator flows pole ward by exposing more sun light cause high photosynthesis in the middle latitude, which was clearly reviled in this study. After reaching a maximum at 10 °N the GOP was started declining towards northern most stations. The center of North Pacific Ocean gyre is oligotrophic in nature, oligotrophic oceanic environment where the plankton biomass is very low and region was assumed to be less productive.

Table 9: The table shows mixed layer depth, 10 days average wind speed, average mixed layer $\Delta^{17}O$. The gross oxygen production was calculated using wind speed and mixed layer $\Delta^{17}O$ according to Luz and bracken 2000 (Luz and Barkan 2000) and Hendricks 2004 (Hendricks et al. 2004). Abbreviations used in the table represents following references, [a]: (Juranek and Quay 2010), b (Quay et al. 2010)

Latitude	Mixed Layer Depth (M)	Wind Speed (M/S)	Avg Mixed Layer $\Delta^{17}O$ (Per meg)	GOP ($mmolO_2m^{-2}d^{-1}$)	Literature Values ($mmolO_2m^{-2}d^{-1}$)
EQ	50	3.2	100	135±70	408±80[a]
5	50	6.8	53	224±86	
10	50	7.3	112	422	109±12[a], 71±16[b], 105±41[b]
15	100	8.1	80	410±186	
20	50	8.0	53	302±16	
24	10	8.1	50	332±10	
30	200	8.0	37	225±108	
36	100	8.6	38	234±136	

4.3 Anomalous argon saturation state in the North Pacific Ocean

In thee ocean water argon anomaly ΔAr is a function of gas exchange and heat flux in the surface mixed layer water and diaphycnal mixing in the subsurface and thermocline water and net heat loss associated polar water mass subduction for deep water (Hamme and Emerson 2002; Ito and Deutsch 2006). The observed argon anomaly was negative in the low latitude north pacific ocean. In the low latitude stations, the solar heating of water cause extensive evaporation of surface water and thus the creation of inter tropical convergence zone (ITCZ). The ITCZ in the equatorial region is associated with high rainfall and comparatively low atmospheric pressure. This heavy rainfall results the freshening of mixed layer water (Figure 20). This change in weather condition could be changing the ΔAr in the low latitude stations.

The measured ΔAr in the subsurface water of North Pacific Ocean was super saturated with argon, and an argon supersaturation zone was observed at a depth around 150 m in the low and middle latitude stations. This argon supersaturation was produced as result of mixing of hot surface mixed layer water and cold subsurface water.

High argon anomaly was observed at deep water (~1000 m) of northern most stations, which were associated with oxygen minimum zone.

I could not find a satisfactory oceanographic process like water mass mixing and water heating to explain such a high argon anomaly below 700 m, thus I would like exploring the possible errors associated with ΔAr calculation. Analytical errors can be a significant for the calculation of ΔAr for samples from oxygen minimum zones (Ito et al. 2007). All the samples were purified using cryogenic method, the errors associated with this method was mainly due to partial elution of oxygen gas, which could happen for samples having low volume especially samples from oxygen minimum zone. Partial elution of oxygen can produce high ΔAr value. Another possible source of error was the over estimation of dissolved oxygen concentration by Winkler method at oxygen minimum zones.

4.4 Significance of triple oxygen isotope ratios and argon anomaly in the North pacific water masses

Through the observation of the temporal distribution of $\Delta^{17}O$ in the north Pacific which was first clarified by this study, it was confirmed that this could be treated as a conservative tracer even after oxygen consumption processes at the hypolimnion layer of the ocean.

North pacific intermediate water is salinity minimum zone in the potential density around 26.8 σ_θ. The thick and low salinity water from the Okhotsk Sea mixes with the war and saline western subarctic water to form the Oyashio water, this water again mixes with Kuroshio Extension to form NPIW. This hot and cold water mass mixing could be traced using argon anomaly in the NPIW. In the winter the surface water temperature of Okhotsk Sea and Kuroshio Extension was about 1 °C and 12 °C respectively, the mixing of these two water masses can produce an argon supersaturation of 1.8 %. After the production of NPIW, it sinks and flows southward having a unique argon supersaturation value along its path. Table 10 shows the measured ΔAr along the path of NPIW in the North Pacific Ocean sampling depth having a density range of 26.8 ±0.1 σ_θ and salinity less than 34.25. The average measured ΔAr of NPIW was 1.7 % (excluding two abnormal values in the table 10) showing good agreement with theoretical calculation. The two abnormal ΔAr along the NPIW path may be due to the analytical errors as explained in the previous section.

Oxygen isotope anomaly $\Delta^{17}O$ in NPIW could have a signature of gross oxygen productivity at the area of formation source waters, which was then mixed together to form NPIW. Table 10 shows the measured $\Delta^{17}O$ of dissolved oxygen along the path of NPIW, those values must be carrying the signature of water mass mixing just before the formation of NPIW. Table 11 shows the averaged $\Delta^{17}O$ values in different water masses along the study area namely NPIW, NPSTMW and AAIW are 65±16, 82±48 and 91±44 respectively. The ΔAr value at NPSTMW is close to zero while it was significantly higher than zero at NPIW.

Table 10: Dissolved oxygen isotope anomaly and argon saturation along the path of north pacific intermediate water. Most of the argon supersaturation shows a good agreement with theoretically calculated value of 1.8 % along the path of NPIW.

Latitude	Depth (M)	Potential Density (σ_θ)	Salinity	$\Delta^{17}O$ (per meg)	Δ Ar (%)
20	600	26.8	34.1	96	-0.47
24	700	26.8	34.0	68	1.58
30	700	26.7	34.0	71	1.50
30	800	26.9	34.0	68	4.85
36	400	26.8	33.9	47	1.83
36	500	26.9	34.0	42	1.93

Table 11: Chemical and isotopic properties of water masses

	Latitudes	Depths (m)	θ	salinity	O_2 (umol/kg)	σ_θ	$\delta^{18}O$ (‰ air)	$\Delta^{17}O$ (per meg)	ΔAr (%)
NPIW	20 ~ 36N	400 ~ 800	5.7±0.9	34.0±0.06	124±23	26.82±0.08	6.01±1.1	65±19	1.8±1.7
NPSTMW	15 ~ 30N	200 ~ 300	17.4±0.6	34.7±0.04	200±16	25.25±0.11	1.65±1.6	82±48	0.2±0.4
AAIW	EQ~15N	800 ~ 1000	4.8±0.5	34.5±0.02	83±13	27.35±0.07	8.4±0.9	91±44	-0.3±1.5

Chapter 5

Conclusion

I revised the method of helium-free cryogenic separation for analysing the triple isotopes of oxygen and the oxygen to argon ratio, which was first reported by Thiemens and Meagher (Thiemens and Meagher 1984). I tested various experimental conditions and found that the use of 1.5 g of MSZ 5A at a temperature of –92 °C were the optimum conditions for separating air samples between 2 and 6.6 mL. I then confirmed the isotope and molecular fractionation during desorption from MSZ, and found that the use of a single pellet (70 mg) of 13X MSZ achieved insignificant isotope fractionation and slight fractionation in the oxygen to argon ratio for 6 mL of atmospheric air. Repeated measurements of atmospheric air samples yielded a reproducibility (±SD) of 0.021 ‰, 0.044 ‰, 15 per meg and 1.9 ‰ for $\delta^{17}O$, $\delta^{18}O$, $\Delta^{17}O$ and $\delta(O_2/Ar)$, respectively, and these average values agreed well with the assigned values.

I have tested and proved this method for purification oxygen–argon mixture in dissolved gas samples. The method was used to determine equilibrium isotope fractionation during gas exchange between air and water. For the stirring of equilibrated DW, the difference in $\delta^{18}O$ values was within the range previously reported, and the difference in $\Delta^{17}O$ was consistent with recent studies and lower than earlier ones. I found a slight difference in $\delta^{18}O$ values between equilibration methods, but no significant difference in $\Delta^{17}O$ values. I have determined $\Delta^{17}O$ during gas exchange between water (seawater and deionized water) and air at equilibrium. In addition, a difference in the $\delta^{18}O$ values of DW and SW occurred at 25 °C.

I have extensively studied the isotope and molecular during gas desorption from molecular sieves. The experiment was carried out for different type and amount of molecular sieves, however the volume of gas mixture used for this experiment was same. I found significant isotope and molecular fractionation during these processes for two and three pellet of molecular sieves, however there was no significant fractionation while using single pellet of molecular sieves. Thus the study suggests the use of single pellet of molecular sieves (preferably 13X) for trapping and transfer of eluted oxygen–argon mixture.

I propose that the cryogenic separation presented here is an alternative analytical method for determining the triple isotopes of oxygen and the oxygen to argon ratio with sufficiently high precision. The device used for sample preparation is much simpler than in the

conventional chromatographic method, with less risk of air contamination for the samples because switching between a vacuum and helium flow system is not necessary. Since the devices used in this method was much simple, and thus the preparation system can be carried on-board very conveniently. The main limitation of this method was that I could not separate oxygen from argon under any of the conditions described in this manuscript. The present method has been calibrated for a range of sample volumes (2–6.6 mL), the samples having a volume beyond this range may require some slight modification in experimental conditions like elution time and/or column temperature. Repeated measurements of atmospheric air samples yielded a reproducibility (±SD) of 0.021‰, 0.044‰, 15 per meg and 1.9‰ for $\delta^{17}O$, $\delta^{18}O$, $\Delta^{17}O$ and $\delta(O_2/Ar)$, respectively, and these average values agreed well with the assigned values.

I propose that the cryogenic separation presented here is an alternative analytical method for determining the triple isotopes of oxygen and the oxygen to argon ratio with sufficiently high precision. The device used for sample preparation is much simpler than in the conventional chromatographic method, with less risk of air contamination for the samples because switching between a vacuum and helium flow system is not necessary.

The method was further used for the purification of oxygen–argon mixture for samples collected during MR 07-01 cruise. The distribution of $\delta^{18}O$, $\Delta^{17}O$ and ΔAr along with hydrographical parameters in the northwestern Pacific Ocean along 155 °N were studied. Oxygen isotope ratios along with argon anomaly can provide valuable information like production of water masses, subsurface water stratification anomaly in the North Pacific Ocean. The $\delta^{18}O$ in mixed layer of low latitude samples were lower than its equilibrium value because of the addition of photosynthetically produced oxygen, which highly depleted isotopic composition while comparing with atmospheric oxygen. The $\Delta^{17}O$ showed strong maxima just below the mixed layer due to accumulation of photosynthetically produced oxygen below thin mixed layer. Measured argon anomaly and modeled results shows similarities at low latitude subsurface and deep water. Theoretically calculated ΔAr for NPIW water shows good agreement with measurement at that region. A strong linear correlation between $\Delta^{17}O$ and ΔAr for NPIW reviled the conservative property of $\Delta^{17}O$ below the photic zone along the path of NPIW.

Cryogenic separation method requires several improvements and modifications, which are listed as future works. (1) The present method was capable only for removing nitrogen in

the samples and the eluted gas will be a mixture of oxygen and argon, this argon in the samples can interfere oxygen isotope analysis. Thus the method should be modified for the purification of pure oxygen in the samples by testing various kinds of molecular sieves. (2) The oxygen isotope ratios of dissolved gas at equilibrium were carried out to check the effect of equilibration method and type water was tested. A future experiment will be conducted to study the effect of temperature on dissolved oxygen isotope ratios at equilibrium. (3) A complete depth distribution of $\delta^{18}O$, $\Delta^{17}O$ and ΔAr in North Pacific Ocean.

This study could confirm that the triple isotope ratio of dissolved oxygen in subsurface ocean plays a role of conservative tracer for past oceanic primary productivity, and the argon anomaly is available for the evaluating diapycnal mixing processes among water masses. By extensive observation among ocean basins, the new picture of ocean interior will be obtained.

References

Abe, O. 2008. Isotope fractionation of molecular oxygen during adsorption/desorption by molecular sieve zeolite. Rapid Communications in Mass Spectrometry **22:** 2510-2514.

Abe, O., and N. Yoshida. 2003. Partial pressure dependency of O-17/O-16 and O-18/O-16 of molecular oxygen in the mass spectrometer. Rapid Communications in Mass Spectrometry **17**.

Angert, A., S. Rachmilevitch, E. Barkan, and B. Luz. 2003. Effects of photorespiration, the cytochrome pathway, and the alternative pathway on the triple isotopic composition of atmospheric O-2. Global Biogeochemical Cycles **17**.

Barkan, E., and B. Luz. 2003. High-precision measurements of O-17/O-16 and O-18/O-16 of O-2 and O-2/Ar ratio in air. Rapid Communications in Mass Spectrometry **17**.

---. 2005. High precision measurements of O-17/O-16 and O-18/O-16 ratios in H2O. Rapid Communications in Mass Spectrometry **19:** 3737-3742.

---. 2011. The relationships among the three stable isotopes of oxygen in air, seawater and marine photosynthesis. Rapid Communications in Mass Spectrometry **25:** 2367-2369.

Battle, M. and others 2003. Measurements and models of the atmospheric Ar/N-2 ratio. Geophysical Research Letters **30:** 4.

Bender, M. L. 1990. THE DELTA-O-18 OF DISSOLVED O2 IN SEAWATER - A UNIQUE TRACER OF CIRCULATION AND RESPIRATION IN THE DEEP-SEA. Journal of Geophysical Research-Oceans **95:** 22243-22252.

---. 2000. Oceanography - Tracer from the sky. Science **288**.

Bender, M. L., S. Kinter, N. Cassar, and R. Wanninkhof. 2011. Evaluating gas transfer velocity parameterizations using upper ocean radon distributions. Journal of Geophysical Research-Oceans **116**.

Benson, B. B., and D. Krause. 1980. THE CONCENTRATION AND ISOTOPIC FRACTIONATION OF GASES DISSOLVED IN FRESH-WATER IN EQUILIBRIUM WITH THE ATMOSPHERE .1. OXYGEN. Limnology and Oceanography **25:** 662-671.

---. 1984. THE CONCENTRATION AND ISOTOPIC FRACTIONATION OF OXYGEN DISSOLVED IN FRESH-WATER AND SEAWATER IN EQUILIBRIUM WITH THE ATMOSPHERE. Limnology and Oceanography **29:** 620-632.

Benson, B. B., D. Krause, and M. A. Peterson. 1979. SOLUBILITY AND ISOTOPIC FRACTIONATION OF GASES IN DILUTE AQUEOUS-SOLUTION .1. OXYGEN. Journal of Solution Chemistry **8:** 655-690.

Bieri, R. H., M. Koide, and E. D. Goldberg. 1966. NOBLE GAS CONTENTS OF PACIFIC SEAWATERS. Journal of Geophysical Research **71:** 5243-&.

Bigeleisen, J., and M. G. Mayer. 1947. CALCULATION OF EQUILIBRIUM CONSTANTS FOR ISOTOPIC EXCHANGE REACTIONS. Journal of Chemical Physics **15:** 261-267.

Blunier, T., B. Barnett, M. L. Bender, and M. B. Hendricks. 2002. Biological oxygen productivity during the last 60,000 years from triple oxygen isotope measurements. Global Biogeochemical Cycles **16**.

Blunier, T., M. L. Bender, B. Barnett, and J. C. Von Fischer. 2012. Planetary fertility during the past 400 ka based on the triple isotope composition of O-2 in trapped gases from the Vostok ice core. Climate of the Past **8:** 1509-1526.

Brenninkmeijer, C. A. M., and T. Rockmann. 1998. A rapid method for the preparation of O-2 from CO2 for mass spectrometric measurement of O-17/O-16 ratios. Rapid Communications in Mass Spectrometry **12:** 479-483.

Broecker, W. S. 1970. A BOUNDARY CONDITION ON EVOLUTION OF ATMOSPHERIC OXYGEN. Journal of Geophysical Research **75:** 3553-&.

Cepeda-Morales, J., G. Gaxiola-Castro, E. Beier, and V. M. Godinez. 2013. The mechanisms involved in defining the northern boundary of the shallow oxygen minimum zone in the eastern tropical Pacific Ocean off Mexico. Deep-Sea Research Part I-Oceanographic Research Papers **76:** 1-12.

Chapman, S. 1930. On ozone and atomic oxygen in the upper atmosphere. Philosophical Magazine **10:** 369-383.

Chiappini, C., D. Romano, and F. Matteucci. 2003. Oxygen, carbon and nitrogen evolution in galaxies. Monthly Notices of the Royal Astronomical Society **339:** 63-81.

Clayton, R. N., L. Grossman, and T. K. Mayeda. 1973. COMPONENT OF PRIMITIVE NUCLEAR COMPOSITION IN CARBONACEOUS METEORITES. Science **182:** 485-488.

Craig, H. 1957. ISOTOPIC STANDARDS FOR CARBON AND OXYGEN AND CORRECTION FACTORS FOR MASS-SPECTROMETRIC ANALYSIS OF CARBON DIOXIDE. Geochimica Et Cosmochimica Acta **12:** 133-149.

Craig, H., and T. Hayward. 1987. OXYGEN SUPERSATURATION IN THE OCEAN - BIOLOGICAL VERSUS PHYSICAL CONTRIBUTIONS. Science **235:** 199-202.

Craig, H., and Kroopnic.P. 1970. O-18 VARIATIONS IN DISSOLVED OXYGEN IN SEA. Transactions-American Geophysical Union **51:** 325-&.

Del Giorgio, P. A., and C. M. Duarte. 2002. Respiration in the open ocean. Nature **420:** 379-384.

Dole, M. 1936. The relative atomic weight of oxygen in water and in air - A discussion of the atmospheric distribution of the oxygen isotopes and of the chemical standard of atomic weights. Journal of Chemical Physics **4:** 268-275.

Emerson, S. 1987. SEASONAL OXYGEN CYCLES AND BIOLOGICAL NEW PRODUCTION IN SURFACE WATERS OF THE SUB-ARCTIC PACIFIC-OCEAN. Journal of Geophysical Research-Oceans **92:** 6535-6544.

Emerson, S., T. Ito, and R. C. Hamme. 2012. Argon supersaturation indicates low decadal-scale vertical mixing in the ocean thermocline. Geophysical Research Letters **39**.

Emerson, S., P. D. Quay, C. Stump, D. Wilbur, and R. Schudlich. 1995. CHEMICAL TRACERS OF PRODUCTIVITY AND RESPIRATION IN THE SUBTROPICAL PACIFIC-OCEAN. Journal of Geophysical Research-Oceans **100:** 15873-15887.

Falkowski, P. G. 1994. THE ROLE OF PHYTOPLANKTON PHOTOSYNTHESIS IN GLOBAL BIOGEOCHEMICAL CYCLES. Photosynthesis Research **39:** 235-258.

Falkowski, P. G., R. T. Barber, and V. Smetacek. 1998. Biogeochemical controls and feedbacks on ocean primary production. Science **281:** 200-206.

Farquhar, G. D. and others 1993. VEGETATION EFFECTS ON THE ISOTOPE COMPOSITION OF OXYGEN IN ATMOSPHERIC CO2. Nature **363:** 439-443.

Farquhar, J., M. H. Thiemens, and T. Jackson. 1998. Atmosphere-surface interactions on Mars: Delta O-17 measurements of carbonate from ALH 84001. Science **280:** 1580-1582.

Gehrie, E., D. Archer, S. Emerson, C. Stump, and C. Henning. 2006. Subsurface ocean argon disequilibrium reveals the equatorial Pacific shadow zone. Geophysical Research Letters **33:** 5.

Grande, K. D. and others 1989. PRIMARY PRODUCTION IN THE NORTH PACIFIC GYRE - A COMPARISON OF RATES DETERMINED BY THE C-14,O-2 CONCENTRATION AND O-18 METHODS. Deep-Sea Research Part a-Oceanographic Research Papers **36:** 1621-1634.

Guy, R. D., M. L. Fogel, and J. A. Berry. 1993. PHOTOSYNTHETIC FRACTIONATION OF THE STABLE ISOTOPES OF OXYGEN AND CARBON. Plant Physiology **101:** 37-47.

Hamme, R. C., and S. R. Emerson. 2002. Mechanisms controlling the global oceanic distribution of the inert gases argon, nitrogen and neon. Geophysical Research Letters **29**.

---. 2004. The solubility of neon, nitrogen and argon in distilled water and seawater. Deep-Sea Research Part I-Oceanographic Research Papers **51:** 1517-1528.

---. 2006. Constraining bubble dynamics and mixing with dissolved gases: Implications for productivity measurements by oxygen mass balance. Journal of Marine Research **64:** 73-95.

Hathorn, B. C., and R. A. Marcus. 1999. An intramolecular theory of the mass-independent isotope effect for ozone. I. Journal of Chemical Physics **111:** 4087-4100.

---. 2000. An intramolecular theory of the mass-independent isotope effect for ozone. II. Numerical implementation at low pressures using a loose transition state. Journal of Chemical Physics **113:** 9497-9509.

Helman, Y., E. Barkan, D. Eisenstadt, B. Luz, and A. Kaplan. 2005. Fractionation of the three stable oxygen isotopes by oxygen-producing and oxygen-consuming reactions in photosynthetic organisms. Plant Physiology **138:** 2292-2298.

Hendricks, M. B., M. L. Bender, and B. A. Barnett. 2004. Net and gross O-2 production in the Southern Ocean from measurements of biological O-2 saturation and its triple isotope composition. Deep-Sea Research Part I-Oceanographic Research Papers **51**.

Hendricks, M. B., M. L. Bender, B. A. Barnett, P. Strutton, and F. P. Chavez. 2005. Triple oxygen isotope composition of dissolved O-2 in the equatorial Pacific: A tracer of mixing, production, and respiration. Journal of Geophysical Research-Oceans **110**.

Ito, T., and C. Deutsch. 2006. Understanding the saturation state of argon in the thermocline: The role of air-sea gas exchange and diapycnal mixing. Global Biogeochemical Cycles **20**.

Ito, T., C. Deutsch, S. Emerson, and R. C. Hamme. 2007. Impact of diapycnal mixing on the saturation state of argon in the subtropical North Pacific. Geophysical Research Letters **34**.

Ito, T., R. C. Hamme, and S. Emerson. 2011. Temporal and spatial variability of noble gas tracers in the North Pacific. Journal of Geophysical Research-Oceans **116**.

Javoy, M. and others 2010. The chemical composition of the Earth: Enstatite chondrite models. Earth and Planetary Science Letters **293:** 259-268.

Juranek, L. W., and P. D. Quay. 2005. In vitro and in situ gross primary and net community production in the North Pacific Subtropical Gyre using labeled and natural abundance isotopes of dissolved O-2. Global Biogeochemical Cycles **19**.

---. 2010. Basin-wide photosynthetic production rates in the subtropical and tropical Pacific Ocean determined from dissolved oxygen isotope ratio measurements. Global Biogeochemical Cycles **24**.

---. 2013. Using Triple Isotopes of Dissolved Oxygen to Evaluate Global Marine Productivity, p. 503-524. *In* C. A. Carlson and S. J. Giovannoni [eds.], Annual Review of Marine Science, Vol 5. Annual Review of Marine Science.

Juranek, L. W., P. D. Quay, R. A. Feely, D. Lockwood, D. M. Karl, and M. J. Church. 2012. Biological production in the NE Pacific and its influence on air-sea CO2 flux: Evidence from dissolved oxygen isotopes and O-2/Ar. Journal of Geophysical Research-Oceans **117**.

Kaiser, J. 2011. Technical note: Consistent calculation of aquatic gross production from oxygen triple isotope measurements. Biogeosciences **8**.

Kaiser, J., and O. Abe. 2012. Reply to Nicholson's comment on 'Consistent calculation of aquatic gross production from oxygen triple isotope measurements' by Kaiser (2011). Biogeosciences **9:** 2921-2933.

Kaiser, J., M. K. Reuer, B. Barnett, and M. L. Bender. 2005. Marine productivity estimates from continuous O-2/Ar ratio measurements by membrane inlet mass spectrometry. Geophysical Research Letters **32**.

Karl, D. M., E. A. Laws, P. Morris, P. J. L. Williams, and S. Emerson. 2003. Global carbon cycle - Metabolic balance of the open sea. Nature **426:** 32-32.

Keedakkadan, H. R., and O. Abe. 2015. Cryogenic separation of an oxygen-argon mixture in natural air samples for the determination of isotope and molecular ratios. Rapid Communications in Mass Spectrometry **29:** 775-781.

Keeling, R. F. 1993. ON THE ROLE OF LARGE BUBBLES IN AIR-SEA GAS-EXCHANGE AND SUPERSATURATION IN THE OCEAN. Journal of Marine Research **51:** 237-271.

Kirkwood, D. S. 1992. STABILITY OF SOLUTIONS OF NUTRIENT SALTS DURING STORAGE. Marine Chemistry **38:** 151-164.

Knox, M., P. D. Quay, and D. Wilbur. 1992. KINETIC ISOTOPIC FRACTIONATION DURING AIR-WATER GAS TRANSFER OF O-2, N-2, CH-4, AND H-2. Journal of Geophysical Research-Oceans **97:** 20335-20343.

Kroopnic.P, and H. Craig. 1972. ATMOSPHERIC OXYGEN - ISOTOPIC COMPOSITION AND SOLUBILITY FRACTIONATION. Science **175:** 54-&.

Kroopnick, P., and H. Craig. 1976. OXYGEN ISOTOPE FRACTIONATION IN DISSOLVED-OXYGEN IN DEEP-SEA. Earth and Planetary Science Letters **32:** 375-388.

Lammerzahl, P., T. Rockmann, C. A. M. Brenninkmeijer, D. Krankowsky, and K. Mauersberger. 2002. Oxygen isotope composition of stratospheric carbon dioxide. Geophysical Research Letters **29**.

Landais, A., J. Lathiere, E. Barkan, and B. Luz. 2007. Reconsidering the change in global biosphere productivity between the Last Glacial Maximum and present day from the triple oxygen isotopic composition of air trapped in ice cores. Global Biogeochemical Cycles **21**.

Levine, N. M., M. L. Bender, and S. C. Doney. 2009. The delta O-18 of dissolved O-2 as a tracer of mixing and respiration in the mesopelagic ocean. Global Biogeochemical Cycles **23**.

Luz, B., and E. Barkan. 2000. Assessment of oceanic productivity with the triple-isotope composition of dissolved oxygen. Science **288**.

---. 2009. Net and gross oxygen production from O-2/Ar, O-17/O-16 and O-18/O-16 ratios. Aquatic Microbial Ecology **56:** 133-145.

---. 2010. Variations of O-17/O-16 and O-18/O-16 in meteoric waters. Geochimica Et Cosmochimica Acta **74**.

---. 2011. The isotopic composition of atmospheric oxygen. Global Biogeochemical Cycles **25**.

Luz, B., E. Barkan, M. L. Bender, M. H. Thiemens, and K. A. Boering. 1999. Triple-isotope composition of atmospheric oxygen as a tracer of biosphere productivity. Nature **400**.

Luz, B., E. Barkan, Y. Sagi, and Y. Z. Yacobi. 2002. Evaluation of community respiratory mechanisms with oxygen isotopes: A case study in Lake Kinneret. Limnology and Oceanography **47**.

Lyons, T. W., C. T. Reinhard, and N. J. Planavsky. 2014. The rise of oxygen in Earth's early ocean and atmosphere. Nature **506:** 307-315.

Lysne, J., and C. Deser. 2002. Wind-driven thermocline variability in the Pacific: A model-data comparison. Journal of Climate **15:** 829-845.

Maes, C., M. J. Mcphaden, and D. Behringer. 2002. Signatures of salinity variability in tropical Pacific Ocean dynamic height anomalies. Journal of Geophysical Research-Oceans **107**.

Mahata, S., S. K. Bhattacharya, C. H. Wang, and M. C. Liang. 2013. Oxygen Isotope Exchange between O-2 and CO2 over Hot Platinum: An Innovative Technique for Measuring Delta O-17 in CO2. Analytical Chemistry **85:** 6894-6901.

Matsuhisa, Y., J. R. Goldsmith, and R. N. Clayton. 1978. MECHANISMS OF HYDROTHERMAL CRYSTALLIZATION OF QUARTZ AT 250-DEGREES-C AND 15 KBAR. Geochimica Et Cosmochimica Acta **42:** 173-&.

Mauersberger, K. 1981. MEASUREMENT OF HEAVY OZONE IN THE STRATOSPHERE. Geophysical Research Letters **8:** 935-937.

---. 1987. OZONE ISOTOPE MEASUREMENTS IN THE STRATOSPHERE. Geophysical Research Letters **14:** 80-83.

Mehler, A. H. 1951. STUDIES ON REACTIONS OF ILLUMINATED CHLOROPLASTS .1. MECHANISM OF THE REDUCTION OF OXYGEN AND OTHER HILL REAGENTS. Archives of Biochemistry and Biophysics **33:** 65-77.

Miller, M. F. 2002. Isotopic fractionation and the quantification of O-17 anomalies in the oxygen three-isotope system: an appraisal and geochemical significance. Geochimica Et Cosmochimica Acta **66**.

Molina, L. T., and M. J. Molina. 1987. PRODUCTION OF CL2O2 FROM THE SELF-REACTION OF THE CIO RADICAL. Journal of Physical Chemistry **91:** 433-436.

Molina, M. J., and F. S. Rowland. 1974. STRATOSPHERIC SINK FOR CHLOROFLUOROMETHANES - CHLORINE ATOMIC-CATALYSED DESTRUCTION OF OZONE. Nature **249:** 810-812.

Morrison, J. M. and others 1999. The oxygen minimum zone in the Arabian Sea during 1995. Deep-Sea Research Part Ii-Topical Studies in Oceanography **46:** 1903-1931.

Munro, D. R., P. D. Quay, L. W. Juranek, and R. Goericke. 2013. Biological production rates off the Southern California coast estimated from triple O-2 isotopes and O-2 : Ar gas ratios. Limnology and Oceanography **58:** 1312-1328.

Navon, O., and G. J. Wasserburg. 1985. SELF-SHIELDING IN O-2 - A POSSIBLE EXPLANATION FOR OXYGEN ISOTOPIC ANOMALIES IN METEORITES. Earth and Planetary Science Letters **73:** 1-16.

Nier, A. O. 1950. A REDETERMINATION OF THE RELATIVE ABUNDANCES OF THE ISOTOPES OF CARBON, NITROGEN, OXYGEN, ARGON, AND POTASSIUM. Physical Review **77:** 789-793.

Nightingale, P. D., P. S. Liss, and P. Schlosser. 2000. Measurements of air-sea gas transfer during an open ocean algal bloom. Geophysical Research Letters **27:** 2117-2120.

Oki, T., and S. Kanae. 2006. Global hydrological cycles and world water resources. Science **313:** 1068-1072.

Oneil, J. R. 1986. THEORETICAL AND EXPERIMENTAL ASPECTS OF ISOTOPIC FRACTIONATION. Reviews in Mineralogy **16:** 1-40.

Paulmier, A., and D. Ruiz-Pino. 2009. Oxygen minimum zones (OMZs) in the modern ocean. Progress in Oceanography **80:** 113-128.

Quay, P. 1997. Was a carbon balance measured in the equatorial Pacific during JGOFS? Deep-Sea Research Part Ii-Topical Studies in Oceanography **44:** 1765-1781.

Quay, P. D., S. Emerson, D. O. Wilbur, C. Stump, and M. Knox. 1993. THE DELTA-O-18 OF DISSOLVED O2 IN THE SURFACE WATERS OF THE SUB-ARCTIC PACIFIC - A TRACER OF BIOLOGICAL PRODUCTIVITY. Journal of Geophysical Research-Oceans **98:** 8447-8458.

Quay, P. D., C. Peacock, K. Bjoerkman, and D. M. Karl. 2010. Measuring primary production rates in the ocean: Enigmatic results between incubation and non-incubation methods at Station ALOHA. Global Biogeochemical Cycles **24**.

Quay, P. D., D. O. Wilbur, J. E. Richey, A. H. Devol, R. Benner, and B. R. Forsberg. 1995. THE O-18/O-16 OF DISSOLVED-OXYGEN IN RIVERS AND LAKES IN THE AMAZON BASIN - DETERMINING THE RATIO OF RESPIRATION TO PHOTOSYNTHESIS RATES IN FRESH-WATERS. Limnology and Oceanography **40:** 718-729.

Ramanathan, V., P. J. Crutzen, J. T. Kiehl, and D. Rosenfeld. 2001. Atmosphere - Aerosols, climate, and the hydrological cycle. Science **294:** 2119-2124.

Reuer, M. K., B. A. Barnett, M. L. Bender, P. G. Falkowski, and M. B. Hendricks. 2007. New estimates of Southern Ocean biological production rates from O-2/Ar ratios and the triple isotope composition of O-2. Deep-Sea Research Part I-Oceanographic Research Papers **54:** 951-974.

Robinson, C. and others 2002. Plankton respiration in the Eastern Atlantic Ocean. Deep-Sea Research Part I-Oceanographic Research Papers **49**.

---. 2009. Comparison of in vitro and in situ plankton production determinations. Aquatic Microbial Ecology **54:** 13-34.

Sarma, V., and O. Abe. 2006. Short-term variation of triple oxygen isotopes and gross oxygen production in the Sagami Bay, central Japan. Limnology and Oceanography **51:** 1432-1442.

Sarma, V., O. Abe, and T. Saino. 2003. Chromatographic separation of nitrogen, argon, and oxygen in dissolved air for determination of triple oxygen isotopes by dual-inlet mass spectrometry. Analytical Chemistry **75**.

Sarma, V., O. Abe, N. Yoshida, and T. Saino. 2006. Continuous shipboard sampling system for determination of triple oxygen isotopes and O-2/Ar ratio by dual-inlet mass spectrometry. Rapid Communications in Mass Spectrometry **20:** 3503-3508.

Sarma, V. V. S. S., O. Abe, M. Honda, and T. Saino. 2010. Estimating of Gas Transfer Velocity Using Triple Isotopes of Dissolved Oxygen. Journal of Oceanography **66**.

Schueler, B., J. Morton, and K. Mauersberger. 1990. MEASUREMENT OF ISOTOPIC ABUNDANCES IN COLLECTED STRATOSPHERIC OZONE SAMPLES. Geophysical Research Letters **17:** 1295-1298.

Solomon, S., R. R. Garcia, F. S. Rowland, and D. J. Wuebbles. 1986. ON THE DEPLETION OF ANTARCTIC OZONE. Nature **321:** 755-758.

Stanley, R. H. R., W. J. Jenkins, D. E. Lott, Iii, and S. C. Doney. 2009. Noble gas constraints on air-sea gas exchange and bubble fluxes. Journal of Geophysical Research-Oceans **114**.

Stanley, R. H. R., J. B. Kirkpatrick, N. Cassar, B. A. Barnett, and M. L. Bender. 2010. Net community production and gross primary production rates in the western equatorial Pacific. Global Biogeochemical Cycles **24**.

Sweeney, C. and others 2007. Constraining global air-sea gas exchange for CO2 with recent bomb C-14 measurements. Global Biogeochemical Cycles **21**.

Talley, L. D. 1991. AN OKHOTSK SEA-WATER ANOMALY - IMPLICATIONS FOR VENTILATION IN THE NORTH PACIFIC. Deep-Sea Research Part a-Oceanographic Research Papers **38:** S171-S190.

---. 1993. DISTRIBUTION AND FORMATION OF NORTH PACIFIC INTERMEDIATE WATER. Journal of Physical Oceanography **23:** 517-537.

Thiemens, M. H. 2002. Mass-independent isotope effects and their use in understanding natural processes. Israel Journal of Chemistry **42**.

Thiemens, M. H., and J. E. Heidenreich. 1983. THE MASS-INDEPENDENT FRACTIONATION OF OXYGEN - A NOVEL ISOTOPE EFFECT AND ITS POSSIBLE COSMOCHEMICAL IMPLICATIONS. Science **219:** 1073-1075.

Thiemens, M. H., T. Jackson, E. C. Zipf, P. W. Erdman, and C. Vanegmond. 1995. CARBON-DIOXIDE AND OXYGEN-ISOTOPE ANOMALIES IN THE MESOSPHERE AND STRATOSPHERE. Science **270:** 969-972.

Thiemens, M. H., and D. Meagher. 1984. CRYOGENIC SEPARATION OF NITROGEN AND OXYGEN IN AIR FOR DETERMINATION OF ISOTOPIC-RATIOS BY MASS-SPECTROMETRY. Analytical Chemistry **56:** 201-203.

Treguer, P., D. M. Nelson, A. J. Vanbennekom, D. J. Demaster, A. Leynaert, and B. Queguiner. 1995. THE SILICA BALANCE IN THE WORLD OCEAN - A REESTIMATE. Science **268:** 375-379.

Urey, H. C. 1947. THE THERMODYNAMIC PROPERTIES OF ISOTOPIC SUBSTANCES. Journal of the Chemical Society**:** 562-581.

Wajsowicz, R. C., and P. S. Schopf. 2001. Oceanic influences on the seasonal cycle in evaporation over the Indian Ocean. Journal of Climate **14:** 1199-1226.

Wanninkhof, R. 1992. RELATIONSHIP BETWEEN WIND-SPEED AND GAS-EXCHANGE OVER THE OCEAN. Journal of Geophysical Research-Oceans **97:** 7373-7382.

Wedepohl, K. H. 1995. THE COMPOSITION OF THE CONTINENTAL-CRUST. Geochimica Et Cosmochimica Acta **59:** 1217-1232.

Williams, P. J. L., P. J. Morris, and D. M. Karl. 2004. Net community production and metabolic balance at the oligotrophic ocean site, station ALOHA. Deep-Sea Research Part I-Oceanographic Research Papers **51:** 1563-1578.

Yasuda, I. 1997. The origin of the North Pacific Intermediate Water. Journal of Geophysical Research-Oceans **102:** 893-909.

Yeung, L. Y., E. D. Young, and E. A. Schauble. 2012. Measurements of (OO)-O-18-O-18 and (OO)-O-17-O-18 in the atmosphere and the role of isotope-exchange reactions. Journal of Geophysical Research-Atmospheres **117**.

Young, E. D., A. Galy, and H. Nagahara. 2002. Kinetic and equilibrium mass-dependent isotope fractionation laws in nature and their geochemical and cosmochemical significance. Geochimica Et Cosmochimica Acta **66:** 1095-1104.

Yung, Y. L., A. Y. T. Lee, F. W. Irion, W. B. Demore, and J. Wen. 1997. Carbon dioxide in the atmosphere: Isotopic exchange with ozone and its use as a tracer in the middle atmosphere. Journal of Geophysical Research-Atmospheres **102:** 10857-10866.